SYNTHESIS AND CHARACTERIZATION OF SILICALITE-1 SUPPORTED NICKEL-BASED CATALYSTS FOR CO_2 REFORMING OF METHANE

BY

ABDUL-RASHID BAWAH

A Thesis Presented to the

DEANSHIP OF GRADUATE STUDIES

KING FAHD UNIVERSITY OF PETROLEUM & MINERALS

DHAHRAN, SAUDI ARABIA

In Partial Fulfillment of the
Requirements for the Degree of

MASTER OF SCIENCE

In

CHEMICAL ENGINEERING

NOVEMBER 2017

KING FAHD UNIVERSITY OF PETROLEUM & MINERALS

DHAHRAN- 31261, SAUDI ARABIA

DEANSHIP OF GRADUATE STUDIES

This thesis, written by **Abdul-Rashid Bawah** under the direction of his thesis advisor and approved by his thesis committee, has been presented and accepted by the Dean of Graduate Studies, in partial fulfilment of the requirements for the degree of **MASTER OF SCIENCE IN CHEMICAL ENGINEERING.**

Dr. Zuhair O. Malaibari
(Advisor)

Dr. Mohammed Ba-Shammakh
Department Chairman

Oki Muraza

Dr. Oki Muraza
(Co-Advisor)

Dr. Salam A. Zummo
Dean of Graduate Studies

A. Al Amer

Dr. Adnan Al-Amer
(Member)

17/1/2018
Date

Mozahar Hossain

Dr. Mohammad Mozahar
(Member)

Shaikh Abdur Razzak

Dr. Shaikh Abdurrazak
(Member)

Dedication

I dedicate this piece of work to my loving mother, Alima, whose hard work, prayers and desire to see me succeed got me to this point in life.

I also dedicate this work to my wife, Asiah, who exercised patience and endured my absence throughout those times I was away from her, working on my research.

This work is dedicated to my entire family for their prayers and support for my education.

ACKNOWLEDGMENTS

First and foremost, sincere gratitude goes to the Almighty Allah, the most gracious, the most merciful, the most beneficent, for the life, health and provisions granted me.

My acknowledgement goes to King Fahd University of Petroleum and Minerals and the Ministry of Higher Education, Kingdom of Saudi Arabia for granting me admission and scholarship to pursue the MSc degree. I highly appreciate the time and effort put in by the secretarial and technical staff of the Chemical Engineering department to help me go through my studies.

It is imperative to mention that this research accomplishment is due, in part, to the guidance and support provided by my thesis advisor Dr. Zuhair Omar Malaibari; co-adviso, Dr. Oki Muraza Muluk; committee members Dr. Adnan Al-Amer, Dr. Mohammad Mozahar Hossain and Dr. Shaikh Abdurrazak. I also am very grateful for the time they took out of their usually occupied schedules to read my thesis and make suggestions for corrections.

This work would not have been a possibility without the laboratory, facilities and financial support provided by the Centre for Research Excellence in Nanotechnology (CENT), Research Institute, KFUPM. I would like to extend sincere gratitude to Dr. Zain Hassan Abdullah Yamani (Director, CENT) for allowing me to be a member of the CENT family. I thank the administrative and technical staff of CENT for the help and vital services they provided to me during my research—most especially, Dr. Hakim S. Abbas, for his astute technical guidance on material characterization techniques, not forgetting Mohammed Sanhoob, Saheed Ganiyu Adewale, Idris Akolade Bakare and

the entire Oki group. I would like to thank every member of all research groups at CENT for any assistance they have provided in one way or another during my research. It was an invaluable experience to have worked with such diligent people.

I am thankful to the entire Ghanaian community at KFUPM and Dhahran at large for being there at all times when I needed them.

TABLE OF CONTENTS

LIST OF TABLES

LIST OF FIGURES

LIST OF ABBREVIATIONS

- ATM: Autothermal reforming of methane
- BET: Brunauer–Emmett–Teller
- CTMABr: Hexadecyl trimethylammonium bromide
- DRM: Dry reforming of methane
- EDX: Energy-dispersive X-ray spectroscopy
- MCM: Mobile composition of matter
- POM: Partial oxidation of methane
- RWGS: Reverse water gas shift
- SBA: Santa Barbara Amorphous
- SEM: Scanning electron microscopy
- SRM: Steam reforming of methane
- TEM: Transmission electron microscopy
- TEOS: Tetraethyl orthosilicate
- TGA: Thermogravimetric analysis
- TPR: Temperature programmed reduction
- XPS: X-ray photoelectron spectroscopy
- XRD: X-ray diffraction
- SiC: Silicon carbide
- GHSV: Gas hourly space velocity
- TPABr: Tetrapropyl ammonium bromide
- FE-SEM: Field emission scanning electron microscopy

ABSTRACT

Full Name : Abdul-Rashid Bawah

Thesis Title : SYNTHESIS AND CHARACTERISATION OF SILICALITE-1 SUPPORTED NICKEL-BASED CATALYSTS FOR CO_2 REFORMING OF METHANE.

Major Field : Chemical Engineering

Date of Degree : January 2018

The conversion of carbon dioxide and methane to syngas is one of the most environmentally benign routes for methane reforming where CO_2, a major greenhouse gas, is converted to hydrogen or syngas (H_2 and CO). Mesoporous silicalite-1 was prepared in one-step by the microwave-assisted hydrothermal synthesis (MAHyS) approach. Ni particles with loadings of 5, 10, 15 and 20 wt.% were impregnated on the silicalite-1, as well as modified silicalite-1. The mesopore volume of the 20 wt.% Ni on S-1 catalyst increased from 0.0712 cm^3/g to 0.1159 cm^3/g after ion-exchanging the Na on silicalite-1 with Ce, prior to impregnation. The structural integrity of the catalysts was maintained as proved by characterization with XRD, FESEM, TEM, N_2-physisorption, XPS and FTIR. H_2-TPR measurements showed that the addition of a second metal enhanced Ni reducibility. The 20 wt.% Ni on silicalite-1 was found to be more active than 10 and 15 wt.% on silicalite-1. Upon modification of the zeolite support material before impregnation of the 20 wt.% Ni, it was observed that Ce-ion-exchanged silicalite-1 supported Ni catalyst was the most active catalyst during 12 h time-on-stream (TOS). Ca promoted Ni on silicalite-1 catalyst produced syngas with H_2/CO ratio of ca. 1, the desired feedstock to produce dimethyl ether. Raman

spectroscopy, TGA-DSC, and TEM revealed that the carbon deposits on the surfaces of the spent catalysts were predominantly multi-walled carbon nanotubes with defects.

ملخص الرسالة

الاسم الكامل: عبد الرشيد باوه

عنوان الرسالة: تصنيع وتخصيص مادة السليكالايت-1 (Silicalite-1) المدعمة بالنيكل كمادة محفزة لتفاعل إعادة تشكيل الميثان بوجود ثاني اوكسيد الكاربون.

التخصص: الندسة الكيميائية

تاريخ الدرجة العلمية: يناير 2018

تعد عملية تحويل ثاني أوكسيد الكاربون والميثان إلى غاز التصنيع من أكثر الطرق الحميدة للبيئة بالنسبة للاعادة تشكيل الميثان، حيث يتم استخدام ثاني أوكسيد الكاربون الغاز الرئيس للإنحباس الحراري وتحويله الى غاز التصنيع، والذي يتكون من الهيدروجين وأول أوكسيد الكاربون. في هذه الدراسة تم تحضير مادة الزيولايت من نوع (silicalite-1) عن طريق التوليف الحراري باستخدام المايكرويف، وتم ترسيب عنصر النيكل بنسب 5 و 10 و 15 و20 % على مادة الزيولايت المصنعة والمعدلة بعد التصنيع. ان حجم المسامات (mesopore volume) للزيولايت ذات ال 20% نيكل ارتفع من 0.0712 سم^2 لكل جرام الى 0.1159 سم^2 لكل جرام بعد ان تم إستبدال الأيونات بالسيريوم. وعند تخصيص المادة باستخدام XRD و FESEM وTEMو XPSو FTIR وعملية امتصاص النيتروجن، تبين أن هيكل المادة المحفزة قد تم الحفاظ عليه، واظهرت نتائج جهاز H_2-TPR ان إضافة عنصر آخر قد عزز القدرة على تقليل النيكل. وأظهرت الدراسة ان الزيولايت ذات الـ 20% نيكل كان أكثر فعالة من الزيولايت ذات النسب الـ 10 والـ 15%. وعند تعديل المادة المحفزة وقبل ترسيب النيكل (20%)، وجد أن الزيولايت المدعم بالنيكل والذي تم تبديل ايوناته بالسيريوم كان الاكثر فعالية خلال 12 ساعة من بدأ التفاعل. وعند استخدام مادة الزيولايت المدعمة بالنيكل والكالسيوم انتجت غاز التصنيع بنسبة $H_2/CO = 1$، والذي يعد الخليط المناسب لانتاج ثنائي ايثيل الايثر وكذلك عملية Fischer-Tropsch، و أظهرت دراسة RAMAN و TGA-DSC و TEM ان رواسب الكاربون على سطح المادة المحفزة التي تم استخدامهما كانت في الغالب شكل أنابيب نانوية كاربونية متعددة الجدران مع وجود العيوب. ان ترسب الكاربون خلال التفاعل قد أسهم بشكل إيجابي بزيادة نسبة H_2/CO .

Chapter 1

INTRODUCTION

1.1 Background

Used mainly as an energy source, methane is obtained primarily from natural gas along with Carbon dioxide. Both gases constitute a major component of the greenhouse gases. On a global scale, over the last few decades, researchers have sought to find economic ways of reducing global warming, and this includes efforts to reduce greenhouse gas emissions. One major area is the control of Carbon dioxide emissions from the combustion of natural gas. This is particularly imperative for economies like that of Saudi Arabia which does not only largely depend on oil exports, but is also the largest domestic consumer of products of fossil fuels in the Middle East and 12th largest consumer of primary energy which is mainly petroleum products [1].

As a consequence of the need for more economic and clean energy, some research work has been done in the areas of hydrogen and syngas ($H_2 + CO$) production [2, 3]. Globally, carbon dioxide emissions from consumption of products of fossil fuel amounted to 34.5 billion tonnes in the year 2012 with average growth in concentration for that year amounting to 2.45 ppm [4]. *Figure 1-1* and *Table 1-1* indicate growth rates and levels of CO_2 emissions for some major economic players in the world including Saudi Arabia. Table 1-1 shows that the growth of Saudi Arabia's CO_2 emissions, from 1971 to 2013, was higher than that of some more industrialized countries like Canada, Germany, Japan and USA.

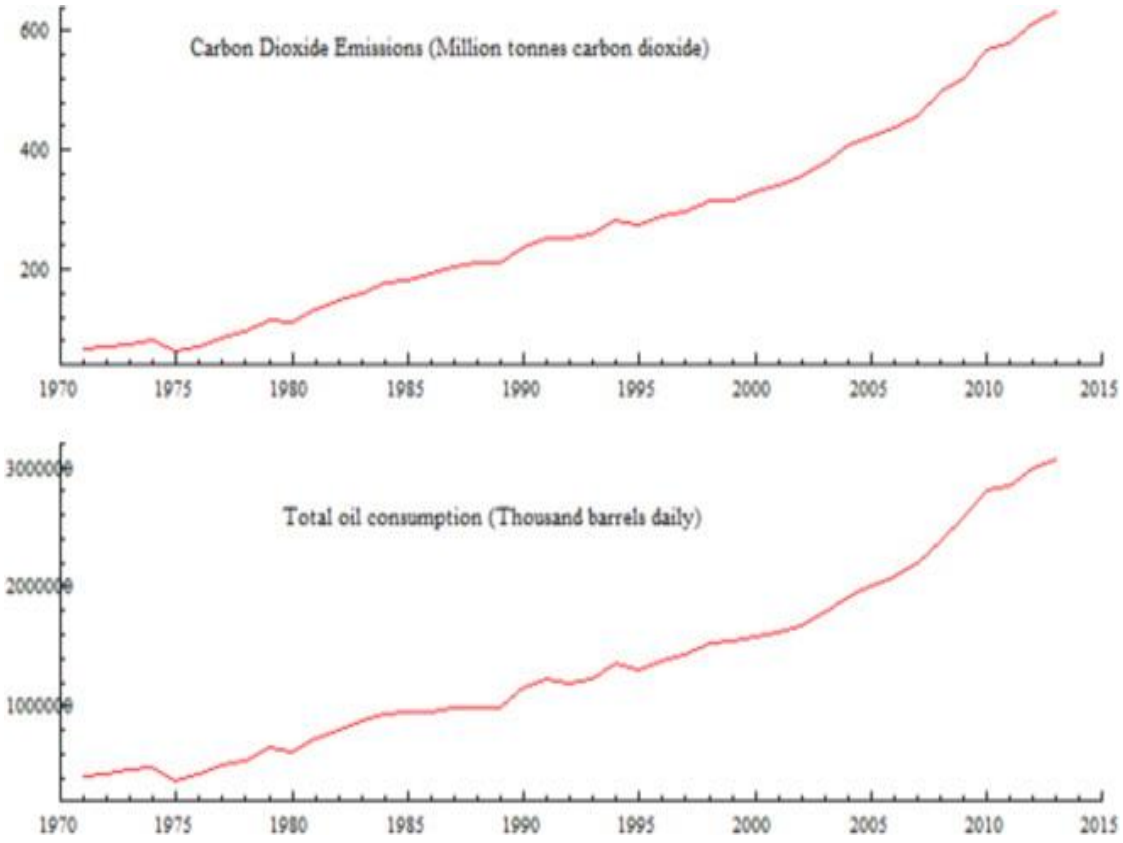

Figure 1-1: CO_2 emissions and oil consumption for Saudi Arabia (1971–2013). Source: [1]

Table 1-1: CO_2 Emissions, 1971–2013

				Average yearly growth, Percent				
Country	**1971 CO_2 emissions in mt**	**2013 CO_2 emissions in mt**	**Percent growth Growth, 1971-2013**	**1971-2013**	**1971-1979**	**1980-1989**	**1990-1999**	**2000-2013**
Saudi Arabia	66.1	632	856.3	5.8	7.2	6.4	4.2	5.2
Germany	1056.4	842.8	−20.2	−0.49	1.25	−1.14	−1.53	−0.37
Japan	857.1	1397.4	56	1.2	2.5	0.57	1.7	0.53
Canada	371.4	616.7	66	1.28	2.9	0.98	1.27	0.54
China	749.7	9524.3	978	6.2	7.8	5.2	3.3	7.8
U.S.A	4682.8	5931.4	616.7	0.59	1.52	0.31	1.25	−0.27
World	15,463.90	35,094.40	126.9	2.02	3.1	1.4	0.94	2.5

(World Bank BP statistical review of world energy, June 2014)[1]

mt: million tonnes

Synthesis gas (syngas), an important source of high value chemicals can be obtained from various sources such coal gasification, and hydrocarbon reforming reactions. The production of syngas by processes such as reforming of heavy hydrocarbons or coal are relatively more expensive than methane reforming. Methane can be catalytically converted to syngas through reforming reactions, as illustrated in Figure 1-3. Syngas, an intermediate product, can be further processed to obtain other useful chemicals such as methanol, ammonia, dimethyl ether, acetic acid, formic acid and also used as feed into the Fischer-Tropsch process which produces liquid fuels [5, 6], Figure 1-2.

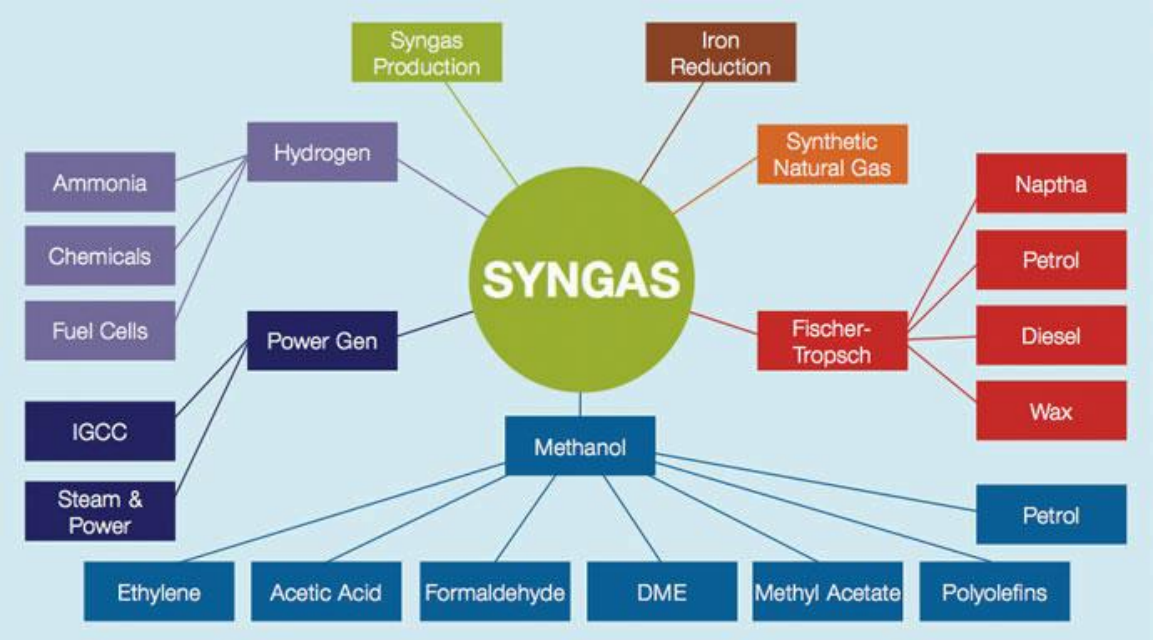

Figure 1-2. Schematic of uses of syngas

1.2 Reforming Technologies

1.2.1 Steam reforming of Methane (SRM)

This reforming technique (Eq. 1) is the major and conventional process implemented in the conversion of methane in natural gas to synthesis gas. Industrially, the SRM is occurs at very high temperatures- (600-900 ^{o}C) and low pressures (1 to 35 atm) [7, 8, 9, 10]. Syngas produced by SRM consists of H_2/CO ratio of about 2.2-4.8 [7, 11].

$$CH_4 + H_2O \rightleftharpoons CO + 3H_2 \; \Delta H_{298\,K} = +206 \text{ kJ/mol} \qquad \text{Eq. 1}$$

1.2.2 Partial Oxidation of Methane (POM)

This reforming technology (Eq. 2) eliminates the costs involved with supplying steam at very high temperatures and can attain equilibrium much faster than steam reforming [12]. However partial oxidation of methane does require a supply of oxygen to combust the methane- this attracts an extra cost as well.

$$CH_4 + 1/2O_2 \rightarrow CO + 2H_2 \; \Delta H_{298K} = -36 \text{ kJ/mol} \qquad \text{Eq. 2}$$

1.2.3 Autothermal Reforming of Methane (ATM)

ATM is a technology that combines partial oxidation (exothermic reaction) and steam reforming (highly endothermic reaction) (Eq. 3) [13] or combines CO_2 reforming and POM (Eq. 4) in the production of syngas. In this reforming technology the H_2/CO_2 ratio can be altered by changing the ratio of oxygen to steam or carbon dioxide as desired [12].

$$4CH_4 + O_2 + 2H_2O \rightarrow 10H_2 + 4CO \qquad \text{Eq. 3}$$

$2CH_4 + O_2 + CO_2 \rightarrow 3H_2 + 3CO + H_2O$ Eq. 4

1.2.4 Dry (CO_2) Reforming of Methane (DRM)

DRM (Eq. 5) is a syngas production technology utilizing carbon dioxide and methane as reactants. Despite its high endothermic nature [14], a catalyst is needed to obtain significant conversions even at such high temperatures [5]. This process yields syngas with a H_2/CO ratio of approximately 1, making it simple for conversion to acetic acid without having to further adjust the ratio.

$CO_2 + CH_4 \rightleftharpoons 2H_2 + 2CO \quad \Delta H_{298K} = +247 \text{ kJ/mol}$ Eq. 5

One major challenge in dry reforming of methane is the competing reverse water gas shift reaction (RWGS) (Eq. 6).

$CO_2 + H_2 \rightleftharpoons CO + H_2O \quad \Delta H_{298} = +41 \text{ kJ/mol}$ Eq. 6

The effect of the RWGS reaction is manifested in the quantity of CO produced. The additional CO from the RWGS reaction results in H_2/CO being less than one.

1.2.5 Bi-Reforming

Another reforming reaction that has gained interests of researchers is bi-reforming of methane. This technology utilizes both CO_2 and steam in a reaction with methane to produce syngas with a H_2/CO ratio of 2 ($H_2/CO = 2$) [6].

$3CH_4 + CO_2 + 2H_2O \rightleftharpoons 4CO + 8H_2 \quad \Delta H_{298\,K} = +220 \text{ kJ/mol}$ Eq. 7

A relatively newer process that seeks to combine the three major catalytic reforming technologies (steam, oxidation and dry reforming) in one reactor is tri-reforming [15].

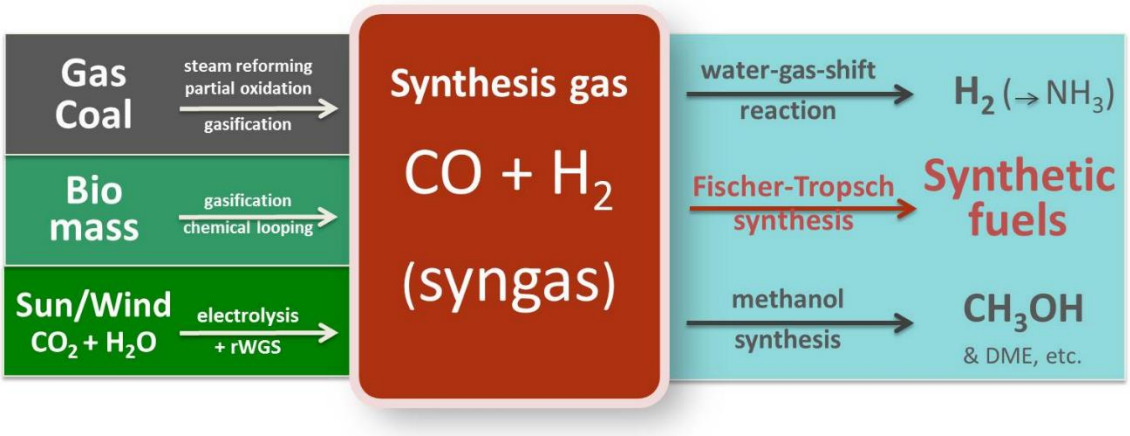

Figure 1-3. Schematic of syngas production from other sources

1.3 Advantages of CO_2 Reforming of Methane

Dry reforming of methane offers the cheapest way to obtain syngas from methane and converts CO_2 into useful products (CO_2 mitigation) and has the potential to reduce the carbon footprint from the combustion of natural gas to produce heat or electricity.. In steam-methane reforming there is a higher possibility of agglomeration and subsequent sintering of metal particles of the catalyst due to the presence of water, whereas CO_2 reforming is a dry process. POM incurs an extra cost with the supply of oxygen to combust the methane whereas DRM utilizes CO_2, a readily available gas that is produced along with natural gas.

1.4 Carbon Deposition in DRM

Methane decomposition (Eq. 8) is the major reaction responsible for carbon deposition in DRM [16]. The effect of the methane cracking reaction can be ameliorated by adjusting CO_2/CH_4 to be greater than unity [17], however, this will also ultimately lead to $H_2/CO < 1$ and will require hydrogen addition in order to be used as feed to the processes that require 1/1 of H_2/CO. Carbon formation may also emanate from the Boudouard reaction (Eq. 9) which is also the reverse of the CO_2 activation reaction. In the reverse boudouard reaction carbon is reacted with CO_2 to yield CO. Since this reaction is endothermic, high temperatures increase the forward reaction, thus producing CO and low temperatures the reverse reaction producing CO_2 [4]. The reaction is also referred to as the CO disproportionation reaction.

$$CH_4 \rightarrow 2H_2 + C \quad \text{Eq. 8}$$

$$C + CO_2 \rightleftharpoons 2CO, \Delta H_{298\,K} = 172\ \text{kJ/mol} \quad \text{Eq. 9}$$

Carbon formation is not energetically favoured on the surfaces of small Ni particles. Thus quite some work have been done to control nickel particles sizes [18, 19] in nickel based catalysts.

1.5 Objectives

The main objectives of this work are explained as follows:

- To synthesize mesoporous silicalite-1 zeolite by the microwave-assisted hydrothermal method.
- To design and synthesize nickel-based catalysts supported on the silicalite-1 zeolite support and study the catalysts using various characterization methods
- To evaluate the performance of the catalysts in the CO_2 reforming of methane reaction in the temperature range: 600 – 900 ^oC.
- To test the catalysts for stability in the CO_2 reforming of methane at 750 ^oC and study the carbon deposited after reaction.

Chapter 2

LITERATURE REVIEW

2.1 Background

A highly endothermic reaction, notwithstanding, CO_2 reforming of methane requires the aid of a catalyst to occur. Temperatures as high as 800-1000^oC are required in dry reforming reactions to achieve equilibrium conversions of the reacting components (CO_2 and CH_4) as well as reduce carbon formation (which subsequently deactivates the catalyst) [20]. Catalyst deactivation resulting from carbon deposition is a major stumbling block to the implementation of DRM on a commercial scale. Thus, this necessitates the need to design catalyst with desirable activity and stability [21]. Noble metal catalysts are highly active and stable in CO_2 reforming reactions [21, 22, 23, 24] but are not economical (are highly expensive), hence cannot be commercially implemented. Nickel based catalysts on the other hand are economically attractive and possess significant activity in dry reforming reactions, but deactivate quickly due to carbon deposition [25, 26]. Ni, Co and Pt have been a major interest for DRM as a result of their significant performance in the reaction [7, 27, 28].

2.2 Catalysts for CO_2 Reforming of Methane

Desperate to find suitable catalysts for the DRM reaction, scientists have investigated many catalysts of various types. However, a striking similarity amongst these catalysts are the use of Nickel. This is due to its availability and activity as well as the fact that it is much less expensive that the noble metals.

2.2.1 Perovskite Type Catalysts

The name perovskite stems from the material $CaTiO_3$ which lends its name to all mixed metal oxides with a similar crystal structure. $CaTiO_3$ was first found by Gustav Rose in the Russian Ural Mountains. This metal oxide was named after Lev Perovski, a Russian mineralogist. Generally, perovskites are donated as ABO_3. A is usually a/an rare/alkaline earth metal and the B position mostly occupied by a transition metal. This type of structure and composition can be tailored during design and synthesis [29]. The perovskite structure can accommodate a considerably large number of different metal types by complete and/or partial substitution at the A and B sites [30, 31, 32].

The most common perovskite catalyst used for dry reforming reactions is the La-Ni-based perovskite ($LaNiO_3$). Its popularity is due the high activity provided by nickel and the high thermal stability provided lanthanum. Partial substitutions of La and Ni can be done in the perovskite structure to improve upon the thermal stability and activity respectively. Substitutions of metal elements in perovskite catalysts do not all the time lead to improved catalytic performance- some substitutions tend to degrade the performance of the catalyst.

2.2.1.1 Performance of Some Perovskite Catalysts in DRM

In the work of Yang et al. $LaNi_{0.5}Fe_{0.5}O_3$ was shown to have achieved lower conversions than when it was doped with the promoters, Sr and Ca at the A-site [33]. These promoters were said to have increased the Basicity of the perovskite, hence increased CO_2 adsorption capacity. The higher activities were ascribed to the quick removal of carbon source from the catalyst active sites. It has been shown by Sutthiumporn et al. [34] that Fe-doped La-Ni based perovskites exhibit less carbon formation due to the formation of the $La_2O_2CO_3$ phase in the process.

Moradi et al. investigated the effects of doping Zn at the B-site in $LaNiO_3$ on DRM [35]. It was shown that perovskites that were partially substituted with degree of x=0.2 and 0.4 achieved higher CH_4 and CO_2 conversions than as-synthesized catalyst ($LaNiO_3$) but the conversions fell drastically when x>=0.6. It was also observed that for all catalysts, CO_2 conversions are higher than CH_4 conversions and H_2/CO is less than unity. This was be attributed to the reverse water gas shift reaction (which consumes the CO_2) which is thermodynamically favourable at these temperatures and occurs simultaneously with the reforming reaction. The activity and stability was ascribed to the structures' resistance to carbon deposition which is an indication that the La_2O_3 phase is highly favoured. By TGA analysis, the x=0.2 Zn doped perovskite showed better resistance to carbon deposition than the as-synthesized perovskite catalyst.

Supported perovskite presented the highest activity in terms of CH_4 and CO_2 conversions with $LaNiO_3$/MCM-41 showing superior performance over the others

[36]. This was attributed to the strong interaction between the supports (SBA-15 and MCM-41), thereby promoting high dispersion of nickel particles the matrix. However, testing for long term stability, $LaNiO_3$/SBA-15 had achieved superior performance over the other catalysts. The higher stability was ascribed to the better anchoring effect of $LaNiO_3$/SBA-15.

Table 2-1: Performance of Some Perovskite Catalysts

Catalyst	Conversion, %		Carbon deposit	H_2/CO	Conditions	Ref
	CH_4	CO_2				
$LaNiO_3$	59.1	74.3	-	0.77-0.87	750° C,1 atm,30 mL min^{-1}, CH_4/CO_2=1/1, 20 hrs	[35]
$LaNi_{0.8}Cu_{0.2}O_3$	72.8	90.9	-	0.84	750° C,1 atm,30 mL min^{-1}, CH_4/CO_2=1/1, 20 hrs	[37]
$La_{0.6}Sr_{0.4}Ni_{0.4}Co_{0.6}O_3$	90.0	92.6	-	1.02	755° C, 1 atm, WHSV= 151 $h^{-1}g^{-1}$, CH_4/CO_2=1/1	[38]
$La_{0.5}Na_{0.5}Ni_{0.3}Al_{0.7}O_3$	95.00	96.00	0.0315 $g_{car}g_{cat}^{-1}h^{-1}$	0.99	880° C, 1 atm, GHSV=30000 cm^3 g_{cat}^{-1} h^{-1}, CH_4/CO_2=1/1, 6 h	[39]
$LaNiO_3$	64.29	68.75	-	0.73	800° C, 1 atm, GHSV=36000 $mLh^{-1}g_{cat}^{-1}$, CH_4/CO_2=1	[36]
$LaNiO_3/SiO_2$	90.18	79.46	-	0.83	800° C, 1 atm, GHSV=36000 $mLh^{-1}g_{cat}^{-1}$, CH_4/CO_2=1	[36]
$LaNiO_3$/SBA-15	91.96	80.36	-	1.04	800° C, 1 atm, GHSV=36000 $mLh^{-1}g_{cat}^{-1}$, CH_4/CO_2=1	[36]
$LaNiO_3$/MCM-41	98.21	81.25	-	0.98	800° C, 1 atm, GHSV=36000 $mLh^{-1}g_{cat}^{-1}$, CH_4/CO_2=1	[36]

Sagar et al. partially substituted Ce at the B-site of LaNiO3 with a substitution degree of y =0 – 1.0 in steps of 0.2 [40]. The perovskite catalyst with a Ce substitution degree of y = 0.4 was found to have achieved superior activity (CO_2 and CH_4 conversions were > 90%) over the other samples (Fig. 1). This catalyst was further subjected to a stability test (Fig. 2). Methane and CO_2 conversions were found to remain above 80% after 9 h on stream.

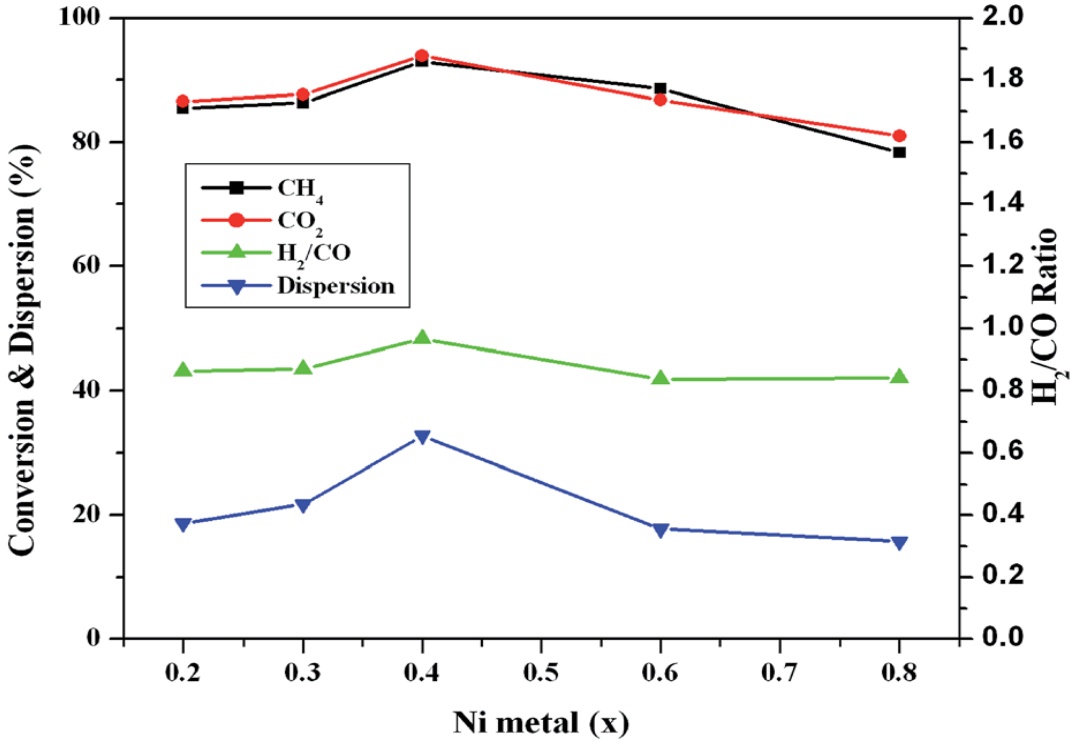

Figure 2-1: Conversion and selectivity test of LaNiy-1CeyO3 catalyst in DRM (Sagar, et al. 2014)

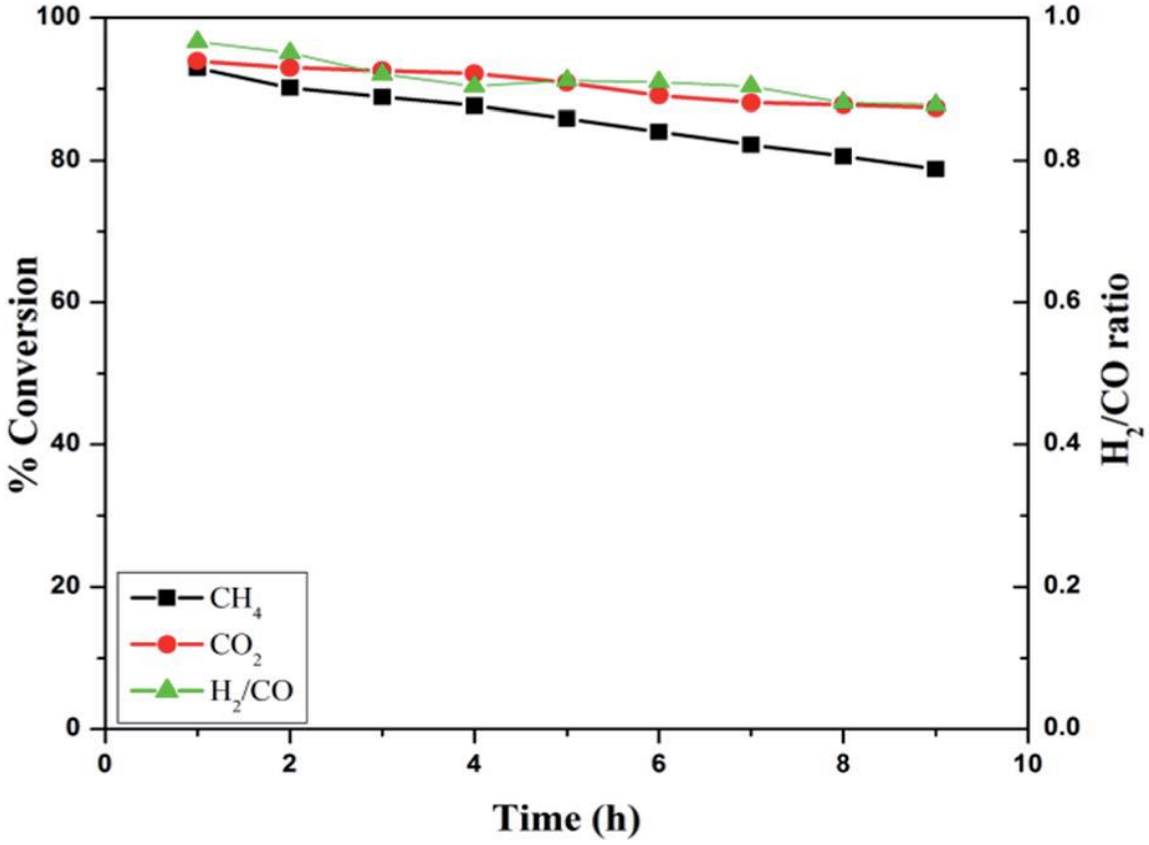

Figure 2-2: Stability test of LaNiy-1CeyO3 catalyst in DRM. [40]

2.2.2 Supports for DRM catalysts

Besides the metal function which provides the activity, a support when applied tends to play an imperative role. Several different materials have been applied as supports in DRM. Amongst such materials are mesoporous silica (SBA-15, MCM-41), alumina as well as zeolites [41]. As stated earlier in this text, the major challenges with the DRM are coke deposition, quick deactivation of the catalysts as well as sintering at very high temperatures (since DRM is highly endothermic). In the quest to achieve high activity and stability in CO_2 reforming of methane, a substantial amount of effort has been put in to investigate catalyst supports and their performances [42]. Zeolites possess high CO_2 affinity and high thermal stability and are therefore suitable to be used as supports for catalysts in CO_2 reforming of methane.

2.2.2.1 Ni Supported on Zeolites for DRM

Owing to their uniform pore size, high pore volume and high surface area, mesoporous material when used as supports for DRM catalysts achieve high catalytic activity [43]. Coupled with the uniform pores size distribution, the high pore volume results in ease of accessibility to the active sites. This can however be reduced by the confined larger size Ni particles. Despite the prime importance of the metal function of DRM catalysts, a well-prepared support if included tends to improve upon the stability and activity of metal-based catalysts in DRM. It has been shown that supports provide the advantage of being able to control the size of Ni nanoparticles [44, 45, 46]. Highly dispersed Ni particles on hierarchical porous materials with strong metal-support interaction coupled with high number of basic sites is a recipe to control carbon deposition and sintering of the Ni particles [47]. In recent years, zeolites have attracted much interest

as supports for DRM due to their uniform microporosity, high thermal stability and the ability to maintain high metal dispersion during the reaction [48]. Zeolites also offer good affinity for CO_2, specific micropore structure and high surface area [49, 50] all of which are desired properties for DRM catalyst support [11]. However, the zeolite framework may be lost due to excessive heat from the high temperature [51] nature of the CO_2 reforming of methane reaction. This necessitates improvement in the thermal stability of the zeolite material prior to being used a support.

The application of zeolites as supports for nickel-based catalysts in CO_2 reforming of methane has been investigated in quite several published works as will be discussed in this text. One such example is the work by Chang et al. [52] in which Ni on ZSM-5 was found to possess high activity and high stability during the dry reforming of methane. As discovered by Zhang et al. [53], the good performance of the ZSM-5 was attributed to its possession of a well-defined structure and the larger surface area (about 340 m^2/g). These properties together facilitate high metal dispersion on the surface. In the work of Chang et al [52] the impact of alkaline promoters (Ca and K) on the reaction was investigated. It was found out that use of Ca as a promoter suppressed carbon deposition and enhanced the activity of the catalyst.

Estephane et al. [54] investigated the performance of a series of Co-Promoted Ni/ZSM-5 catalysts in CO_2 reforming of methane. They found the catalyst doped with the most Co to have high activity and stability as compared to other samples. The suppression of carbon deposition was ascribed to the presence of Co as a promoter. In another work [55], Estephane et al. doped Ni/NaY with a small amount (0.1 wt%)

of Rh and observed drastic improvement in the CO_2 reforming of methane reaction. This outcome is expected since Rh is a noble metal and noble metals are known to have exceptional activities and stabilities in DRM reaction. Nonetheless, their expensive nature inhibits their commercial use as catalysts in CO_2 reforming of methane.

Zeolites KL, KH and clinoptiolite [56] compared to Al_2O_3 were found to possess higher activities and stabilities in dry reforming of methane and they are reported to be suitable supports for the reaction. In these same works, the essence of promoter metals and nickel loading were investigated. In a quest to investigate their stabilities as well activities, Zeolites A, X, and ZSM-5 were applied in dry reforming of methane as result of the thermal stabilities of these materials [57, 58].

It was observed that the nature of the zeolite support has a significant effect on the overall catalytic performance when different zeolites were used as active metal supports in CO_2 reforming of methane [56, 59]. Ni-particles deposited on various kinds of zeolites by the wetness impregnation method showed Ni/zeolite Y to have higher catalytic performance and stability than zeolites X, A and ZSM-5 [42]. Pinheiro et al. [11] applied dealuminated FAU-type Y and BEA zeolites as supports in dry reforming of methane. They reported an improvement in accessibility as a result of the dealumination. The BEA zeolite was observed to be highly stable as well as having an increased catalytic activity.

In an investigation [60], Ni/ZSM-5 was found to achieve higher conversion of CH_4 (96.1%) than that of Ni supported on MCM-22, SBA-15 and MCM-41. The higher

stability and activity were ascribed to the larger surface area (216.7 m2/g) and the small nature of the mesoporous structures (3 – 10 nm)- these are much needed properties for mass transfer [61]. A higher catalytic activity was reported for Ni/ZSM-5 when compared to Ni/HZSM-5, 68.9% and Ni/SiO-Al_2O_3, 62.1%. The acidity of the HZSM-5 contributed to its low catalytic activity by causing a reduction in CO_2 chemisorption thus leading to more carbon forming and subsequent deposition [60]. Due to quick deactivation emanating from the carbon deposition, HZSM-5 is a support material is not suitable for use in CO_2 reforming of methane. Delaminated zeolite (ITQ-6), MCM-41 and Silicalite-1 were investigated for their effects as supports for Ni in CO_2 reforming of methane [62]. A higher stability and catalytic activity was observed for Ni/ITQ-6, with a CH_4 conversion of 80% CH_4 conversion, whereas Ni/MCM-41 achieved a CH_4 conversion of 75% and that of Ni/Silicalite-1 was 63%. The better performance of ITQ-6 was ascribed to a strong interaction between the support and metal particles, high metal dispersion, its resistance to sintering and low coke deposition of 2.1 wt%.

Using the ion exchange method, a series of catalysts, based on Ni, were prepared and tested in dry reforming of methane in the work of Halliche et al. [63]. By H_2-TPR and NH_3-TPD techniques, Ni/ZSM-5 was found to have the highest reducibility and acidity. They reported that the catalytic performance in CO_2 methane reforming reaction had a simultaneous dependence on the reducibility, acidity and zeolite structure. Carbon formation in DRM catalysts can be incited by higher acidity. Due to its lesser acidity, Ni/USY was found to have a higher catalytic performance than Ni/g-Al_2O_3 and Ni/ZSM-5 [63]. Kaengsilalai et al. [59] found the morphology of the zeolite material to

play an imperative role in the performance of the catalyst. They reported that flower-shaped and dog-bone KH zeolites proved to be more active in the DRM reaction when compared to KH zeolite with a disordered morphology. The flower-shaped and dog-bone KH zeolites also showed lesser amounts of carbon formation as wells higher yield of H_2. After 65 h time on stream, the Ni based KH zeolite catalyst exhibited a higher stability than that of Ni/Al_2O_3 [59]. In the work of Frontera et al. [49] involving the investigation of the effects of the external surface of zeolites as supports for Ni in CO_2 reforming of methane reaction, they reported a large amount of silanol groups on silicalite-1 surface. It was observed that these silanol groups lead to low carbon deposition thus preserving the catalyst. The catalytic performance and stability of Ni/sililated-silicalite-1 was improved as a result of replacing the OH groups with larger organosilane groups, Figure 2-3 [49, 64]

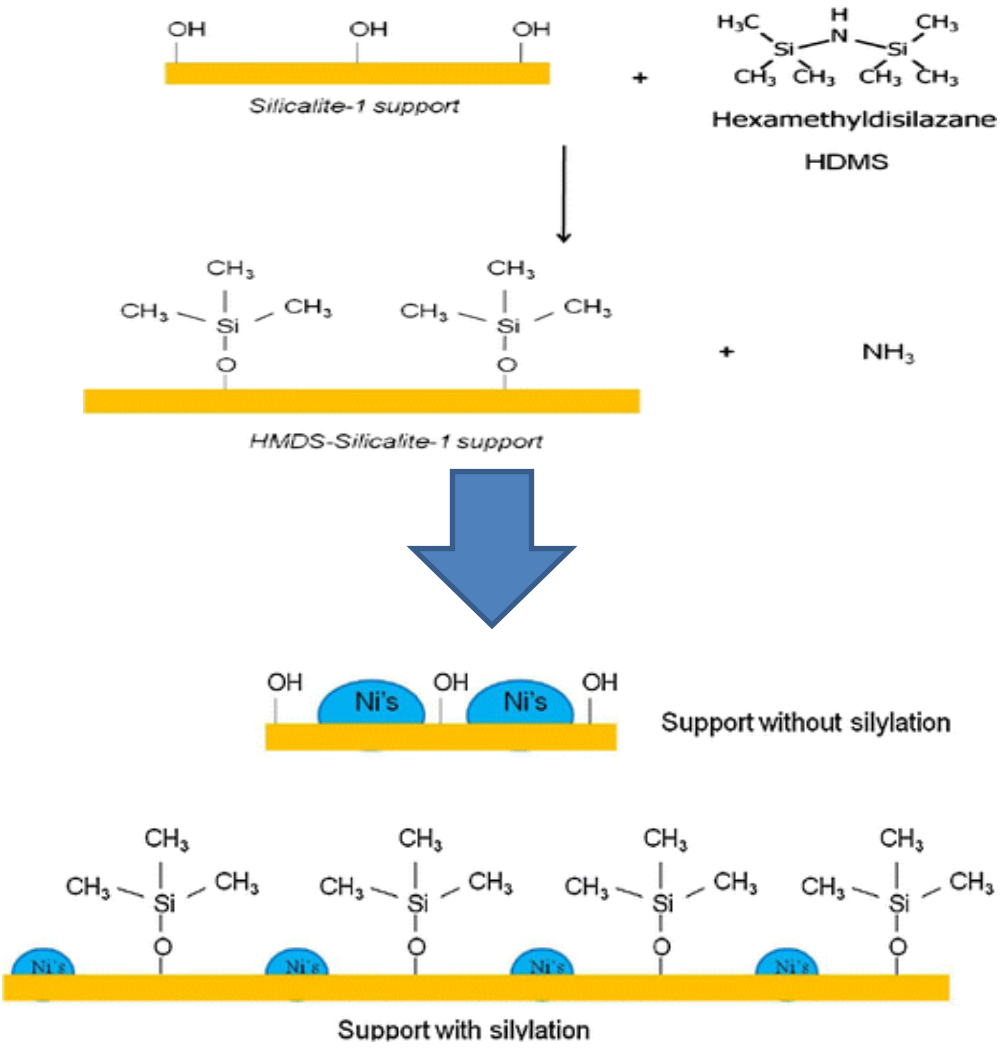

Figure 2-3. Schematic of sylilation mechanism

[64]

Table 2-2. Performance of some zeolite supported catalysts in DRM.

	Conversion, %					
Catalyst	CH_4	CO_2	Carbon deposits	H_2/CO ratio	Conditions	Ref.
Ni/Zeolite Y (A), Si/Al = 5.1	21	28	21%	-	700 °C, 1 atm, 0.6 g_{cat}, 40 ml/min, CH_4/CO_2=1, 9 h	[65]
La-Ni/Zeolite Y (A), Si/Al = 5.1	21	31	20%	-	700 °C, 1 atm, 0.6 g_{cat}, 40 ml/min, CH_4/CO_2=1, 9 h	[65]
Ca-Ni/Zeolite Y (A), Si/Al = 5.1	18	31	25%	-	700 °C, 1 atm, 0.6 g_{cat}, 40 ml/min, CH_4/CO_2=1, 9 h	[65]
Ni/Zeolite Y (B), Si/Al = 12	30	41	6%	-	700 °C, 1 atm, 0.6 g_{cat}, 40 ml/min, CH_4/CO_2=1, 9 h	[65]
La-Ni/Zeolite Y (B), Si/Al = 12	4	10	24%	-	700 °C, 1 atm, 0.6 g_{cat}, 40 ml/min, CH_4/CO_2=1, 9 h	[65]
Ca-Ni/Zeolite Y (B), Si/Al = 12	18	30	23%	-	700 °C, 1 atm, 0.6 g_{cat}, 40 ml/min, CH_4/CO_2=1, 9 h	[65]
Ni/ZSM-5, Si/Al_2 = 23	66	73	46.4%	0.95	800 °C, 1 atm, 100 mg_{cat}, 60,000 mL g^{-1} hr^{-1}, CH_4/CO_2=1	[54]
2Ni1Co/ZSM-5, Si/Al_2 = 23	77	82	20.6%	0.97	800 °C, 1 atm, 100 mg_{cat}, 60,000 mL g^{-1} hr^{-1}, CH_4/CO_2=1	[54]
1Ni1Co/ZSM-5, Si/Al_2 = 23	77	84	-	0.96	800 °C, 1 atm, 100 mg_{cat}, GHSV=60,000 mL g^{-1} hr^{-1}, CH_4/CO_2=1	[54]
1Ni2Co/ZSM-5, 425 Si/Al_2 = 23	81	86	5%	0.97	800 °C, 1 atm, 100 mg_{cat}, 60,000 mL g^{-1} hr^{-1}, CH_4/CO_2=1	[54]

Co/ZSM-5, $Si/Al_2 = 23$	68	79	3.6%	0.89	800 °C, 1 atm, 100 mg_{cat}, 60,000 mL g^{-1} hr^{-1}, CH_4/CO_2=1	[54]
0.1RhNi7.5/NaY	100	100	-	-	550 °C, 1 atm, 40 mg_{cat}, GHSV (193,500 mL·g^{-1}·h), CH_4/CO_2=1	[55]
Ni7.5S/NaY	85	92	-	-	750 °C, 1 atm, 40 mg_{cat}, GHSV (193,500 mL·g−1·h), CH_4/CO_2=1	[55]
Ni7.5I/NaY	85	90	-	-	750 °C, 1 atm, 40 mg_{cat}, GHSV (193,500 mL·g−1·h), CH_4/CO_2=1	[55]
0.1RhNi7.5/NaY (Stability test, 12 h)	59	70	-	-	550 °C, 1 atm, 40 mg_{cat}, GHSV (193,500 mL·g^{-1}·h), CH_4/CO_2=1, 12 h	[55]
1.5Ni/S-1	Initaill y ~70% but reduce s to 0% after 1 h	Initailly ~78% but reduce s to 0% after 1 h	31%	-	800 °C, 1 atm, 200 mg, GHSV = 72000 ml g^{-1} h^{-1}, and CH_4/CO_2 = 1:1 (v/v), 1 h	[48]
1.5Ni@Hol S-1	67% after 6 h	72% after 6 h	10.3%	-	800 °C, 1 atm, 200 mg, GHSV = 72000 ml g^{-1} h^{-1}, and CH_4/CO_2 = 1:1 (v/v), 6 h	[48]

1.5Ni–0.5Pt/S-1	Initaill y ~70% but reduce s to 0% after 1 h	Initailly ~78% but reduce s to 0% after 1 h	11.4%	-	800 °C, 1 atm, 200 mg, GHSV = 72000 ml g^{-1} h^{-1}, and CH_4/CO_2 = 1:1 (v/v), 6 h	[48]
1.5Ni–0.5Pt@Hol S-1	70% after 6 h	80% after 6 h	1%	-	800 °C, 1 atm, 200 mg, GHSV = 72000 ml g^{-1} h^{-1}, and CH_4/CO_2 = 1:1 (v/v), 6 h	[48]
Rh-Ni/Zeolite L (Disc), Si/Al_2 = 30	65	96	-	0.95	1073 K, 1 atm, 340 mg_{cat}, WHSV= 75 h^{-1}, CH_4/CO_2=60/40, 90 min	[66]
Ni/Zeolite L (Disc), Si/Al_2 = 30	81	92	-	1.26	1073 K, 1 atm, 340 mg_{cat}, WHSV= 75 h^{-1}, CH_4/CO_2=60/40, 90 min	[66]
Rh-Ni/Zeolite L (30-60 nm), Si/Al_2 = 20	64	95	-	0.90	1073 K, 1 atm, 340 mg_{cat}, WHSV= 75 h^{-1}, CH_4/CO_2=60/40, 90 min	[66]
Ni/Zeolite L (30-60 nm), Si/Al_2 = 20	61	94	-	0.85	1073 K, 1 atm, 340 mg_{cat}, WHSV= 75 h^{-1}, CH_4/CO_2=60/40, 90 min	[66]

Rh-Ni/Zeolite L (1-3 μm), $Si/Al_2 = 30$	52	86	-	0.83	1073 K, 1 atm, 340 mg_{cat}, WHSV= 75 h^{-1}, CH_4/CO_2=60/40, 90 min	[66]
Ni/Zeolite L (1-3 μm), $Si/Al_2 = 30$	49	85	-	0.80	1073 K, 1 atm, 340 mg_{cat}, WHSV= 75 h^{-1}, CH_4/CO_2=60/40, 90 min	[66]
Ni(8%)/ZSM-5 synthesized via ultrasound method MFI observed through FESEM, $Si/Al_2 > 25$	82	80	-	0.84	850 °C, 1 atm, GHSV= 24 l/g_{cat}h, CH_4/CO_2=1	[67]
Ni/MCM-41	75	86	4.4%	1.03	700 °C, 1 atm, 0.2 g_{cat}, CH_4/CO_2=1, 10 h	[62]
Ni/ITQ-6 (pure silica delaminated zeolite) Ferrierite type zeolite	77	90	2.1%	1.39	700 °C, 1 atm, 0.2 g_{cat}, CH_4/CO_2=1, 10 h	[62]
Ni/H-S1	62	84	-	1.23	973 K, 1 atm, 0.2 g_{cat}, CH_4/CO_2=1, 10 h	[49]
Ni-/H-S2	63	80	-	1.15	973 K, 1 atm, 0.2 g_{cat}, CH_4/CO_2=1, 10 h	[49]
Ni/S-HMDS-1 (after silylation of H-S1)	74	83	-	1.04	973 K, 1 atm, 0.2 g_{cat}, CH_4/CO_2=1, 10 h	[49]
Ni/S-HMDS-2 (after silylation of H-S2)	77	84	-	1.05	973 K, 1 atm, 0.2 g_{cat}, CH_4/CO_2=1, 10 h	[49]
Ni/Silicalite-1	56	83	5.6%	1.21	700 °C, 1 atm, 0.2 g_{cat}, CH_4/CO_2=1, 24 h	[64]

Ni/Silicalite-111	61	84	6.0%	1.23	700 °C, 1 atm, 0.2 g_{cat}, CH_4/CO_2=1, 24 h	[64]
Ni/Silicalite-111S	74	79	4.2%	1.04	700 °C, 1 atm, 0.2 g_{cat}, CH_4/CO_2=1, 24 h	[64]
8% Ni/flower-shape KH zeolite (Si/Al = 10)	98	90	3.82%	1.58	700 °C, 1 atm, GHSV = 30,000 h^{-1}, CH_4/CO_2 = 1:1	[59]
8% Ni/dog-bone KH zeolite (Si/Al = 10)	90	84	2.78%	1.50	700 °C, 1 atm, GHSV = 30,000 h^{-1}, CH_4/CO_2 = 1:1	[59]
8% Ni/disordered KH zeolite (Si/Al = 10)	85	85	6.40%	1.18	700 °C, 1 atm, GHSV = 30,000 h^{-1}, CH_4/CO_2 = 1:1, 5 h	[59]
Ni(7%)/Zeolite A (Si/Al = 1)	Initial conversion ~70-80% but reduced to 12.3% after 5 h on stream	Initial conversion ~80% but reduced to 20% after 5 h on stream	0.25%	(0.31) 55% H_2 selectivity	700 °C, 1 atm, 0.2 g_{cat}, GHSV = 30,000 cm^3/hg_{cat}, CH_4/CO_2 = 1:1, 5 h	[42]
Ni(7%)/Zeolite X (Si/Al = 1)	Initial conversion was >	CO_2 conversion ~ 80%	0.24%	(1.23)	700 °C, 1 atm, 0.2 g_{cat}, GHSV = 30,000 cm^3/hg_{cat}, CH_4/CO_2 = 1:1, 5 h	[42]

	80. It was 71.5% after 5 h on stream.	after 5 h on stream		60% H_2 selectivity		
Ni(7%)/Zeolite Y (Si/Al = 1)	91.6% CH_4 conversion after 5 h	~92% CO_2 conversion after 5 h	6.83%	(1.79) H_2 selectivity of ~65%	700 °C, 1 atm, 0.2 g_{cat}, GHSV = 30,000 cm^3/hg_{cat}, CH_4/CO_2 = 1:1, 5 h	[42]
Ni/ZSM-5 (Si/Al = 398)	~90% initial CH_4 conversion and 57.8% at 5 h	~90% initial CO_2 conversion and ~70% at 5 h	2.16%	(1.03) H_2 selectivity of ~60%	700 °C, 1 atm, 0.2 g_{cat}, GHSV = 30,000 cm^3/hg_{cat}, CH_4/CO_2 = 1:1, 5 h	[42]

Ni(13%)/H-Zeolite Y	93	86	-	0.94	700 ^{o}C, 1 atm, 1 g_{cat}, 200 ml/min, GHSV = 3500 h^{-1}, $CH_4/CO_2 = 1$, 1 h	[68]
Ni(13%)-Mg(5%)/H-Zeolite Y	~ 90% after 72 h on stream, and ~ 80% after 720 h.	-	21% after 720 h on stream	89% H_2 yield after 1 h	700 ^{o}C, 1 atm, 1 g_{cat}, 200 ml/min, GHSV = 3500 h^{-1}, $CH_4/CO_2 = 1$,	[68]
Ni(13%)-Mn(5%)/H-Zeolite Y	~ 75% after 72 h on stream	-	-		700 ^{o}C, 1 atm, 1 g_{cat}, 200 ml/min, GHSV = 3500 h^{-1}, $CH_4/CO_2 = 1$,	[68]
Ni(13%)-Ca(5%)/H-Zeolite Y	~ 70% after 72 h on stream	-	-		700 ^{o}C, 1 atm, 1 g_{cat}, 200 ml/min, GHSV = 3500 h^{-1}, $CH_4/CO_2 = 1$,	[68]
Ni(13%)-K(5%)/H-Zeolite Y	Reduced to 0% at 30 h on stream	-	-		700 ^{o}C, 1 atm, 1 g_{cat}, 200 ml/min, GHSV = 3500 h^{-1}, $CH_4/CO_2 = 1$,	[68]

Ni(13%)/H-Zeolite Y	~ 30% after 72 h on stream	-	32%		700 ^{o}C, 1 atm, 1 g_{cat}, 200 ml/min, GHSV = 3500 h^{-1}, $CH_4/CO_2 = 1$,	[68]

2.3 Basic Zeolites

Zeolites, a group of well-known environmentally friendly materials with well-defined aluminosilicate, crystalline frameworks and high surface area are widely applied in the field of catalysis [61, 69, 70, 71, 72]. Despite the fact that zeolites have been widely used as solid acid catalysts due to their uniform pores and tunable acidic properties [73, 74, 75] some research has been committed to the basic applications of zeolites- due to their high selectivity and highly dispersed basic sites stemming from the sub-nanometer micropores [74]. It is a challenge to preserve the well-defined crystalline frameworks while creating strong basic sites that are active and highly stable because the catalytic activity is affected by the pore structure, basicity and stability [74, 76].

The basicity in zeolites comes from the negative charge on the oxygen atoms in the framework [77, 78, 79]. The AlO_4^- in the aluminosilicate structure exhibits acidity whereas the SiO_4 is usually neutral. Most basic zeolites are prepared by the impregnation [80, 81] and ion exchange [79, 82, 83]. Basic zeolites were traditionally synthesized by ion-exchanging the charge on the framework to balance the cation with alkali metal cations [84, 85]. The oxygen ions in the framework are to be the origin of basicity in basic zeolites [85].

Isolated metal ion related active sites can be achieved by the doing a one-pot synthesis where the metal salts are added in a single step [86, 87, 88, 89]. One pot-synthesis helps eliminate post-synthesis treatment and also preserves the crystal framework of

the zeolite; it therefore saves time and energy [90]. This technique also provides an efficient platform to tune the acid/base properties of the zeolite [76, 84, 91, 92, 93].

To adjust acidity, alkaline earth metals have been incorporated into aluminophosphates (ALPOs) [94, 95]. The low electronegativities of alkaline earth metals makes them useful to strong basic sites [90]. Zhou et al [90] successfully incorporated alkaline earth metals (Mg, Ca, Ba, and Sr) separately into Silicalite-1 (an MFI pure silica zeolite), in a one-pot hydrothermal synthesis by co-hydrolyzing the alkaline earth metal salts with the silica source in an acidic medium. It was demonstrated by systematic base analysis that strong basicity was exhibited by Mg on S-1 as a result of the framework Mg^{2+} species [90].

A network of secondary mesoporosity was introduced into USY zeolite by treating it with tetrapropylammonium bromide (TPABr) in alkaline medium, nonetheless the crystalline framework was preserved [79].

2.4 Zeolite synthesis techniques

The preparation of zeolites with mesoporosity has been a big challenge in materials science research due to their valuable applications as catalysts [81, 96, 97, 98, 99]. For fast crystallization in the preparation of porous materials, microwave synthesis has been found to useful as it also provides a good opportunity to control the macroscopic morphology [100], phase selectivity [101], and particle size distribution [102]. There have not been many reports on the use of microwave synthesis methods for morphological control of porous materials [100, 103].

Among the many zeolite materials, silicalites, with MFI topological framework have been extensively investigated in the field of catalysis [104, 105] Hwang et al. [87] reported to have synthesized Ti (and other metals) incorporated MFI-framework zeolites by microwave irradiation. This samples were said to be fibrous and exhibited physicochemical properties that are useful as a result of their self-stacking. It was however observed that this technique introduced a dramatic modification in the morphology depending on the composition [87].

2.5 Silicalite-1

Owing to their superior capacities in mass transfer, mesoporous as well as microporous zeolites are highly desirable materials in catalytic and separation applications [61, 106]. The location of the mesopores in zeolites maybe intercrystalline (between aggregates of zeolite crystals) or intracrystalline (on the zeolite crystals) [107]. Given the importance of zeolitic materials in various applications including chromatography, it is beneficial to understand the details of their preparation to help manipulate their properties desirable for different applications. Silicalite-1 is conventionally known as a pure silica analog of ZSM-5. Extensive work has been done to study the growth of silicalite-1 [108, 109, 110, 111, 112]. This is partly because of the unique adsorption and catalytic properties possessed by MFI framework materials. The typical MFI structure composes of 10 straight membered channels of silicate-rings and 10 zigzag sinusoidal membered ring channels as shown in Figure 2-4. These intersect and have pore diameters of approximately 5.5 angstroms [113].

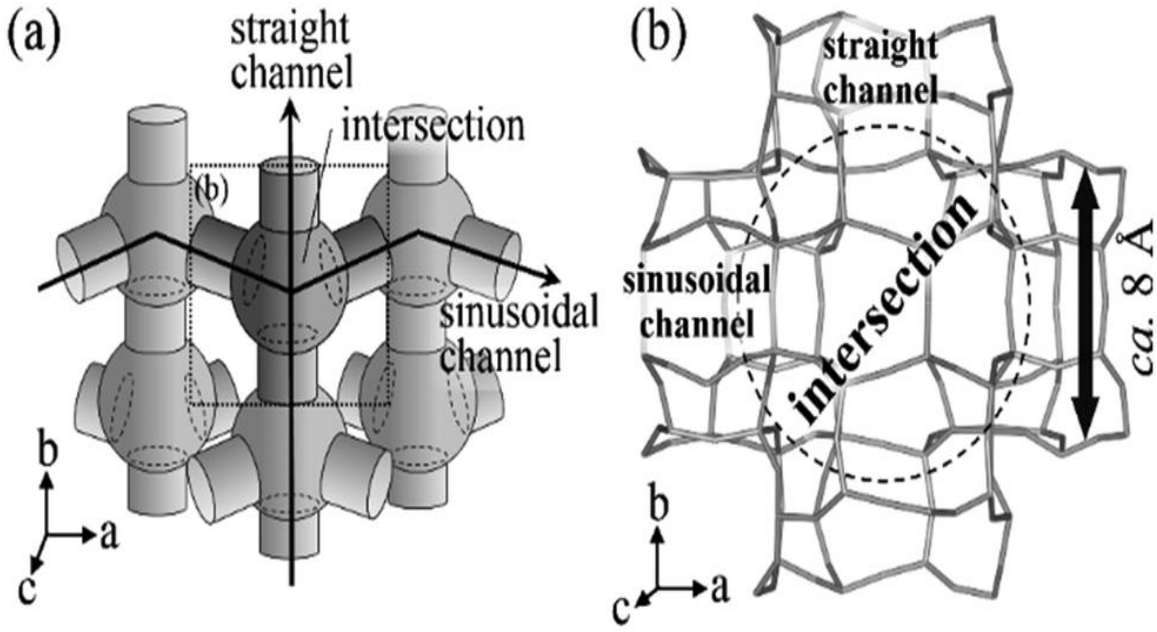

Figure 2-4. channel system of MFI-type zeolite: (a) a schematic illustration of the pore topology and (b) the intersection-centered framework with adjoining channels.

[114]

2.6 Synthesis of Silicalite-1 Crystals

The synthesis route for silicalite-1 crystal is a robust process and can achieved from a clear solution [115, 116, 117, 118, 119, 120, 121] or a gel phase [122, 123, 124]. Using these methods, the mechanisms of nucleation that can be proposed are: homogenous and heterogenous nucleation [123]. Applying various methods (small angle X-ray

scattering, powder X-ray diffraction and ^{1}H-29Si CP MAS NMR) to study the crystallization of silicalite-1 from a gel phase, it has been found to follow a heterogenous pathway [109]. The zeolite community in the last decade has intensively studied the preparation of silicalite-1 using optically transparent solutions of TEOS/TPAOH/H_2O [112, 116, 125, 126]. In some instances, this synthesis is done in a low temperature medium, thus enabling the easy study of such systems involving the optically transparent mixture [127].

Chapter 3

METHODOLOGY

3.1 Experimental

3.1.1 Reagents

- Ludox HS-40 colloidal silica (40 wt% in water; Sigma Aldrich)
- Tetrapropylammonium bromide (98%; Sigma Aldrich)
- Sodium hydroxide (98% purity; Sigma Aldrich) -- NaOH
- Nickel(II) nitrate hexahydrate (98.5% purity; Sigma Aldrich) – $Ni(NO_3)_2.6H_2O$
- Cerium(III) nitrate hexahydrate (99% purity; Sigma Aldrich) – $Ce(NO_3)_3.6H_2O$
- Zinc nitrate hexahydrate (98% purity; Sigma Aldrich) -- $Zn(NO_3)_2.6H_2O$
- Yttrium(iii) nitrate hexahydrate (99.8% purity; Sigma Aldrich) – $Y(NO_3)_3.6H_2O$
- Deionised water

All chemicals were analytical grade and were used as received without further purification.

3.1.2 Catalysts Preparation

3.1.2.1 In-situ Ni-loaded Catalysts

A series of in-situ Ni-loaded silicalite-1 catalysts were synthesized using the initial gel composition of SiO_2 : 0.125 TPABr : 0.125 NaOH : 20 H_2O : $yNi(NO_3)_2.6H_2O$ with y being the mole ratio of Ni/Si. First, a calculated amount of sodium hydroxide (NaOH) was completely dissolved in deionized water followed by the addition of the silica

source under continuous stirring at a rate of 300 rpm until a uniform solution was obtained. The nickel precursor was then added at this stage and the gel was aged for 6 hours under continuous stirring. A solution of tetrapropylammonium bromide was added and again aged under stirring for another 6 hours. The resulting solution was transferred into a Teflon lined autoclave and treated in a microwave at power of 800 W under autogenous pressure at 180 ^{o}C for 6 hours. The Ni on Silicalite-1 crystals thus obtained were washed with deionized water and dried for a period of 12 h in air at room temperature. The dried powder obtained was again dried at 110 ^{o}C for 12 h. Calcination was done in air at 500 ^{o}C for 5 h, to remove the template. Ca and Mg were incorporated by the wet-impregnation method, as promoters for the 20Ni/S-1 catalyst. 4 wt. % of the metals used.

3.1.2.2 Ni-loaded Catalysts by Wet-Impregnation

Also, a series of Ni impregnated Na-Silicalite-1 catalysts were prepared per the method described as follows. Pure Silicalite-1 was prepared by alkaline hydrolyses of the SiO source. Ludox HS-40 was added to an aqueous solution of NaOH and TPABr. The gel obtained was stirred for 6 h at room temperature and then transferred into Teflon lined autoclave and treated under microwave irradiation for another 6 h. The Na-Silicalite-1 crystals obtained were washed with deionized water several times followed by drying at room temperature in air overnight and then dried for 12 hours in air at 110 ^{o}C. Ni was then deposited on the surface of the parent S-1 by incipient wet-impregnation with weight fractions ranging from 5-20%. 10 mL of deionized water per 1 g of the Silicalite-1 crystalswas used in the impregnation process. In a typical impregnation process $Ni(NO_3)_3.6H_2O$ was dissolved in deionized water. The

Silicalite-1 crystals were then added followed by stirring at room temperature for 2 h. The samples obtained were dried in air at room temperature and again at 110 ^{o}C before being calcined at 500 ^{o}C for a period of 5 h, to remove the template.

3.1.2.3 Ni loading on Alkali-Metal-Ion-Exchanged S-1

To carry out the ion-exchange procedure, 1 M of aqueous solutions each containing the precursor ions: Ce, Zn and Y were prepared using deionized water. The reagents used were $Ce(NO_3)_3.6H_2O$ (99% purity; Sigma Aldrich), $Zn(NO_3)_2.6H_2O$ (98% purity; Sigma Aldrich) and $Y(NO_3)_3.6H_2O$ (99.8% purity; Sigma Aldrich), respectively. 20 mL of each aqueou solution was used per 1 g of the Silicalite-1 crystals, stirred and treated under microwave irradiation at a temperature of 85 ^{o}C for 2 h. The resulting samples were retrieved, washed with deionized water and dried at room temperature for 12 h and again at 110^{o}C for 12 h. Ni particles were then deposited on the surface of the alkali metal ion-exchanged Silicalite-1 crystals by the wet incipient impregnation method. The resulting Ni/M-S-1 in aqueous solution was stirred for 2 h, dried for 12 h in air at room temperature, and then calcined in air for 5 h at 500^{o}C.

3.2 Catalysts Characterization

3.2.1 X-ray Diffraction

To identify the phase and determine the crystallinity, X-ray diffraction (XRD) was done in a Rigaku MiniFlex X-ray diffraction instrument equipped with a Cu anode with $K\alpha = 1.5405$, accelerating voltage of 30 kV and tube current of 10 mA. The scanning speed and step were 3^{o}/min and 0.02^{o} respectively in a 2θ range of between 2^{o} and

50^{o}. The identification of the XRD patterns was done with the aid of structure databases, in a Rigaku PDXL software.

3.2.2 Field Emission Scanning Electron Microscopy (FE-SEM)

The morphology of the prepared samples was analysed using a field emission scanning electron microscopy (FESEM; LYRA 3, TESCAN, Czech) with secondary electron and backscattered electron modes at an accelerating voltage of 30 kV. This device was also used for energy-dispersive X-ray (EDX) analysis and elemental mapping.

3.2.3 Physical Properties

Using a Micrometrics ASAP 2020 device, the samples were degassed at 250 ^{o}C for 3 h before performing N_2 physisorption was carried out -196 ^{o}C. The adsorption-desorption data were then applied to evaluate specific surface areas, pore size and pore volumes. The surface areas were calculated using the Barret-Emmet-Teller (BET) method whereas the pore volumes and pore size distribution were both calculated using the Barret-Joyner-Halenda (BJH) method.

3.2.4 X-ray photoelectron spectroscopy

The binding energies and valence states of the chemical species in the catalysts were determined by using X-ray photoelectron spectroscopy (PHI 5000 Versa Probe II, ULVAC-PHI Inc.) A few millimeter thickness of pellet was made from the sample powder. A vacuum condition was created and maintained in the chamber during the analysis.

3.2.5 Fourier Transformation Infrared (FTIR) Spectroscopy

The functional groups in the synthesized silicalite-1 catalysts were studied with application of FTIR. The infrared spectra of the samples were collected in the range of 400 cm^{-1} to 4000 cm^{-1}. The equipment used was Thermo Scientific Nicolet 6700 FT-IR spectrometer.

3.2.6 Temperature-Programmed Reduction

The catalysts were tested for reducibility by H_2-Temperature Programmed Reduction (H_2-TPR) in a Micromeritics (Autochem II-2920) chemisorption analyzer. 10 mg of the sample was treated for 60 mins at 500 ^oC under pure He flow and then cooled down to 80 ^oC. It was then slowly heated to 1000 ^oC under a flow of 20 mL/min (10%H_2 in He) with the H_2 consumption recorded by a thermal conductivity detector (TCD).

3.2.7 Raman Scattering Spectroscopy

Using a green laser with a wavelength 532 nm (300 mW), carbon deposits on the spent catalysts (20Ni/CeS-1 and 20Ni/YS-1) were characterized with a Raman scattering spectrometer.

3.2.8 TGA-DSC

The spent catalysts were evaluated for carbon deposition using the simultaneous TGA-DSC technique in a NETZSCH STA 449 F3 instrument. Approximately 10 mg of the spent catalyst sample, loaded into a microliter Al_2O_3 crucible, was heated from

30°C to 900°C at rate of 15°C/min under 20 mL/min flow of zero air. Argon was used as the protective gas.

3.3 Catalyst evaluation of Methane CO_2 reforming.

The CO_2 reforming of methane reactions were carried out in fixed bed reactor setup equipped with mass flow controllers, a programmable furnace coupled to a micro gas chromatography equipment (Agilent 490 micro GC). The catalysts were evaluated for dry reforming of methane under atmospheric pressure (1 atm) and operated between 600 and 900 °C. The reactor assembly, as shown in Figure 3-1, is made up of a 2.5 cm diameter and 30 cm length tube enclosed in a furnace The tube was made of stainless steel. Temperature in the furnace was monitored with a sensor connected to an Eurotherm temperature controller. Gas flows to the reactor were controlled and monitored by Brooks mass flow controllers. A flow ratio of $CH_4/CO_2/He = 1/1/1$ was used for all reactions with a catalyst weight of 0.3 g corresponding to a gas hourly space velocity (GHSV) of 51400 mL/h.g. The catalyst powders were pelletized to minimize pressure drop across the bed. The catalyst pellets were then mixed with SiC. All samples were loaded in the reaction zone, sandwiched in between quartz wool and SiC in the order: quartz wool-SiC-catalyst-SiC-quartz wool. The two layers of quartz wool were used to keep the bed from moving in the tube. Before commencement of reactions the reactor and its contents were flushed with high purity He. While flowing He over the bed, the temperature was ramped at a rate of 10 °C/min up to 700 °C. The catalysts were then reduced in a 50 mL/min flow of 10%H_2 in He at 700 °C for 1 h. The reduced catalysts were purged with a flow of pure He at a rate of 30 mL/min for 30 min before ramping up to the reaction temperature at a rate of 10 °C/min. The

reaction was commenced by flowing the feed gas (CH_4 and CO_2, using He as carrier gas). Stability tests for selected samples were carried out at 750 ^oC for a period of 12 h unless stated otherwise. Gaseous effluents from the reactor were analysed in a 4 channel Agilent 490 micro GC. Only 2 channels (Molsieve 5A and PoraPlot Q) were used in the analysis.

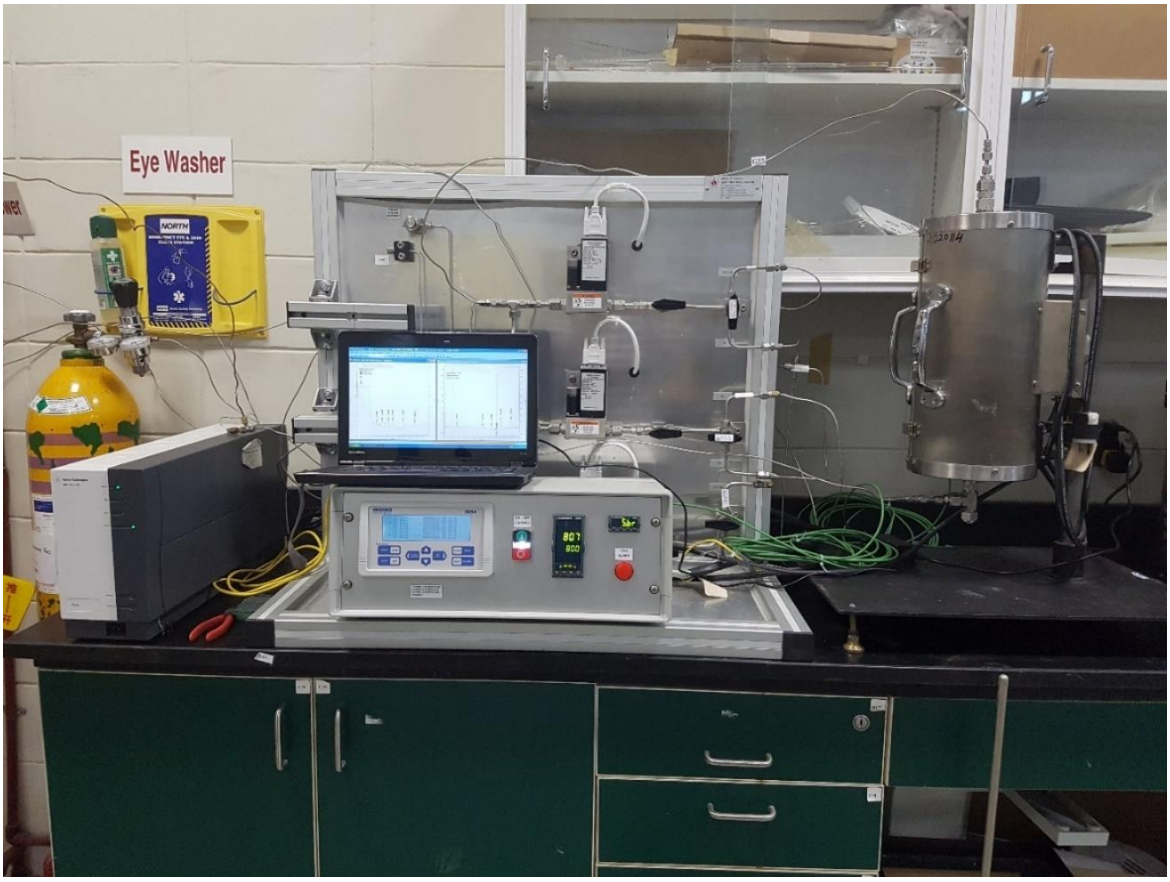

Figure 3-1. The fixed-bed reforming reactor setup

Chapter 4

RESULTS AND DISCUSSION

Well-defined silicalite-1 crystals with significant mesoporosity was successfully prepared in a one-step method by the microwave-assisted hydrothermal synthesis (MAHyS) approach. This was achieved using a cheap template TPABr in alkaline medium. When preparing silicalite-1 crystals in an alkaline medium, the microporous channels are formed by the direct interaction of the inorganic Si with the TPA^+. The mesopores are formed as the Na^+ or TPA^+ cations mediate electrostatically between zeolite nanoparticles that are negatively charged. Mesoporous zeolites have been demonstrated to have improved catalytic performance over conventional zeolites in many environmental and hydrocarbon conversion processes. As a result, much work has been devoted to synthesizing microporous zeolite with some mesopores. Some strategies that have been applied to obtain mesoporous zeolites include the use of different templates, well-ordered mesoporous carbon, as well as desilication and recrystallization [22]. However, some of these templates are expensive. The other preparation strategies are also troublesome. These challenges can still be overcome in most cases.

4.1 X-ray diffraction studies

All synthesized silicalite-1 samples, with different nickel loadings, showed high crystallinity with reflections characteristic of the MFI structure as shown in Figure 4-1. The peaks are broad and less intense suggesting small crystal size. Catalysts prepared

by the wet incipient impregnation method showed peaks for NiO at $2\theta = 37.29^{o}$, 43.342^{o} and 62.95^{o}. These peaks became more prominent with increasing Nickel loading. The X-ray diffraction patterns of 5 wt. %Ni and 10 wt. %Ni impregnated on silicalite-1 showed no NiO peaks. The NiO particles were thus suggested to be well-dispersed on the surface of the silicalite-1 support crystals.

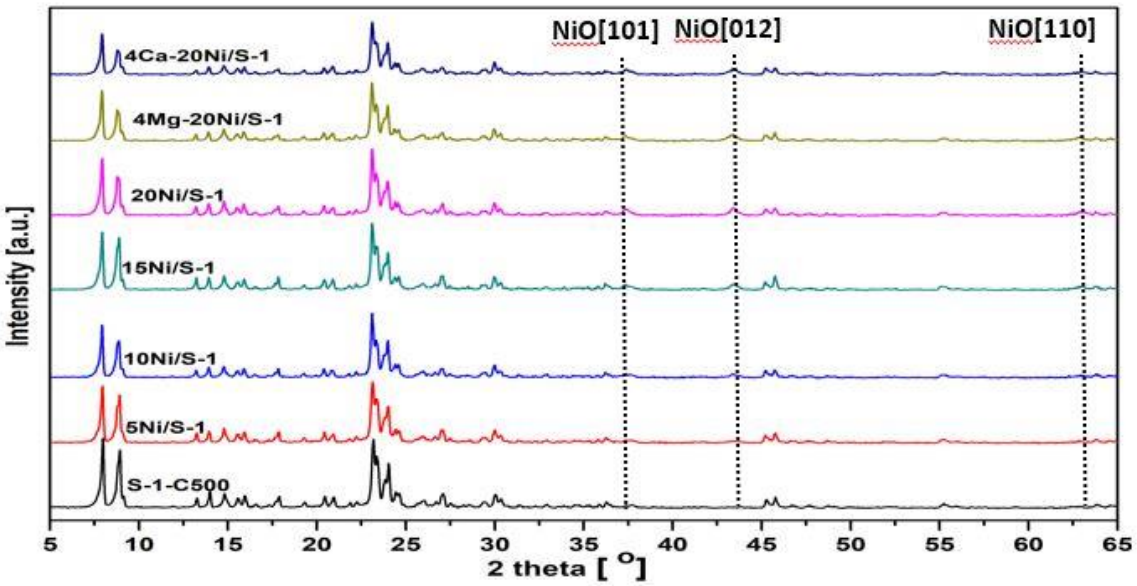

Figure 4-1. X-ray diffraction patterns of Ni supported on MAHyS of silicalite-1.

4.2 Field Emission Scanning Electron Microscopy (FE-SEM)

The high crystallinity as well as absence of amorphous S-1 materials was further proven by the SEM images as seen in Figure 4-2, Figure 4-3 and Figure 4-4. The images show uniform well-defined elongated crystals with prism-like shapes for the NiS-1 samples, synthesized via the one-step method, whereas the parent S-1 and the Ni/S-1 samples depict less elongation, albeit a similar morphology with less uniformity. This observation is in agreement with other works involving one-pot synthesis of TS-1 [128] and [129]. The elongation of the one-pot synthesized samples in this work can be ascribed to the co-hydrolysis of the Ni-precursor with the silica source in the alkaline medium. This is evident from the decreasing elongation with decreasing Ni content. All Ni containing samples show deposits of Ni particles, with sizes ranging from a few nanometers to about 200 nm, on the surfaces of S-1 crystals. The images show uniform well-defined crystals with trigonal shapes for the samples. All Ni containing samples show deposits of Ni particles, with sizes ranging from a few nanometres to about 200 nm, on the surfaces of S-1 crystals.

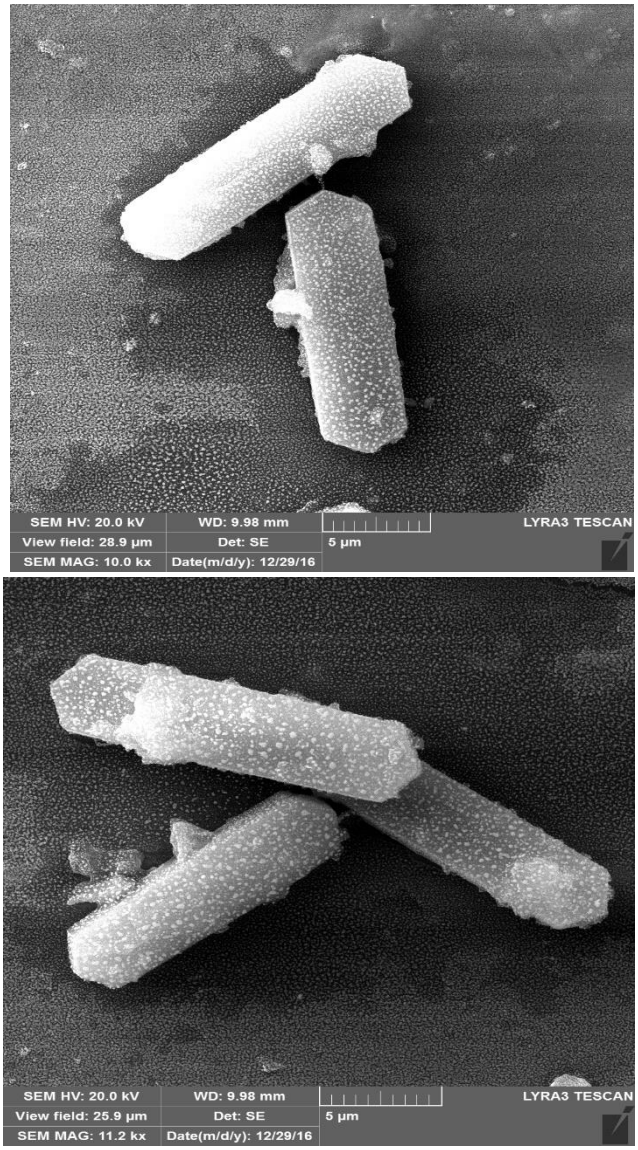

Figure 4-2. FE-SEM micro-graphs of in-situ synthesized catalysts.

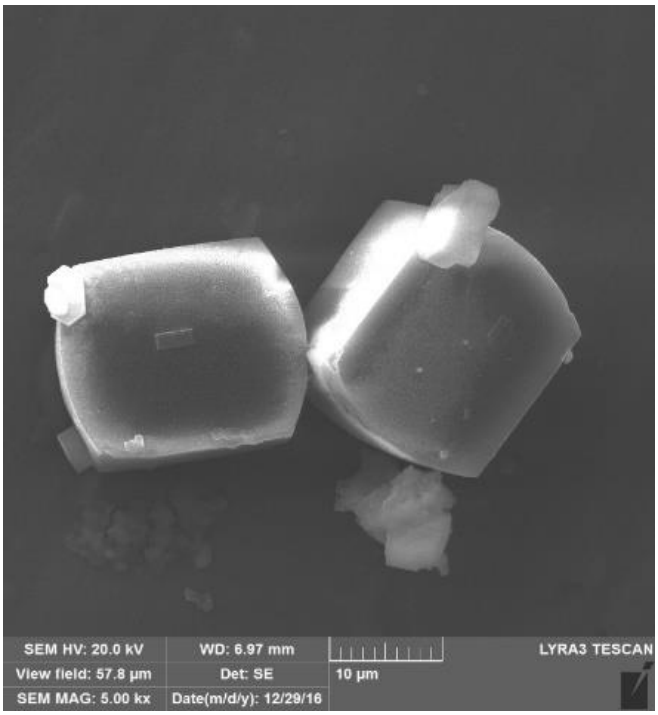
SEM HV: 20.0 kV
WD: 6.97 mm
LYRA3 TESCAN
View field: 57.8 µm
Det: SE
10 µm
SEM MAG: 5.00 kx
Date(m/d/y): 12/29/16

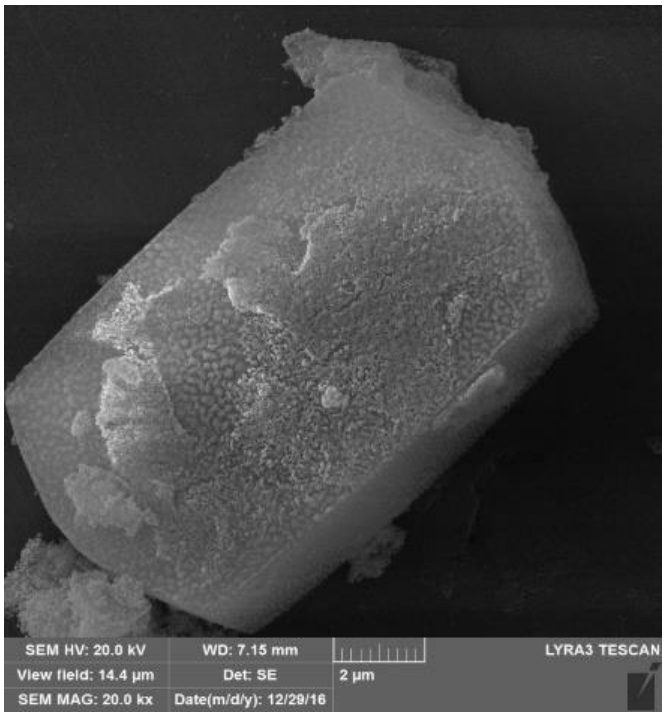
SEM HV: 20.0 kV
WD: 7.15 mm
LYRA3 TESCAN
View field: 14.4 µm
Det: SE
2 µm
SEM MAG: 20.0 kx
Date(m/d/y): 12/29/16

Figure 4-3. FE-SEM micro-graphs of: Top; As-synthesized S-1 crystals, Bottom; S-1 loaded with Ni.

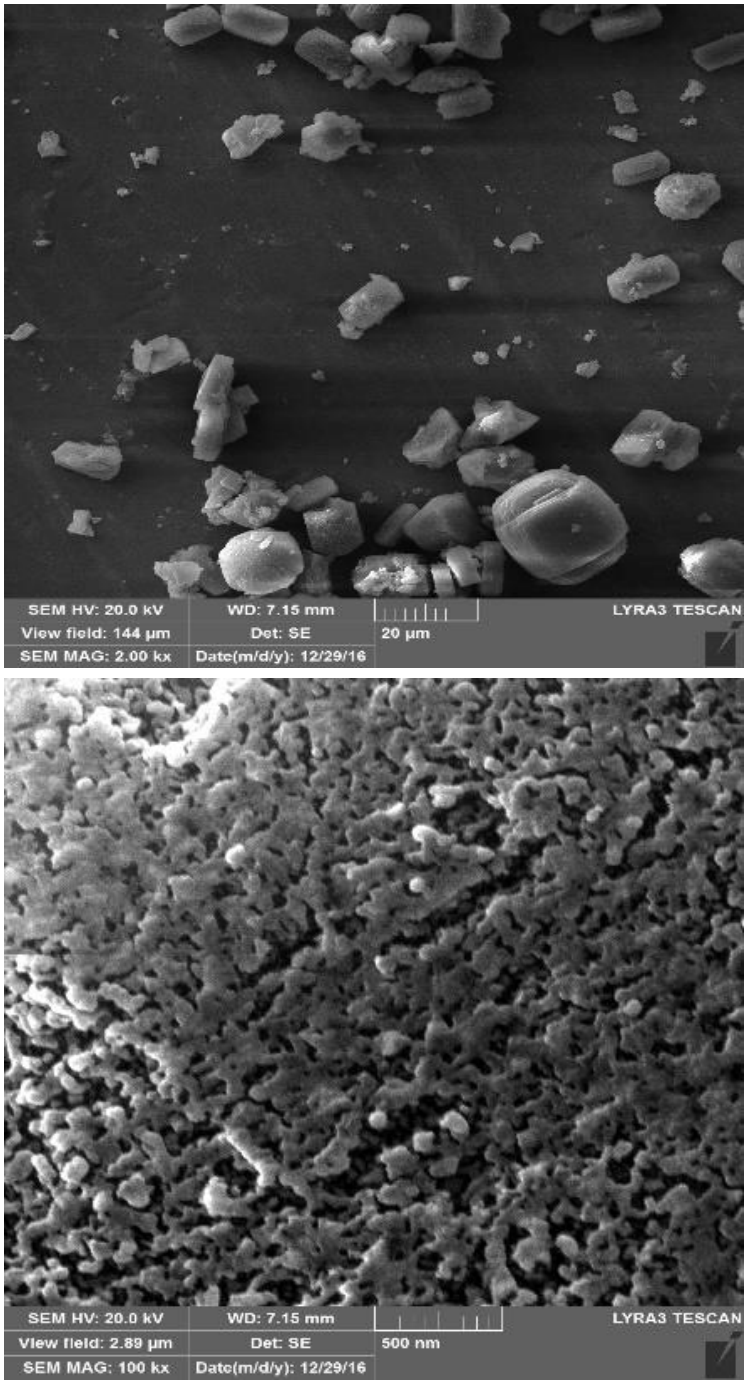

Figure 4-4. FE-SEM micro-graphs of: Top; As-synthesized S-1 crystals, Bottom; Ni nanoparticles on S-1 crystal.

4.3 Physical properties measurement

N_2 physisorption technique was applied to characterize the physical properties of the catalysts. The results of this analysis (pore volumes, pore diameters and BET surface areas) are presented in Table 4-1. All synthesized samples exhibited high BET surface areas with the as-synthesized (not calcined) silicalite-1 having a BET surface area of 237 m^2/g and that of the calcined silicalite-1 being 366 m^2/g. It can be observed from the results that the high surface areas of these catalysts were linked to the internal surface areas which are much higher than the external surface areas. The difference in surface area between the as-synthesized and calcined samples was due the complete or partial removal of the TPABr template after decomposition in air. It is worth noting the decrease in surface area of the catalysts with increasing nickel loading. This observation was ascribed to the presence of the nickel particles in the pores of the silicalite-1 crystals. All catalysts were confirmed to be mesoporous in nature since the average pore diameters all fell within the range (2—50 nm or 20—500 Å) of mesoporous materials as defined by IUPAC [130]. Pore volumes of the catalysts are also presented in Table 4-1. Shown in Figure 4-5, Figure 4-6 and Figure 4-7 are the N_2 adsorption-desorption isotherms for the S-1 based catalysts (all samples were calcined at 500 ^oC for 5 h except S-1-NC which was not calcined). The isotherms of all S-1 catalysts exhibited an H4 hysteresis loop with a step in the desorption branch at approximately $p/p^o = 0.45$. This was not the case with un-calcined S-1. The step is less prominent in the isotherm of S-1-NC. It is worth noting the difference between the isotherms (from $p/p^o = 0.05$ to $p/p^o = 0.45$) of the

transitions metal ion-exchanged samples (20Ni/CeS-1, 20Ni/YS-1 and 20Ni/ZnS-1) and other S-1 based catalysts also calcined at 500 ^{o}C. This variation is manifested in the comparatively lower micropore volumes of the ion-exchanged catalysts. The N_2 adsorption-desorption isotherms of the S-1 samples with nickel loadings of 5 – 20wt% and S-1-C500 do not show any observable difference when comparing between them – an indication that original S-1 structure has been preserved after nickel impregnation. This observation is further corroborated by the relatively constant microporous volumes of these catalysts. Figure 4-8, Figure 4-9 and Figure 4-10 show the pore size distribution profiles obtained from the BJH dV/dW pore volume (desorption branch). From the profiles of all samples it can be inferred that the overall pore size distribution was not affected by the various post-synthesis treatments.

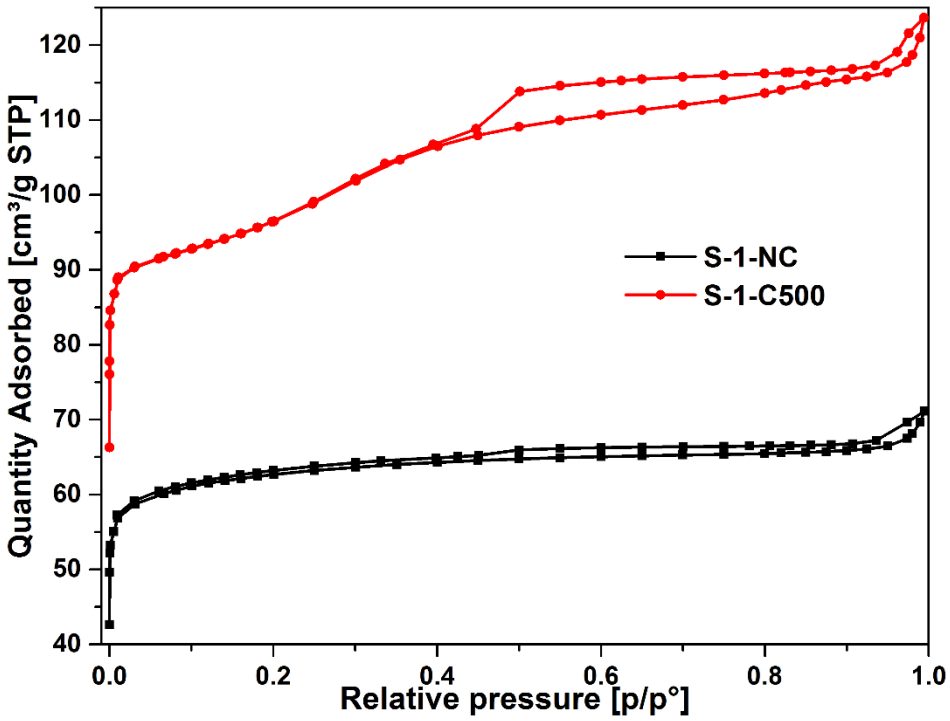

Figure 4-5. N_2 adsorption-desorption isotherms of as-synthesized S-1 and S-1 calcined at 500 °C

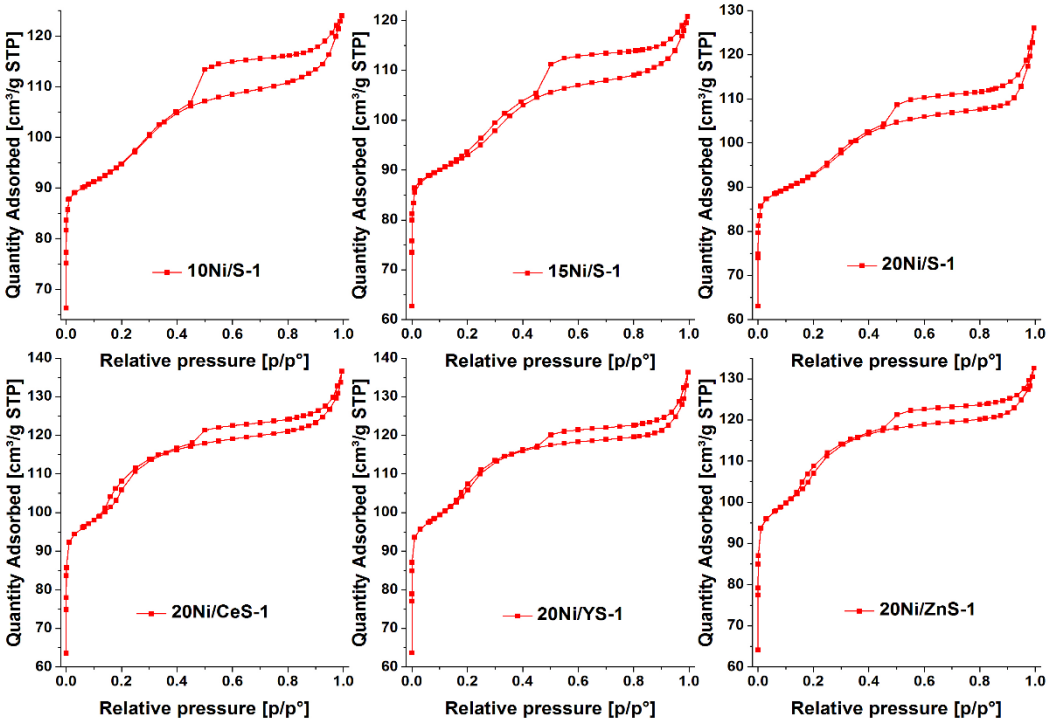

Figure 4-6. N_2 adsorption-desorption isotherms of (Top row) different Ni loadings on silicalite-1, (bottom row) 20 wt.% Ni on [Ce, Y or Zn] ion-exchanged silicalite-1

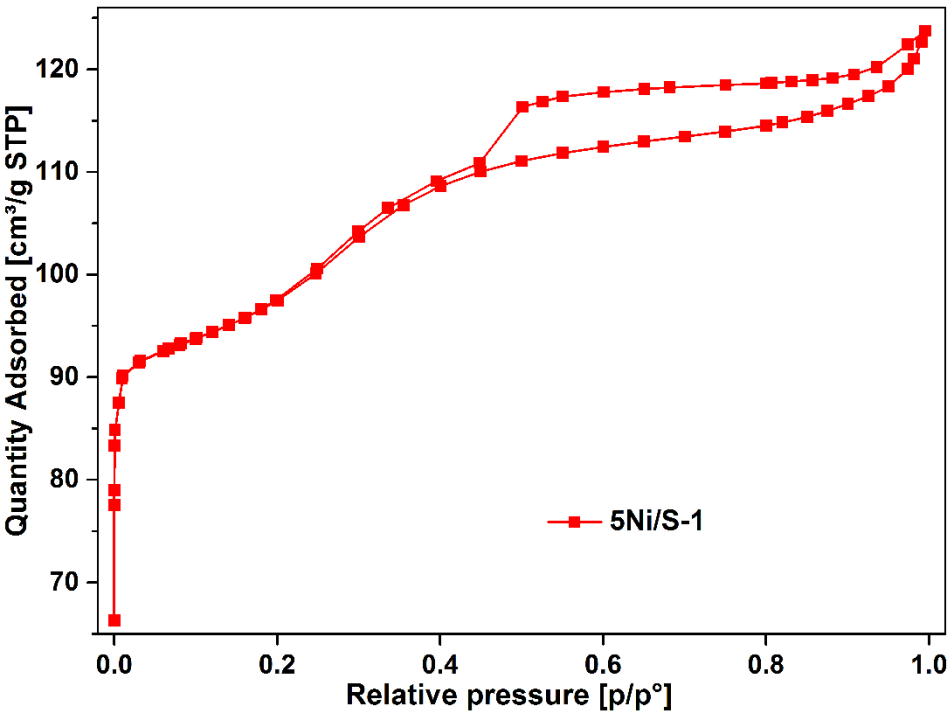

Figure 4-7. N_2 adsorption-desorption isotherms of 5Ni/S-1, calcined at 500 ºC

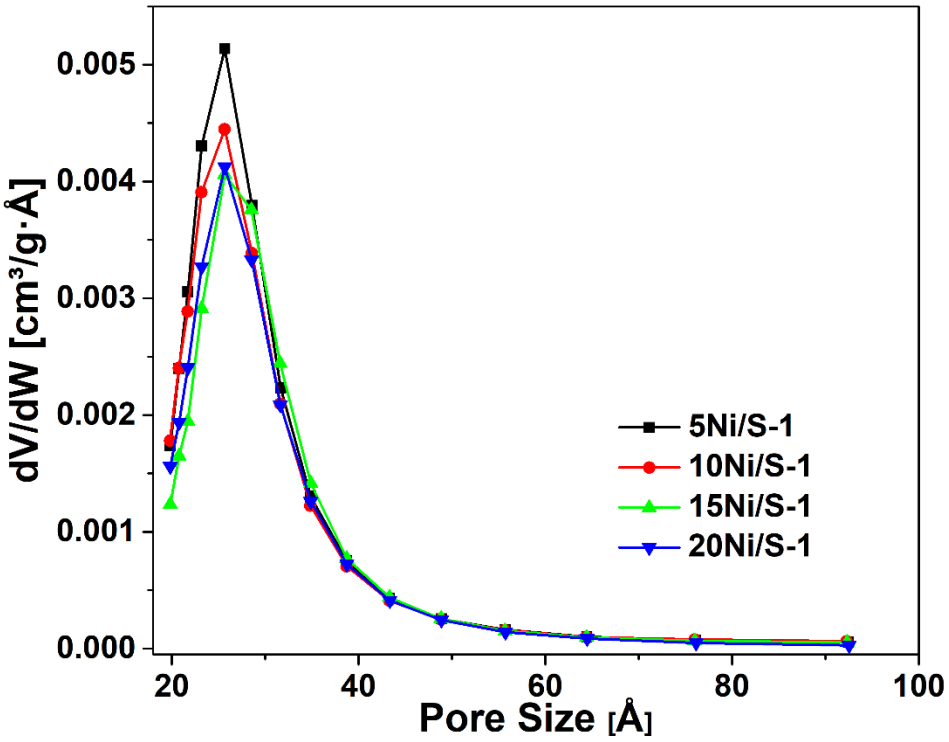

Figure 4-8. Pore-size distribution of the 5 - 20 wt.%Ni on silicalite-1, calcined at 500 ^{o}C.

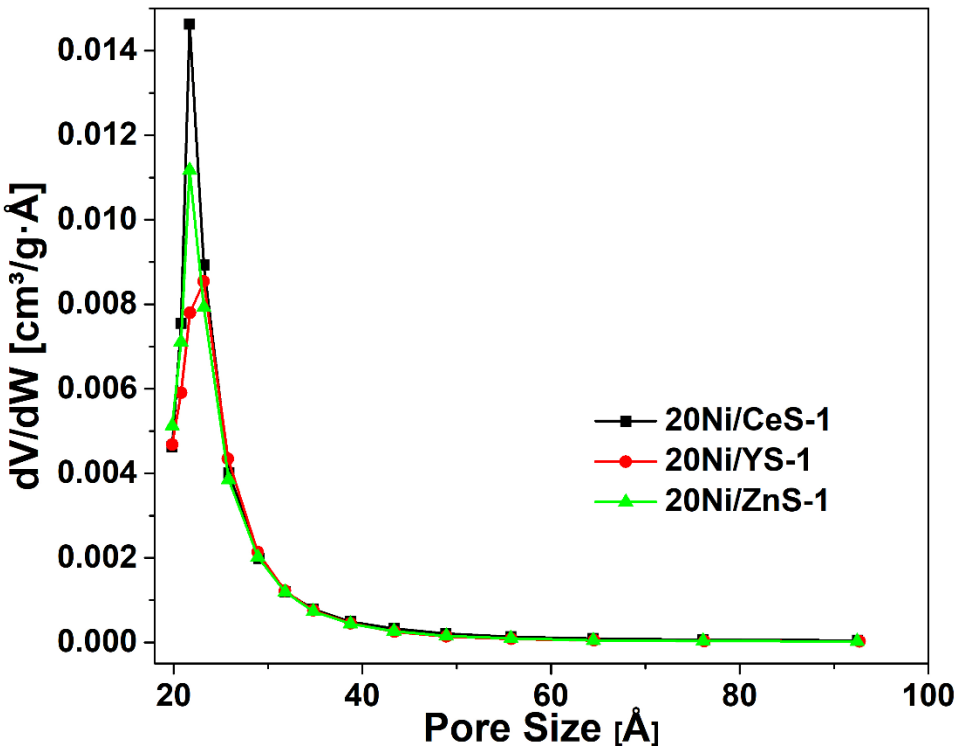

Figure 4-9. Pore size distribution profiles of the 20 wt.%Ni supported on ion-exchanged silicalite-1

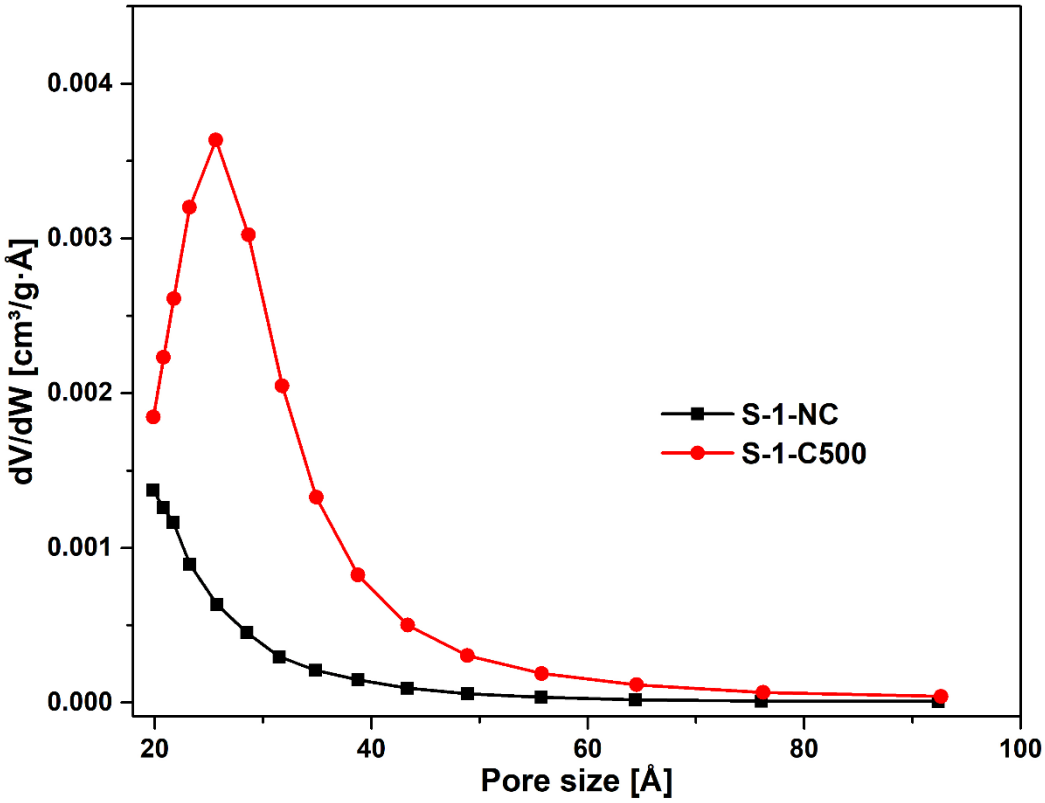

Figure 4-10. Pore size distribution profiles of as-synthesized S-1 and S-1 calcined at 500 °C.

Table 4-1. Physicochemical properties of silicalite-1 based catalysts

Sample	BET Surface	Vmicro [cm^3/g]	Vmeso [cm^3/g]	Average pore diameter [nm]	Micro area

	Area [m^2/g]				
S-1-NC	237	0.0817	0.0227	5.06	203
S-1-C500	400	0.1114	0.0708	3.66	279
5Ni/S-1	369	0.1118	0.0739	3.40	279
10Ni/S-1	357	0.1094	0.0760	3.72	271
15Ni/S-1	353	0.1122	0.0685	3.64	281
20Ni/S-1	350	0.1104	0.0712	4.25	274
20Ni/Ce-S-1	386	0.0845	0.1159	4.10	206
20Ni/Y-S-1	390	0.0968	0.1011	4.11	237
20Ni/Zn-S-1	394	0.0927	0.1044	3.82	228
NiS-1(40)	357	0.0922	0.1115	3.75	227
NiS-1(30)	348	0.0968	0.1017	4.04	238
NiS-1(20)	327	0.0966	0.0994	3.95	239

4.4 X-ray photoelectron spectroscopes of fresh catalysts

In our bid to elucidate and to obtain information about the surface elemental composition of the catalysts, the samples were subjected to XPS analysis. The results of Ni2p XPS spectra are presented in Figure 4-11. When interpreting the XPS spectra

for Ni, one must be careful not to confuse the shake-up satellite peaks with oxidized nickel peaks—Ni XPS spectra complex with a combination of spin-orbitals and satellite features [131].

The spectra from the X-ray photoelectron spectroscopy analysis revealed Ni2p peaks for the samples: 20Ni/YS-1(Figure 4-11**A)** and 20Ni/ZnS-1 (Figure 4-11**B)**. These peaks are an indication of the presence of Ni oxide (NiO) [132] on the surface of the catalysts. As presented in the XPS spectrum for 20Ni/CeS-1, in Figure 4-11**C**, appearing at binding energies of 857.3 eV and 875.3 eV are the two spin-orbit peaks which correspond to $Ni2p_{3/2}$ and $Ni2p_{1/2}$ respectively.

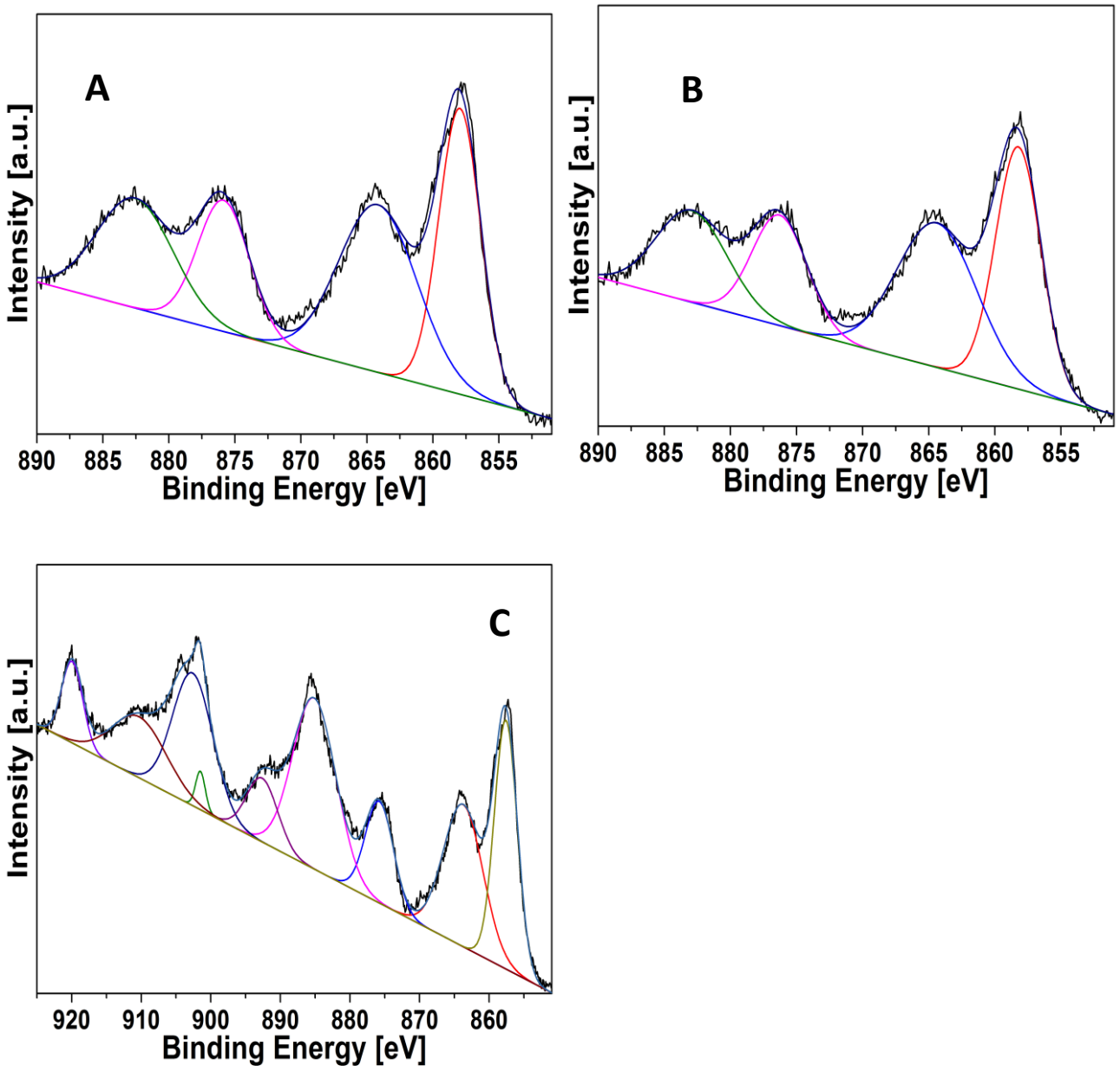

Figure 4-11. XPS spectra of Ni2p of (A) 20Ni/YS-1 and of (B) 20Ni/ZnS-1. Ce3d-Ni2p spectra of (C) 20Ni/CeS-1.

The XPS spectra of ceria-based compounds also show complex features resulting from a number of initial as well as final 4f electronic configurations [133]. It is recommended to deconvolute these types of spectra with non-linear least square fitting before analyzing them. The 3d spectrum recorded from ceria-based materials can be resolved into doublets of three spin-orbits, $3d_{3/2}$ and $3d_{5/2}$ [134]. The Ce3d spectra can be ascribed to the existence of the different oxidation states of Ce^{3+} and Ce^{4+} cations in species of CeO_2. This can further be explained by the fact that the sample was washed only once after ion exchange, thereby leaving some amount of $Ce(NO_3)_3$ on the surface. $Ce(NO_3)_3$ after calcination is converted to CeO_2. On careful observation of the Ce3d-Ni2p spectra, we can see what appears to be an overlap of the $Ni2p_{1/2}$ satellite peak and the first peak of $Ce3d_{5/2}$. This overlap appears at binding energy between 880 eV and 890 eV. Information regarding the oxygen species in the samples was derived from the O1s spectra after deconvolution. Accompanying these peaks are their shake-up (satellite) peaks at ca. 864.1 eV and 885.3 eV. In the Si XPS spectra for the 20Ni/CeS-1 sample, only the Si2p peak appeared at binding energy of ca. 104.3 eV – depicting the Si to be in the form of SiO_2. Two peaks were needed to successfully fit the Si2p peaks. As shown in Figure 4-12**C**, these two peaks ($Si2p_{3/2}$ and $Si2p_{1/2}$) signal the presence of Si in the oxide form. Since no extra peaks were detected, it was confirmed that there were no other forms of Si in the sample. The same phenomenon was observed in the Si XPS spectra for the samples: 20Ni/YS-1 and 20Ni/ZnS-1 in Figure 4-12A and B respectively where the Si2p peaks were at 104.5 eV and 104.3 eV respectively. The difference in binding energies of Ni and Si (ΔE_{Ni} - ΔES_i = $Ni2p_{3/2}$ - Si2p) is applied as a specific indicator for Ni – Si interaction [135].

Coenen [136] reported that the formation of nickel-silicates results in binding energy difference of between 753.2 eV and 753.6 eV. Based on the above inference the binding energy difference for the sample 20Ni/CeS-1 is 753 eV which implies that there was no formation of nickel-silicate in this sample. As shown in Figure 4-13, the O1s XPS signals were each deconvoluted using two peaks. These peaks were attributed to lattice oxygen from silicon oxides. This observation was in agreement with the findings from the Si2p XPS spectra. In the Y3d XPS spectra for 20Ni/YS-1, shown in Figure 4-14**A**, it can be observed that it is not symmetric. After deconvoluting the signal, it was found out that it contained two peaks. These peaks were ascribed to the $Y3d_{5/2}$ appears at binding energy of 155.4 eV and $Y3d_{3/2}$ at binding energy of 159.7 eV. The $Y3d_{5/2}$ signal observation suggests the existence of Y_2O_3 on the surface of the sample. Y carbonate species was confirmed to be on the sample 20Ni/YS-1, most probably due to the adsorption of CO_2 from the atmosphere by Y_2O_3 to form the carbonate species. Also, shown in Figure 4-14**B** is the Y3p XPS signal. Displayed at a binding energy of 301.7 eV is the $Y3p_{3/2}$ peak and at 313.1 eV is the $Y3p_{1/2}$ peak. These spectra are at the inherent binding energies for Y^{3+} ion.

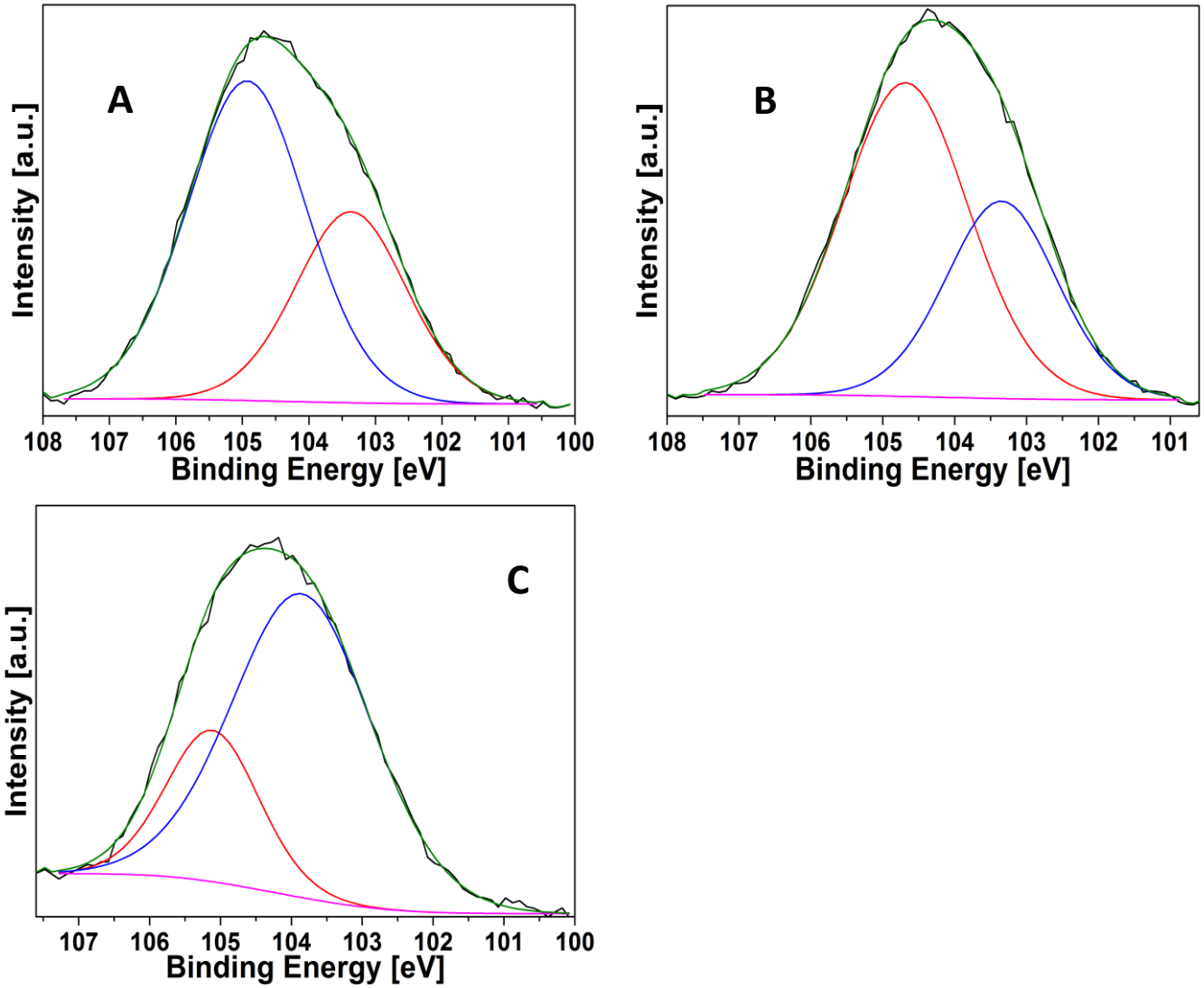

Figure 4-12. Si2p XPS spectra of (A) 20Ni/YS-1 (B) 20Ni/ZnS-1 and (C) 20Ni/CeS-1.

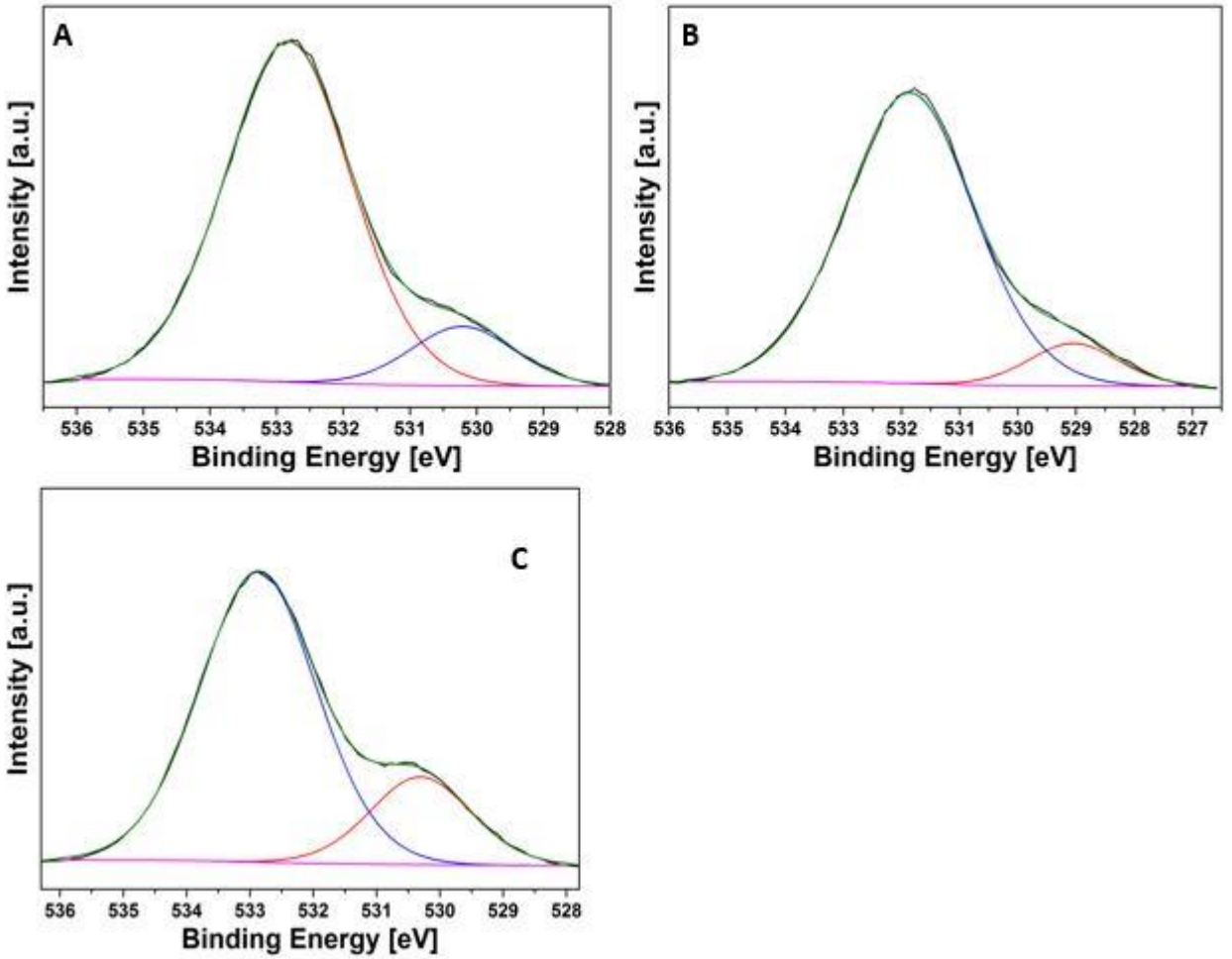

Figure 4-13. XPS O1s spectra of (A) 20Ni/YS-1, (B) 20Ni/ZnS-1 and (C) 20Ni/CeS-1.

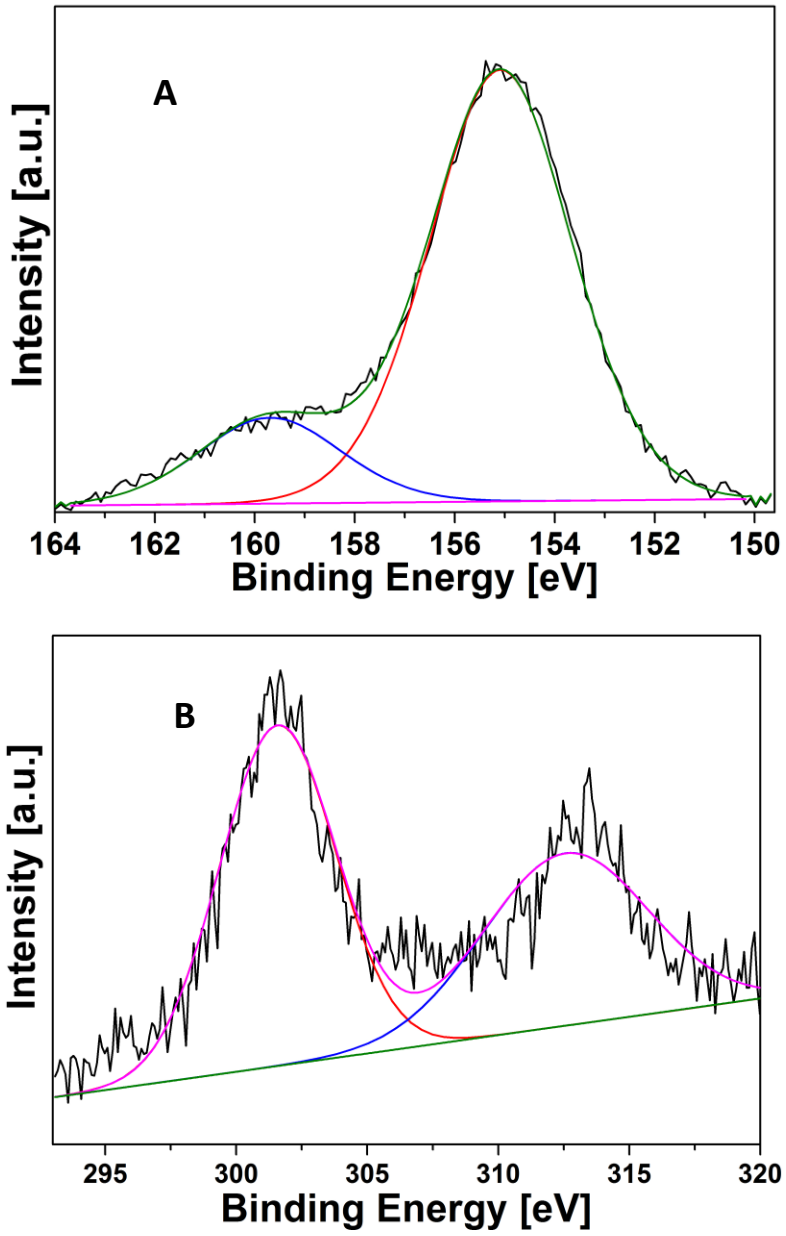

Figure 4-14. XPS spectra of (A) Y3d and (B) Y3p of 20Ni/YS-1 catalyst.

4.5 FTIR spectroscopy of fresh catalysts

The major structural groups of materials such as zeolites can be analyzed with the help of IR spectroscopy. Stretching or bending molecules are responsible for the vibrations in zeolites. There are 2 possible sources of the vibrations in zeolites: the framework internal vibrations or external vibrations emanating from the links of the tetrahedral units [137]. From the IR spectra of the fresh catalysts shown in Figure 4-15, the peaks at wavelength of 440 cm^{-1} are ascribed to the internal tetrahedral Si—O bend. Another peak appears at a wavelength of approximately 540 cm^{-1} and is linked to the vibrations of the double rings in the external linkage. The band at 800 cm^{-1} is ascribed to X—O—X symmetric stretching vibration in the external linkage whereas the band at 1100 cm^{-1} is because of the asymmetric stretching vibrations (where X is Si or other element present). Comparing between FTIR spectra of the S-1-C500, 10Ni/S-1 and 20Ni/CeS-1, the formation of Ni-O or Ce-O bonds could be inferred. The presence of Ni in Si-O-Ni linkage could be ascribed to possible ion-exchange occurring during the wet-impregnation. The intensity of the IR band at 1100 cm^{-1} slightly decreased and was subsequently enveloped between 1110 and 1040 cm^{-1} with increase in Ni loading—indicating the formation of Ni-O bond which replaced the Na-O in Si-O-Na.

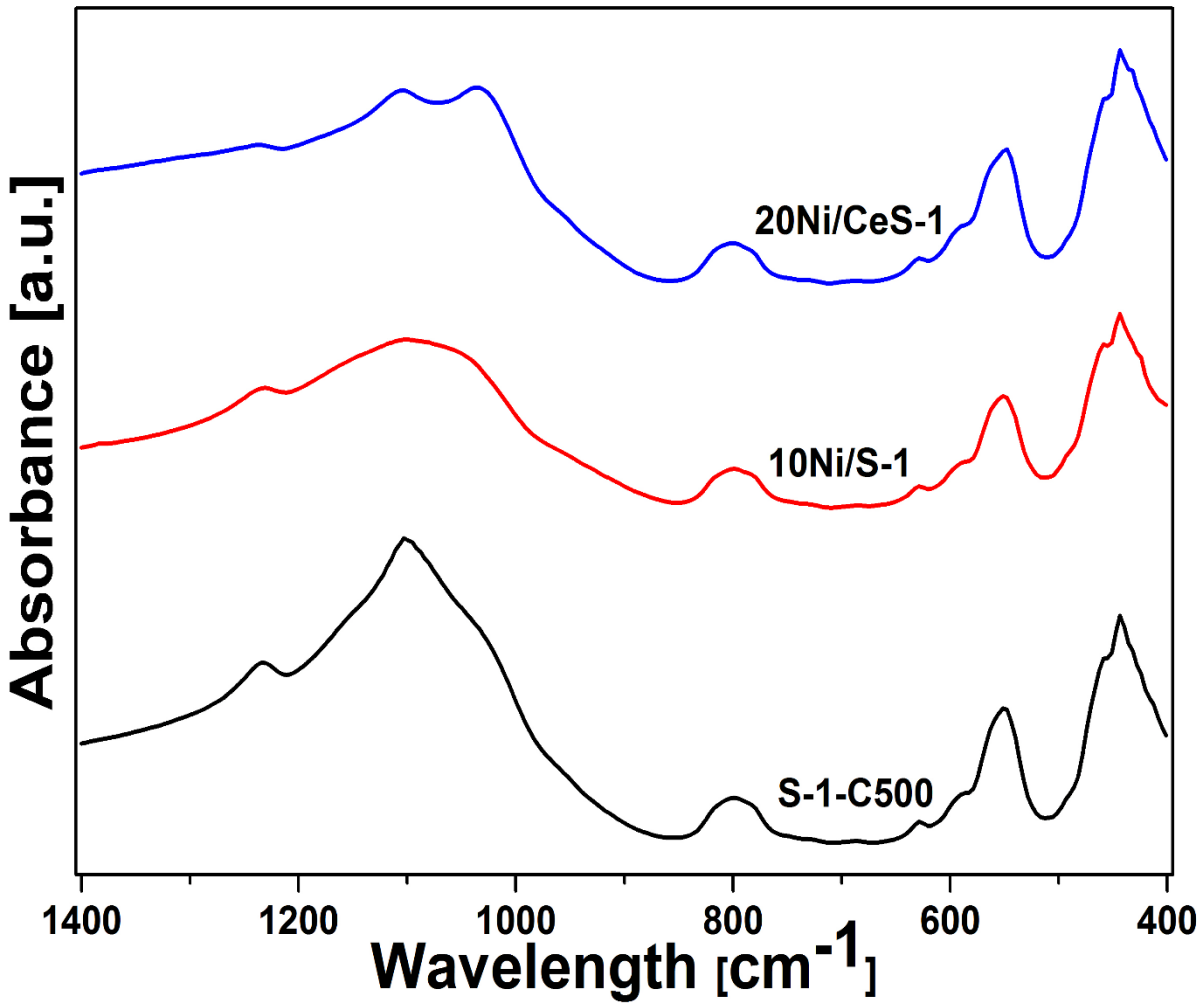

Figure 4-15. FTIR spectra of fresh catalysts.

4.6 Temperature Programmed Reduction

H_2-TPR experiments were performed to better understand the support-metal interactions, as presented in Figure 4-16. The silicalite-1 sample without any modification or metal loading did not yield any peak with regards to reduction over the range of temperatures analyzed. This was as expected since the was no metal loaded on the zeolite. The peaks of hydrogen consumption can be said to emanate from the nickel oxide species in the samples. Ni^{2+} is said to be reduced directly to Ni^0

without producing species of intermediate oxidation states. The H_2 consumption in different temperature regions could be attributed to different nickel species [132] with different extents of interactions with the silicalite-1 support. With reference to the peak positions, the reduction of NiO and H_2 consumption can be divided into three (3) parts, namely, α-, β-, and γ-parts [138]. Free NiO species that have weak metal-support interactions are reduced in low temperature ranges– this part is ascribed α, whereas β is assigned to the stage of reduction of NiO species with moderate metal-support interactions. NiO species with strong interaction with the support are reduced in the temperature range assigned to the γ-stage [138]. For both the 5Ni/S-1 and 10Ni/S-1 catalysts, we can observe reduction peaks of relatively low intensities,. Generally, the broadness and intensity of the peak increased with increasing nickel loading. The maximum reduction temperature increased slightly, with respect to nickel loading, of the 10Ni/S-1 catalyst. This phenomenon is consistent with the previous work of Takahashi et al. [139] and is an implication of stronger metal-support interaction which may be associated with a Si-O-X bond formation, as supported by the results from FT-IR. The reduction profile of 20Ni/S-1 shows a clearly significant symmetrical peak with a maximum at ca. 410 ^{o}C.

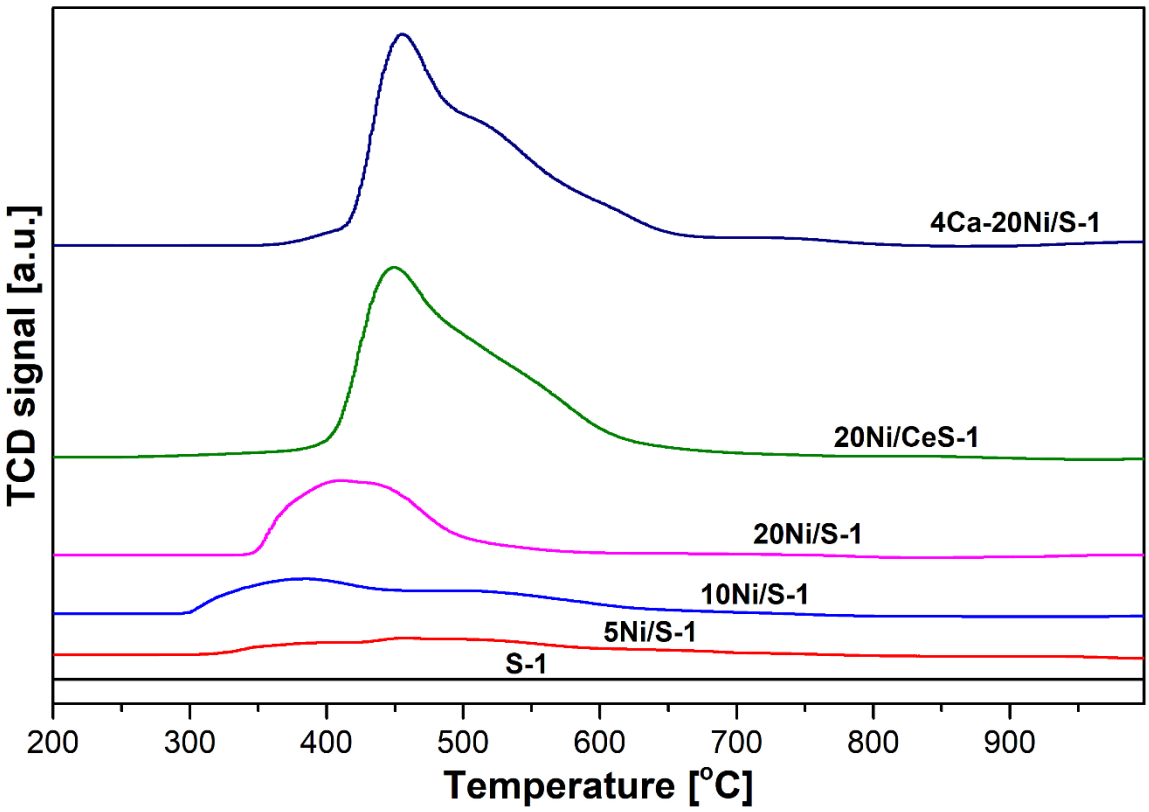

Figure 4-16. H_2 – Temperature Programmed Reduction profiles for fresh catalysts calcined at 500 °C.

The broad peaks observed in the reduction profiles of the nickel loaded silicalite-1 were because of the coalescing of two peaks ascribed to the clumped and dispersed NiO species with slightly different reduction temperature ranges. In the reduction profile of the 20Ni/CeS-1 sample, a broad and relatively more intense reduction peak can be observed in the temperature ranges 400 – 500 °C, with a shoulder between 500 – 600 °C. A similar observation was made for the 4Ca-20Ni/S-1 catalysts. This was attributed to the possible presence of CeO_2 or CaO species, respectively, on the surface

of silicalite-1 as corroborated by the XPS results for 20Ni/CeS-1. Possible significant CeO_2 species on the surface of zeolite were remnants of the ion exchange process whereas the CaO species were from the wet impregnation procedure. The 20Ni/CeS-1 and 4Ca-20Ni/S-1 yielded reduction peaks of significantly high areas than that of the unmodified 20Ni/S-1 catalysts. This observation could suggest that the Ce and Ca promoters effectively improved the Ni particle dispersion. These samples (20Ni/CeS-1 and 4Ca-20Ni/S-1) could perhaps also possess surface oxygen vacancies which significantly facilitate the reduction process of NiO species. These oxygen vacancies possibly formed on the surface may have a strong interaction with a neighboring oxygen on a NiO species, weakening the Ni—O, making it easily removable by hydrogen [140].

4.7 Catalyst evaluation Temperature tests

NS-1-series of catalysts, synthesized via the one-step method were unable to convert methane and carbon dioxide. This could be attributed to the fact that the dry reforming reaction is a surface reaction. In-situ incorporation of nickel resulted in the lodging of the nickel metal in the tetrahedral structure of the zeolite. Ni particles provide the primary actives, therefore restricted access to these sites produces no activity.

Silicalite-1 with varying loadings of nickel were tested at different temperatures, ranging from 600 ^oC to 900 ^oC and the results of CH_4 and CO_2 conversions as well as H_2/CO ratios are shown in Figure 4-17, Figure 4-18 and Figure 4-19 respectivly. It was observed that the conversions of both reactants increased with increasing nickel loading as well as with temperature. The upward trend variation with temperature

can be ascribed to endothermic nature of the reaction—which as such is favored by high temperatures. At 900 ^{o}C, methane conversion of above 90% was obtained over the 20Ni/S-1 catalyst. Also, the conversion increased with higher nickel loading due to the availability of more active sites for reaction to occur. This trend, however, is not sustainable as every support material has its optimum metal loading capacity, beyond which sintering easily occurs at high temperatures. On the average, the H_2/CO ratio was observed to increase with increasing temperature. This occurrence could be a signal of prevalence of the methane decomposition reaction, yielding more H_2 in the process. The conversions H_2/CO obtained in these tests represent the performance of the catalysts after 30 mins on stream, a point at which stability would have been reached.

The H_2/CO ratio obtained for the various catalysts was closest to unity at a temperature of 750 ^{o}C. This could imply that the conversions of both CH_4 and CO_2 were almost the same at this temperature, where side reactions were probably controlled. Again, the H_2/CO ratios decreased slightly with increasing nickel loading. This observation could be attributed to agglomeration of nickel particles at higher weight percent loading, leading to reduced number of active sites per amount of nickel deposited. This affects the overall activity of the catalysts. In this case, the more profound negative effect was on the methane conversion.

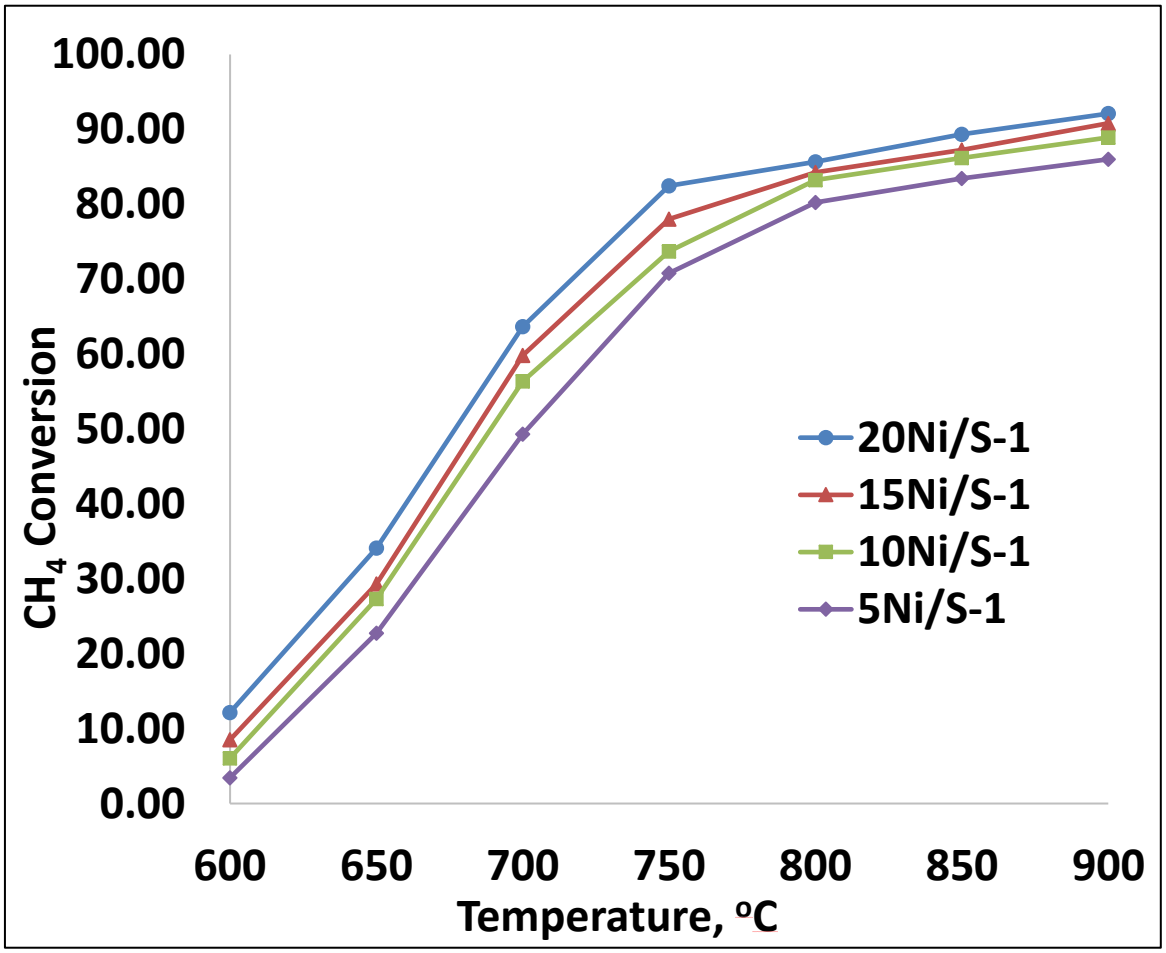

Figure 4-17. CH_4 conversion vs temperature for 5 – 10 wt.% Ni on silicalite-1

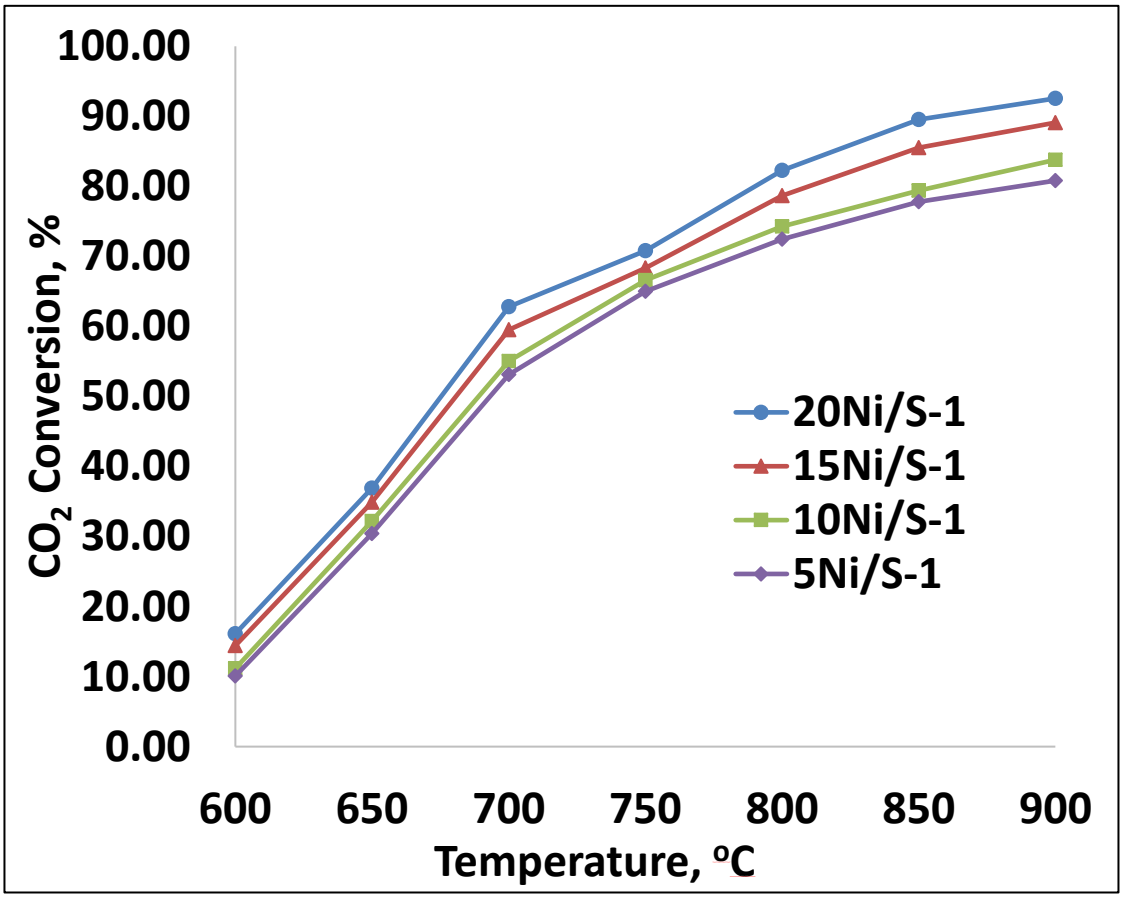

Figure 4-18. CO_2 conversion vs temperature for 5 – 10 wt.% Ni on silicalite-1

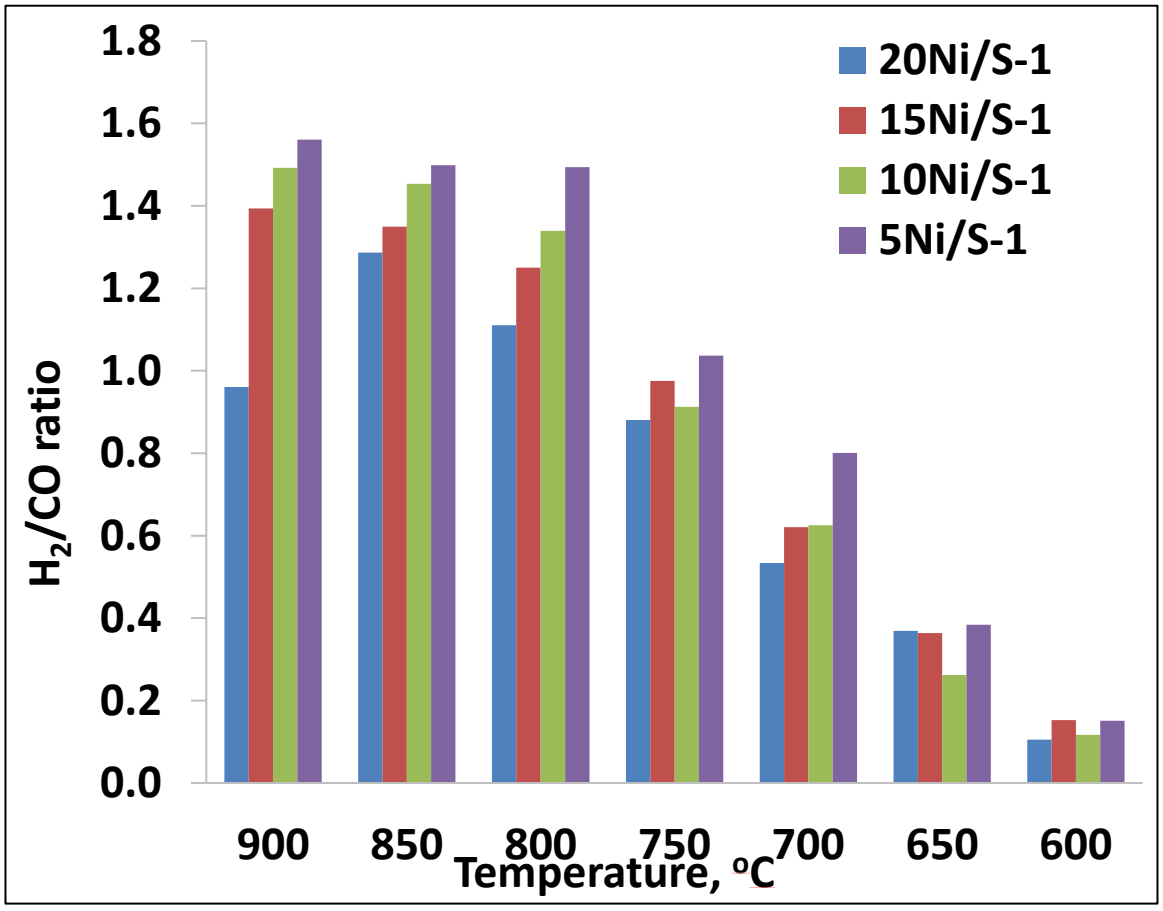

Figure 4-19. H_2/CO ratio vs temperature for 5 – 20 wt.% Ni on silicalite-1

4.8 Catalytic activity, stability and carbon resistance.

CH_4 and CO_2 conversions with time on stream for different loadings of Ni on silicalite-1 are presented in Figure 4-20 and Figure 4-21 respectively. The catalyst with nickel loading of 5 wt.% was observed to have performed poorly, with a very low initial conversion and then declines sharply to zero, most possibly due quick deactivation as a result of few active sites—this was corroborated by the H_2-TPR profile, presented in Figure 4-16. Besides 5Ni/S-1, 10Ni/S-1 is observed to have a relatively low initial CH_4 conversion as compared to all other samples tested for stability but its CH_4 and CO_2 conversions (76.22% and 68.18%, respectively) at 12 h TOS were higher than those of 15Ni/S-1 (70.92% and 64.33% respectively) at 12 h TOS. Moreover, CH_4 conversion seemed to have declined significantly (dropping from 84.58% to 70.92% after 12 h of reaction) with time over 15Ni/S-1. The 10Ni/S-1 catalyst was observed to be more stable than the 15Ni/S-1 catalyst. The apparent higher stability of 10 wt.% on S-1 was justified by plotting conversion per gram of Ni vs Ni wt.% after 12 h of TOS, as presented in Figure 4-23. This phenomenon could be attributed to the agglomeration of Ni particles with higher Ni loading. However, this suggested agglomeration may have been compensated for by the higher number of active sites on the 20 wt.% Ni on S-1. We therefore selected this catalyst (20Ni/S-1) for modification and further stability studies. The 20Ni/S-1 catalyst achieved a CH_4 conversion of 87.02% and a CO_2 conversion of 85.18% after the first hour on stream. These decreased to 87.11% and 72.66% respectively at 12 h TOS. The CH_4 and CO_2 conversions were 77.58% and 60.76% respectively at 18 h TOS. The worst performing catalyst was 5Ni/S-1 with CH_4 and CO_2 conversions of 66.32% and 68.87% respectively after 1 h TOS. These declined rapidly

to 2.06% and 3.22% respectively after just 3 h TOS. When reforming CH_4 using CO_2 in equimolar ratio, we expect to obtain equal conversions [49] and a H_2/CO ratio of one. If this is not the case as we observed in our work, it could be ascribed to side reactions.

As shown in Figure 4-24 and Figure 4-25, Ce, Y and Zn ion-exchanged S-1 catalysts achieved higher CH_4 and CO_2 conversions as compared to the unmodified silicalite-1 based catalysts— up to our knowledge this is the first time such modification of silicalite-1 has been applied in CO_2 reforming of methane. 20Ni/CeS-1 was the most active catalyst—its CH_4 conversion did not decrease during the reaction whereas there was slight decrease (from 88.53% to 82.41) in its CO_2 conversion. As discussed above in the XPS analysis, CeO_2 was formed on the surface of the 20 wt.% Ni on CeS-1. Ceria is known to provide a high amount of mobile oxygen. During the reaction, a good amount of oxygen is made available during through a continuous cycle of reduction/oxidation of the Ce sites, thus enhancing the transfer of oxygen to Ni centers [1]. this makes the actives sites more resistant to carbon. Furthermore, the relatively higher mesoporosity and higher surface area of the 20 wt.% on CeS-1 catalyst could be influencing factors in its improved performance than the unmodified analog, 20 wt.% on S-1. The modified 20 wt.% on CeS-1 had a mesopore volume of 0.1159 cm^3/g, an increase from the mesopore of 0.0712 cm^3/g of the 20 wt.% Ni on unmodified S-1. The mesopores served to reduce mass transfer restriction, as a result increasing catalytic activity. The higher surface also helped to disperse the nickel particles on the surface of the support to expose more active sites for reaction to occur. The apparent increase in CH_4 conversion was most likely due the methane decomposition reaction ($CH_4 \rightarrow C + 2H_2$) being prevalent as a side reaction. This is manifested in the relatively high H_2/CO ratios obtained for this

catalyst. 20Ni/ZnS-1 was found to be relatively less active than 20Ni/CeS-1 but relatively more active and stable than 20Ni/YS-1. At 12 h TOS the CH_4 and CO_2 conversions of 20Ni/ZnS-1 were 84.46% and 75.39% respectively whereas those of 20Ni/YS-1 were 84.45% and 69.62% respectively. Alkaline earth metals are mostly known to enhance the stability of DRM catalysts. Whereas this is true, Ca and Mg when used as promoters for the 20Ni/S-1 did not seem to have superior performance over the 20Ni/CeS-1 catalysts.

Except for 10Ni/S-1 and 15Ni/S-1 catalysts over which H_2/CO ratios of approximately one were obtained, all samples tested for stability had significantly high H_2/CO ratios (high H_2 selectivity) (Figure 4-19). This phenomenon could be ascribed to side reactions which could have been prevalent on stream during the CO_2 reforming of methane reactions. An example is the water gas shift (WGS: $H_2O + CO \leftrightharpoons H_2 + CO_2$) where hydrogen and carbon dioxide are produced resulting in a consumption of carbon monoxide.

Further evidence of this is shown in the low amount of CO and relatively higher quantities of CO_2 than CH_4 in the product stream. Other possible side reactions are the methane decomposition reaction, which is favored by high temperature To determine structural changes after methane reforming reactions, XRD analysis was carried out on the fresh and spent ion-exchanged silicalite-1 catalysts and the results are displayed in Figure 4-27**A** and Figure 4-27**B** respectively. The presence of carbon deposits was clearly observed in the x-ray diffraction peaks of the spent catalysts as compared to that of the fresh catalyst. Apart from the appearance of the carbon peaks

([002] and [100]), no observable structural changes occurred. This implies that the catalysts maintained structural integrity after 12 h on stream at 750 ^{o}C.

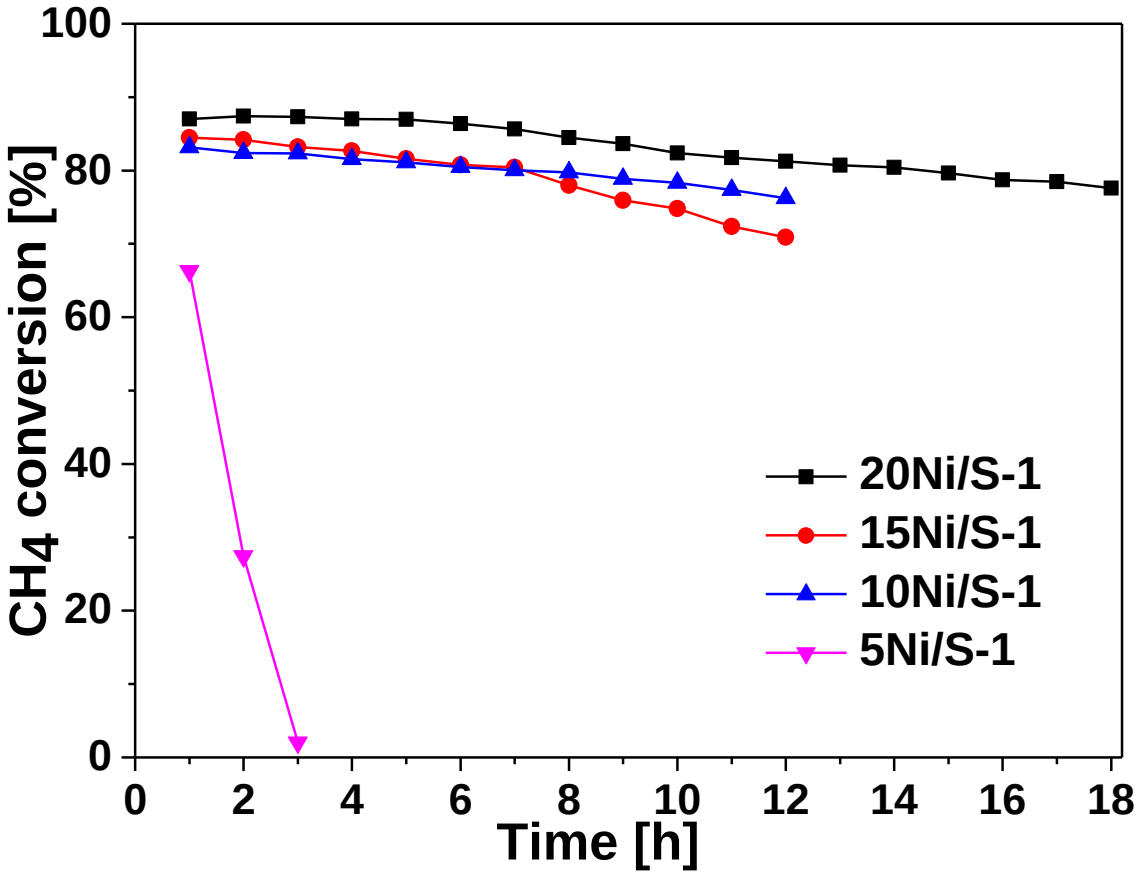

Figure 4-20. CH_4 conversion vrs TOS at 750 ^{o}C for 5-20 wt.% Ni on S-1.

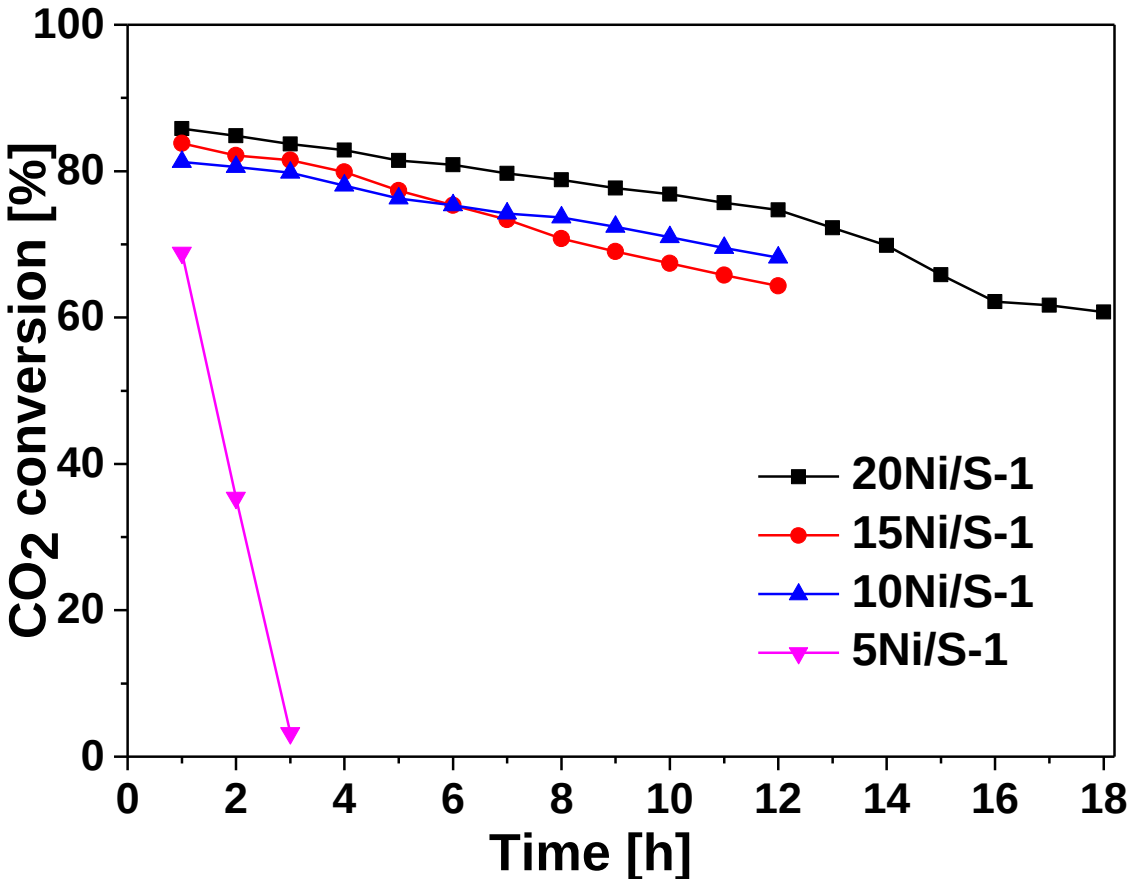

Figure 4-21. CO_2 conversion vrs TOS at 750 ^oC for 5-20 wt.% Ni on S-1.

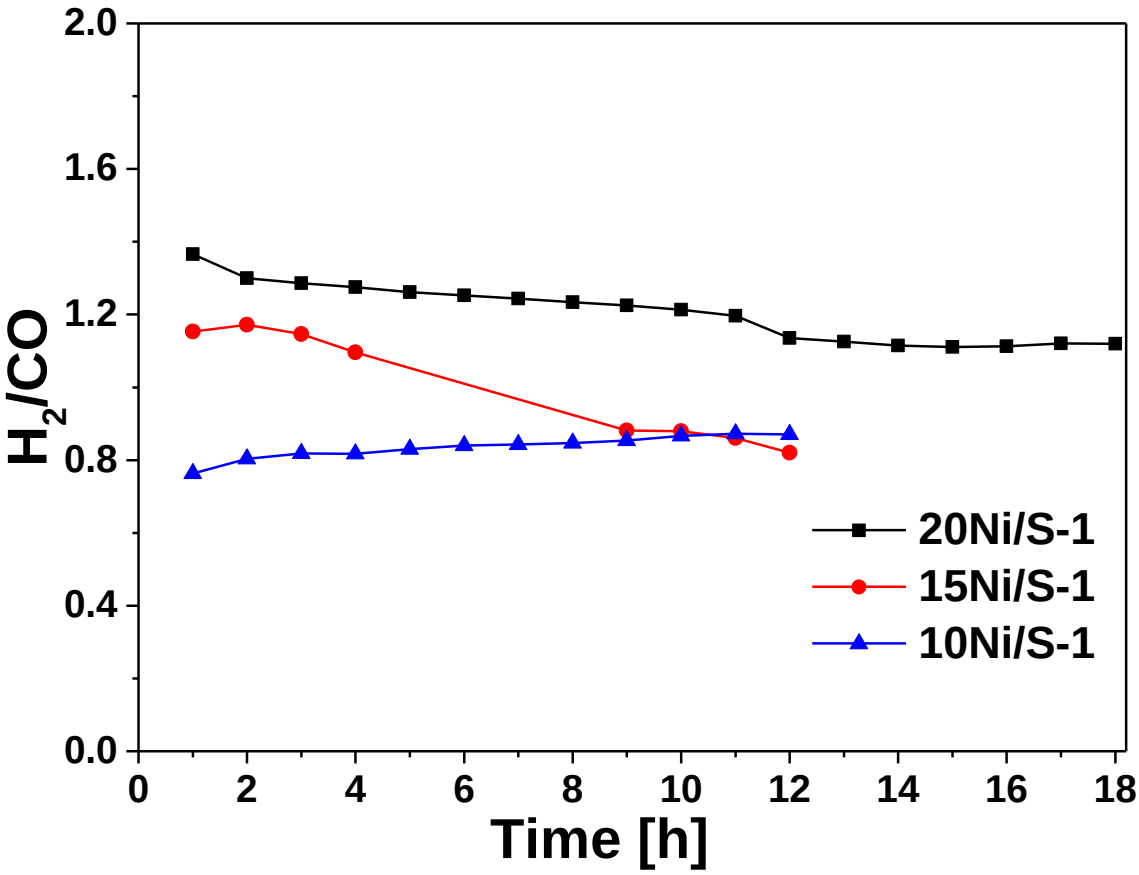

Figure 4-22. H_2/CO ratio vrs TOS at 750 ºC for 5-20 wt.% Ni on S-1.

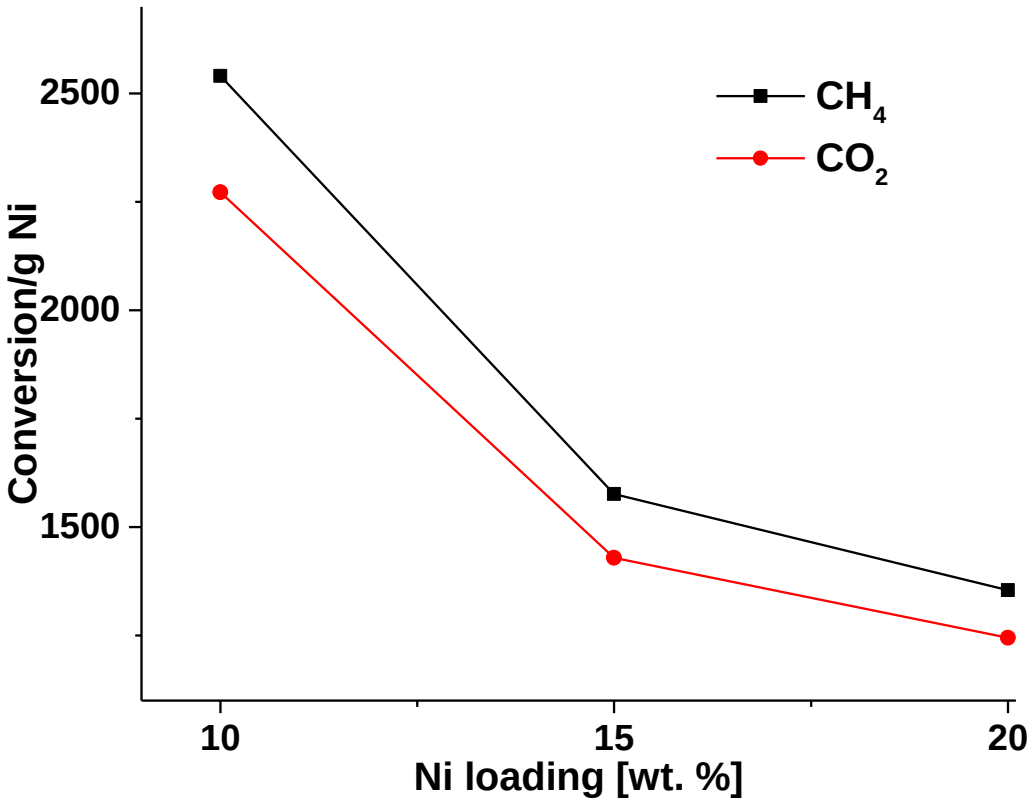

Figure 4-23. Conversion per unit gram Ni vs Ni wt. % after 12 h TOS.

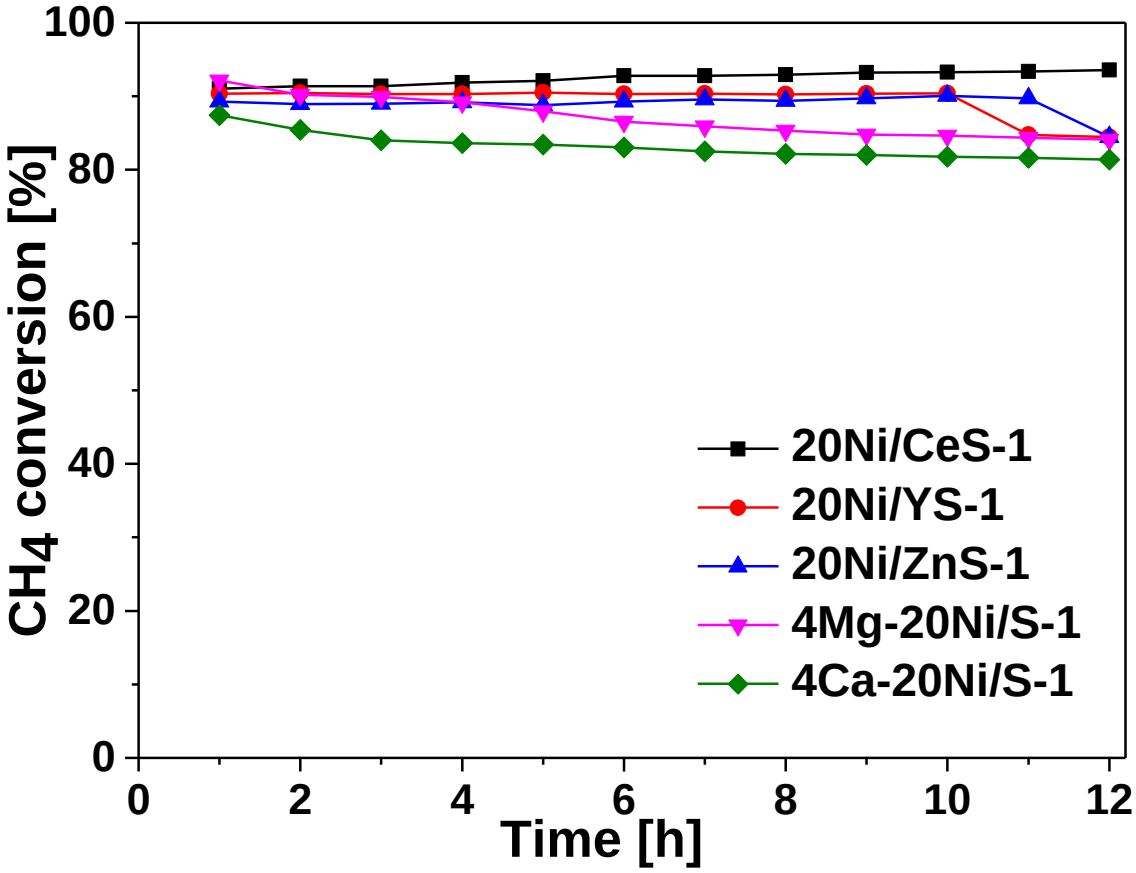

Figure 4-24. CH_4 conversion vrs TOS at 750 ^oC over 20 wt.% Ni on modified S-1 catalysts.

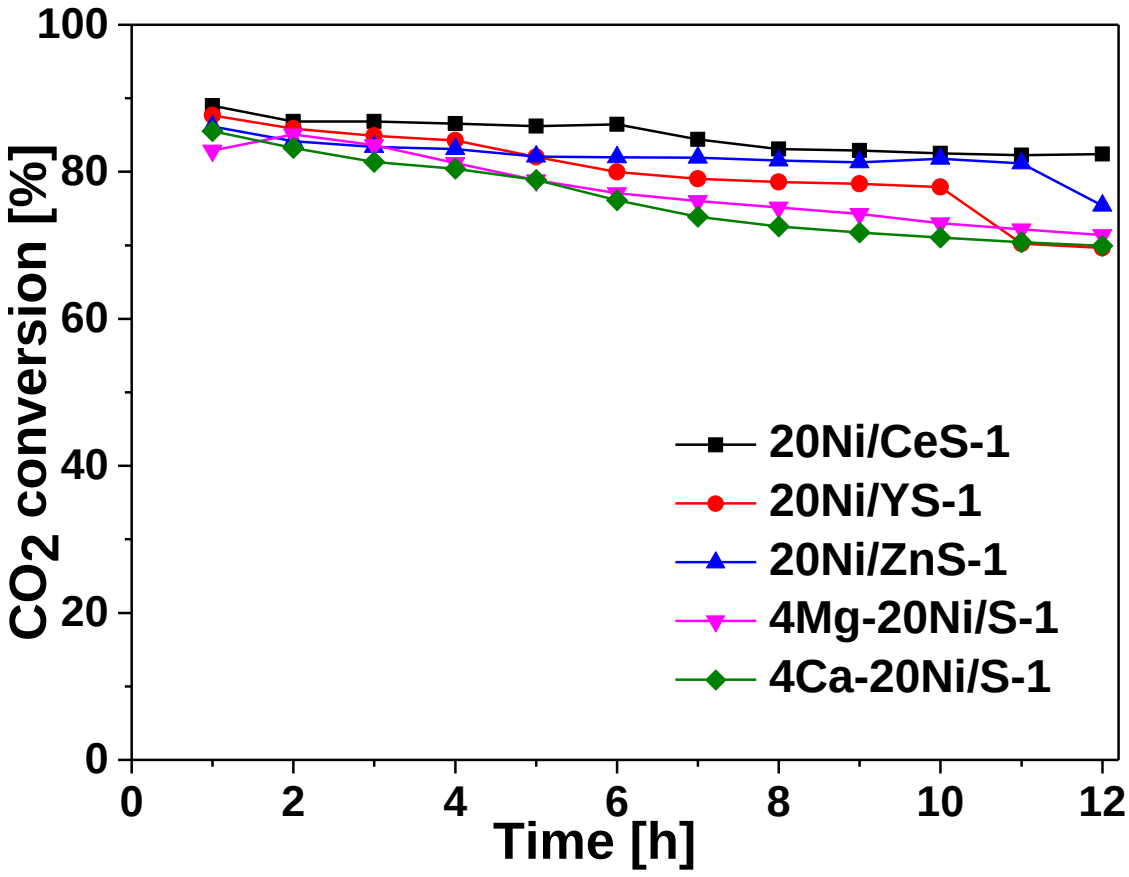

Figure 4-25. CO_2 conversion vrs TOS at 750 ^oC over 20 wt.% Ni on S-1 catalysts.

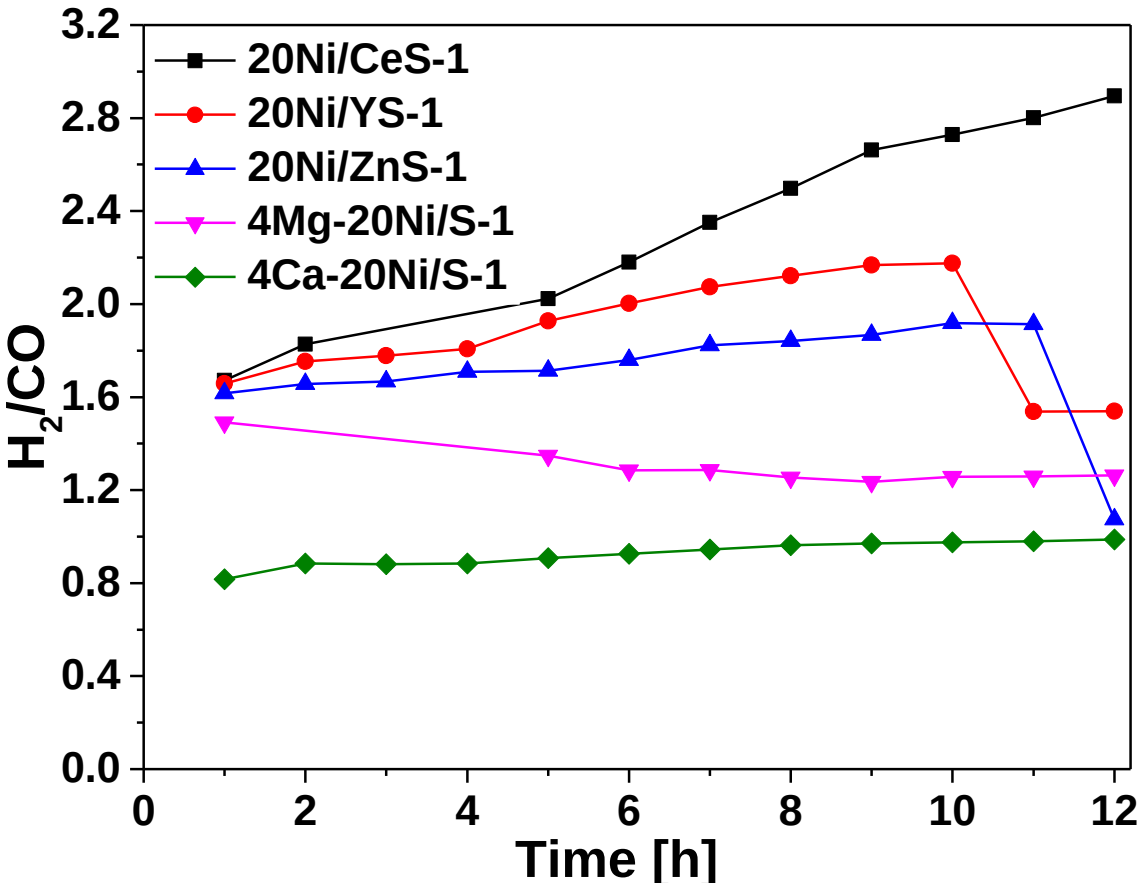

Figure 4-26. H_2/CO ratio vrs TOS at 750 ºC of modified 20 wt.% Ni on S-1 catalysts.

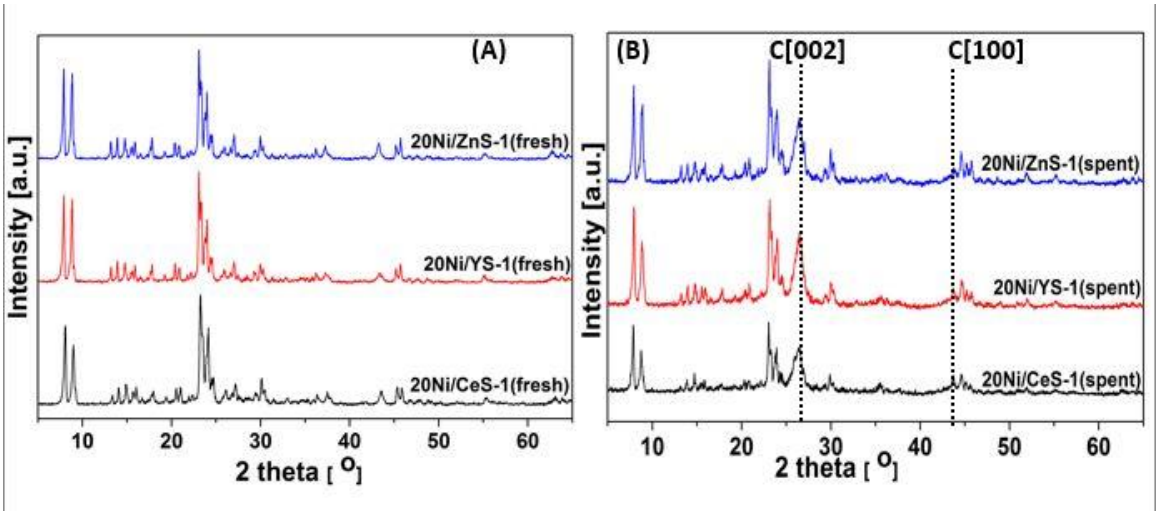

Figure 4-27. XRD patterns of [Ce, Y or Zn] ion-exchanged silicalite-1 after impregnation with 20wt% Ni: (A) before reaction (B) after 12 h of reaction.

4.9 Raman Scattering Spectrometry of spent catalysts

Results of Raman spectrometry for spent catalysts are shown in Figure 4-28. Two bands can be observed at approximately 1337 cm^{-1} and 1576 cm^{-1} which respectively represent the D-band and the G-band. The appearance of these bands after DRM reaction confirms the deposition of carbonaceous materials on the surfaces of the catalysts. These well-defined bands are ascribed to the existence of multi-walled carbon nanotubes on the spent catalysts. The absence of single-walled carbon nanotubes was confirmed by the absence of peaks below the Raman shift of 300 cm^{-1} [142]. The D band is induced by disorderliness and is ascribed to imperfections in the structures of defective carbon materials. The G band represents graphitic carbon, ascribed to the stretching vibrations of pairs of sp^2 atoms' in-plane C-C bonds [143, 144]. The degree of disorderliness or graphitization of carbon species is determined by the relative intensity ratio I_D/I_G. From Figure 4-28, it can be observed that the yield of amorphous carbon deposits was higher than graphitic carbon in the coke deposits on the surfaces of the spent catalysts (20Ni/Ce-S-1 and 20Ni/Y-S-1). A similar trend is seen in Figure 4-29, presenting Raman spectra for 15Ni/S-1, 20Ni/S-1 and 20Ni/Zn-S-1 spent catalysts.

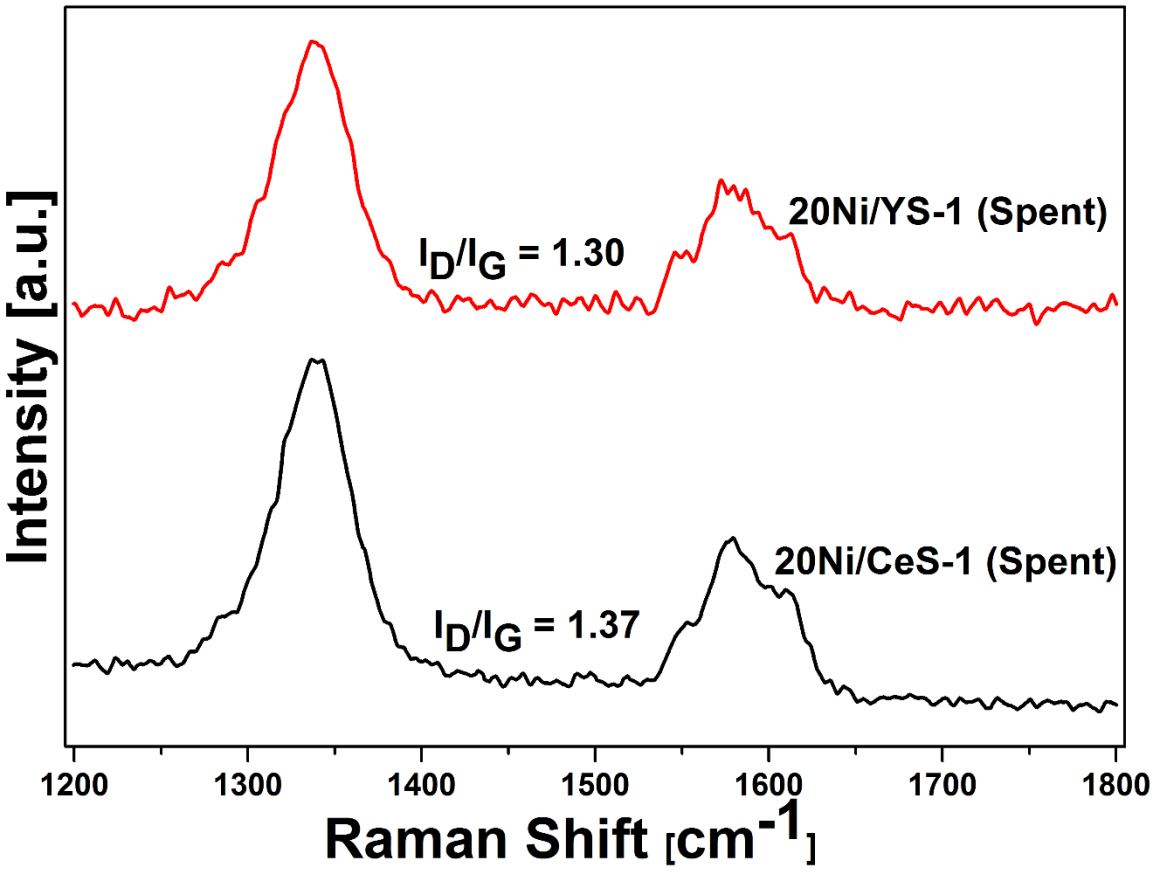

Figure 4-28. Raman spectra of spent catalysts.

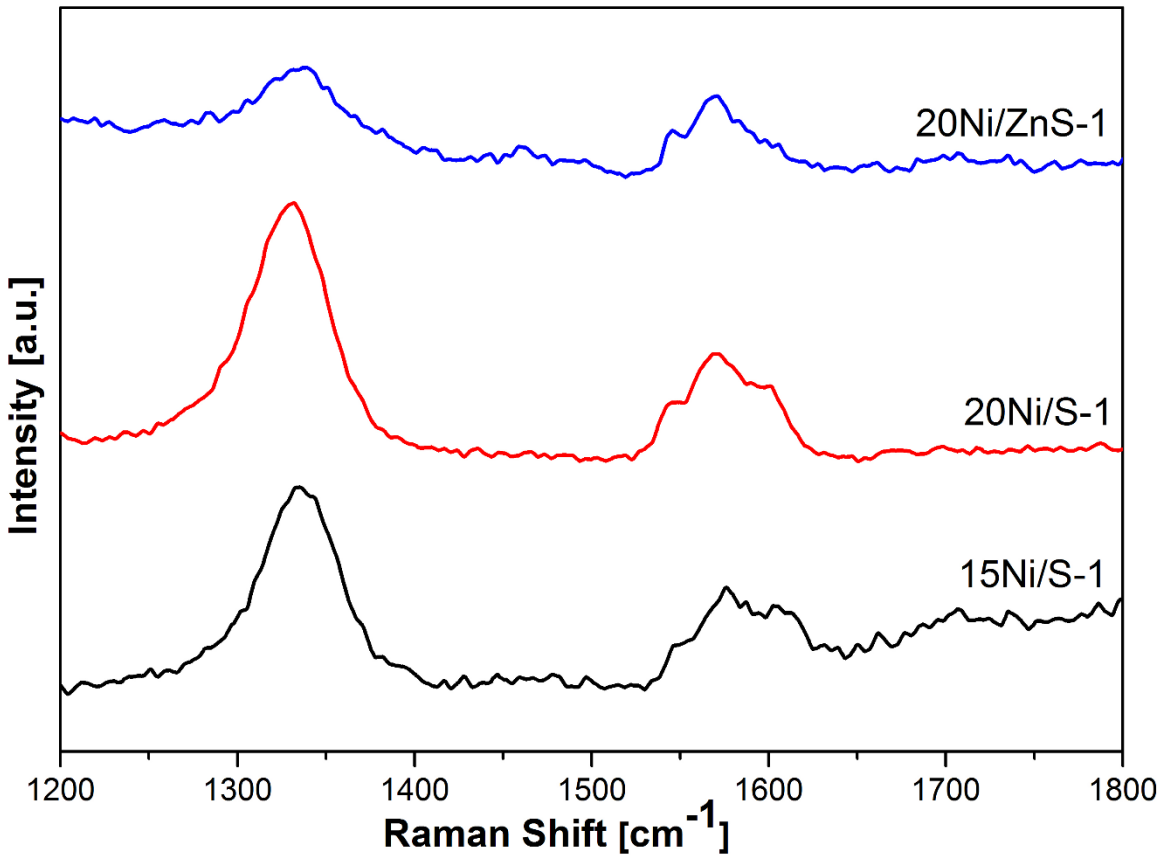

Figure 4-29. Raman spectra of spent: a. 15Ni/S-1, b. 20Ni/S-1 and c. 20Ni/Zn-S-1 catalysts.

4.10 TGA-DSC analyses of spent catalysts

Spent catalysts were analyzed by the TGA-DSC technique to elucidate the amount and types of carbon deposited on the surfaces of the catalysts during the reaction. As shown in Figure 4-30, Figure 4-31 and Figure 4-32, the high change in percent weight for the samples indicate high amount of carbon deposited on the catalysts. These weight losses were due to the oxidation of the carbon structures that were formed during the DRM reactions. This phenomenon agrees with the CH_4 and CO_2 conversions as well as H_2/CO ratios. It can be inferred that high the H_2/CO ratios obtained are because of the carbon not being converted to CO but rather being deposited as solid on the surfaces of the catalysts despite the high conversions of both CH_4 and CO_2 (even though CH_4 decomposition seems to be the prevalent). The DSC profiles reveal a 2-stage process (involving 2 steep endothermic curves) of carbon burn-off from the spent catalysts. The first one is a more intense curve that developed between 450^{o}C and 630^{o}C whereas the second peak (less intense) emerged between 700^{o}C and 800^{o}C. These two stages clearly indicate the presence of 2 types of carbon deposits. The low temperature peak was attributed to the burn-off of amorphous carbon whereas the high temperature peak was ascribed to the graphitic carbon on the surface of the catalysts. The appearance as well as the intensities of these peaks corroborates with the inferences drawn from the Raman spectra of the spent catalysts and the FE-SEM micro graphs of the spent catalysts shown in Figure 4-33. Due to the defects in its structure, amorphous carbon possesses a high chemical activity which makes it easy to burn off. Therefore, it has little impact in catalyst deactivation—this agrees with the good catalytic activity obtained even after 11 h of TOS. [18, 145, 146].

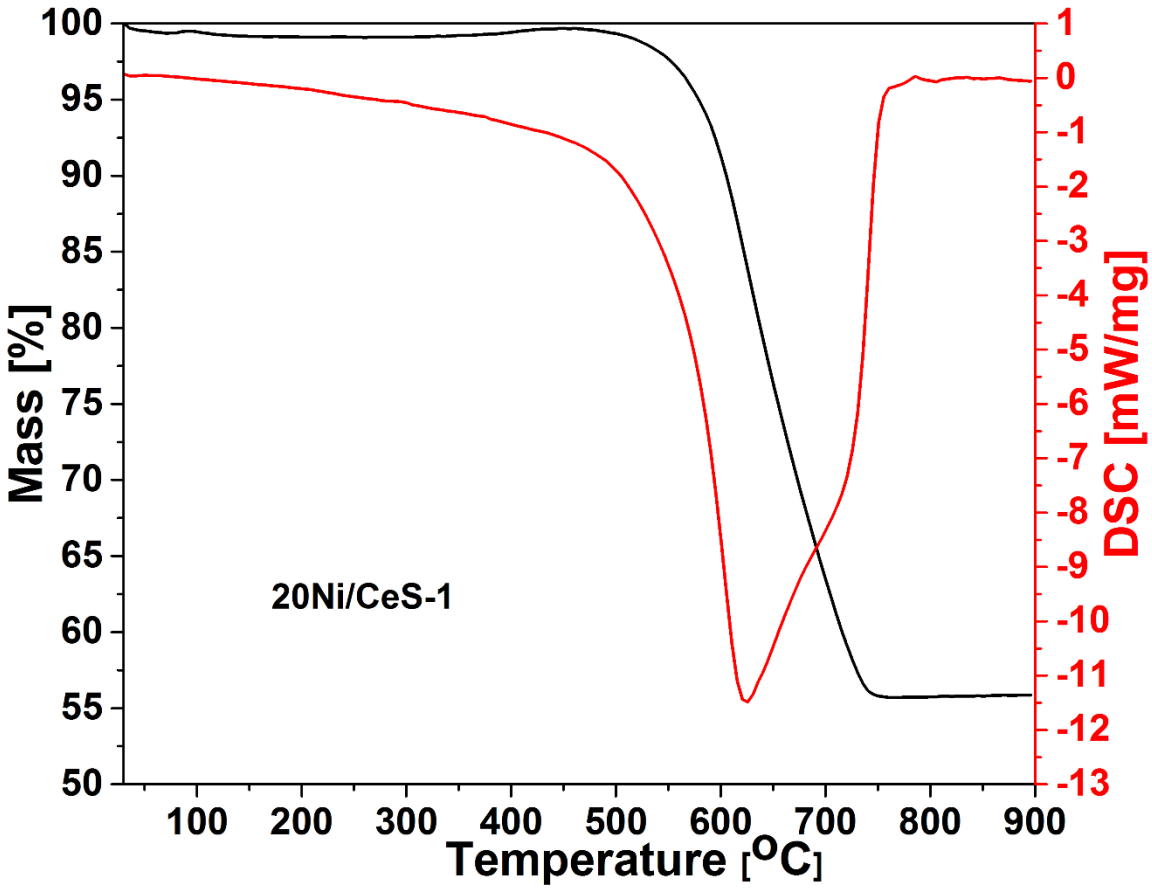

Figure 4-30. TGA - DSC profile 20Ni/CeS-1 spent catalyst

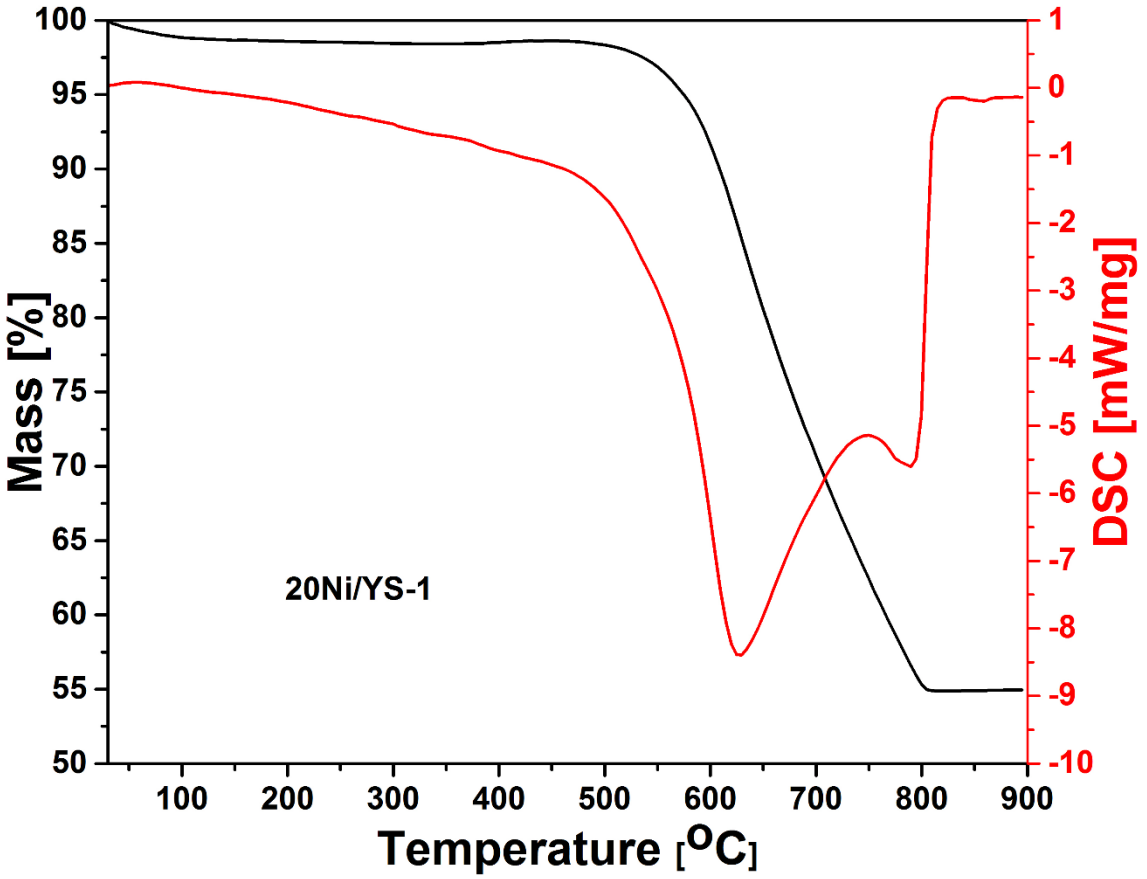

Figure 4-31. TGA - DSC profile 20Ni/Y-S-1 spent catalyst

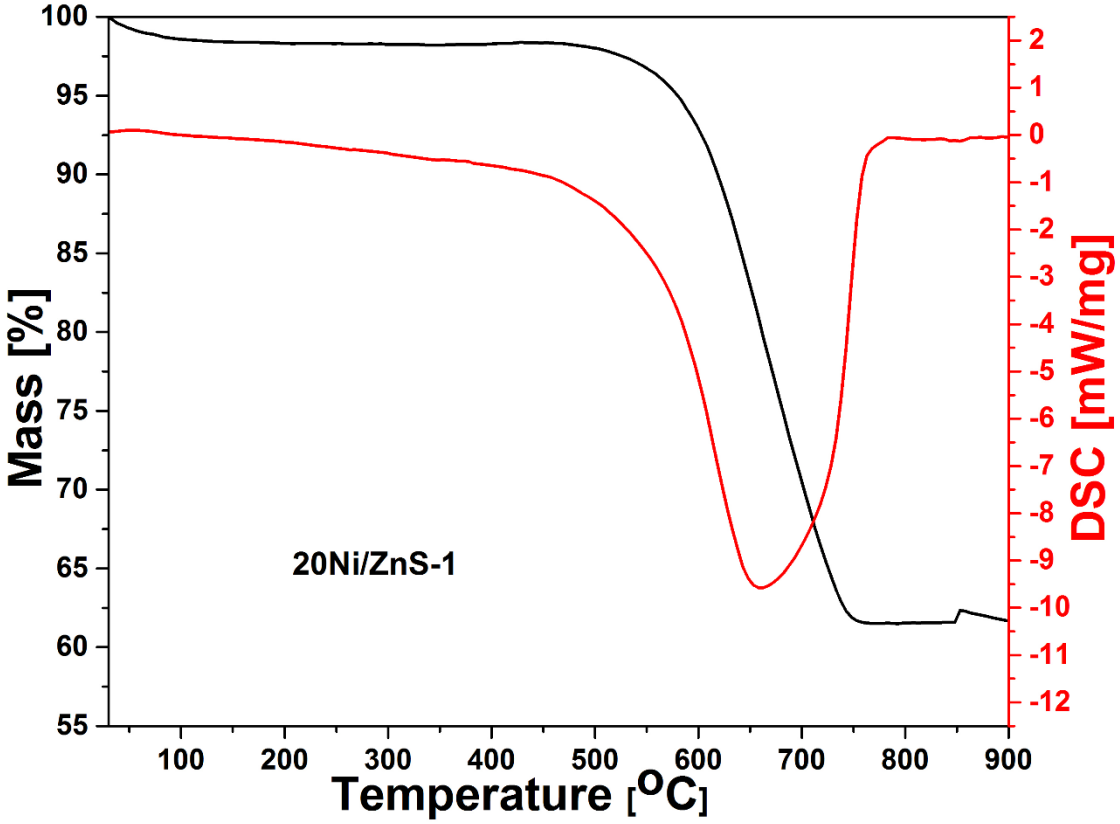

Figure 4-32. TGA - DSC profile 20Ni/ZnS-1 spent catalyst

4.11 FESEM and TEM of spent catalysts

FE-SEM images of spent catalysts are presented in Figure 4-33. Results from TEM analysis allows us to investigate and explain the catalytic behavior of metal based catalysts. The effectiveness of metal particles deposition on fresh catalysts and morphology of carbon deposits formed on post-mortem catalysts can determined by this technique. In this work, among the catalysts tested in dry reforming of methane, the 20Ni/CeS-1 proved to be superior in both methane and CO_2 conversions. But this high activity was not without carbon formation. As can be observed in Table 4-2 the carbon deposited on the spent 20Ni/CeS-1 was 44.13% despite it being still substantially active after 11 h on stream. This phenomenon was attributed to the formation of amorphous carbon nanotubes on the catalyst surface.

Table 4-2. Carbon deposits on spent catalysts.

Catalyst	Carbon, wt%
20Ni/CeS-1	44.13
20Ni/YS-1	45.05
20Ni/ZnS-1	38.31

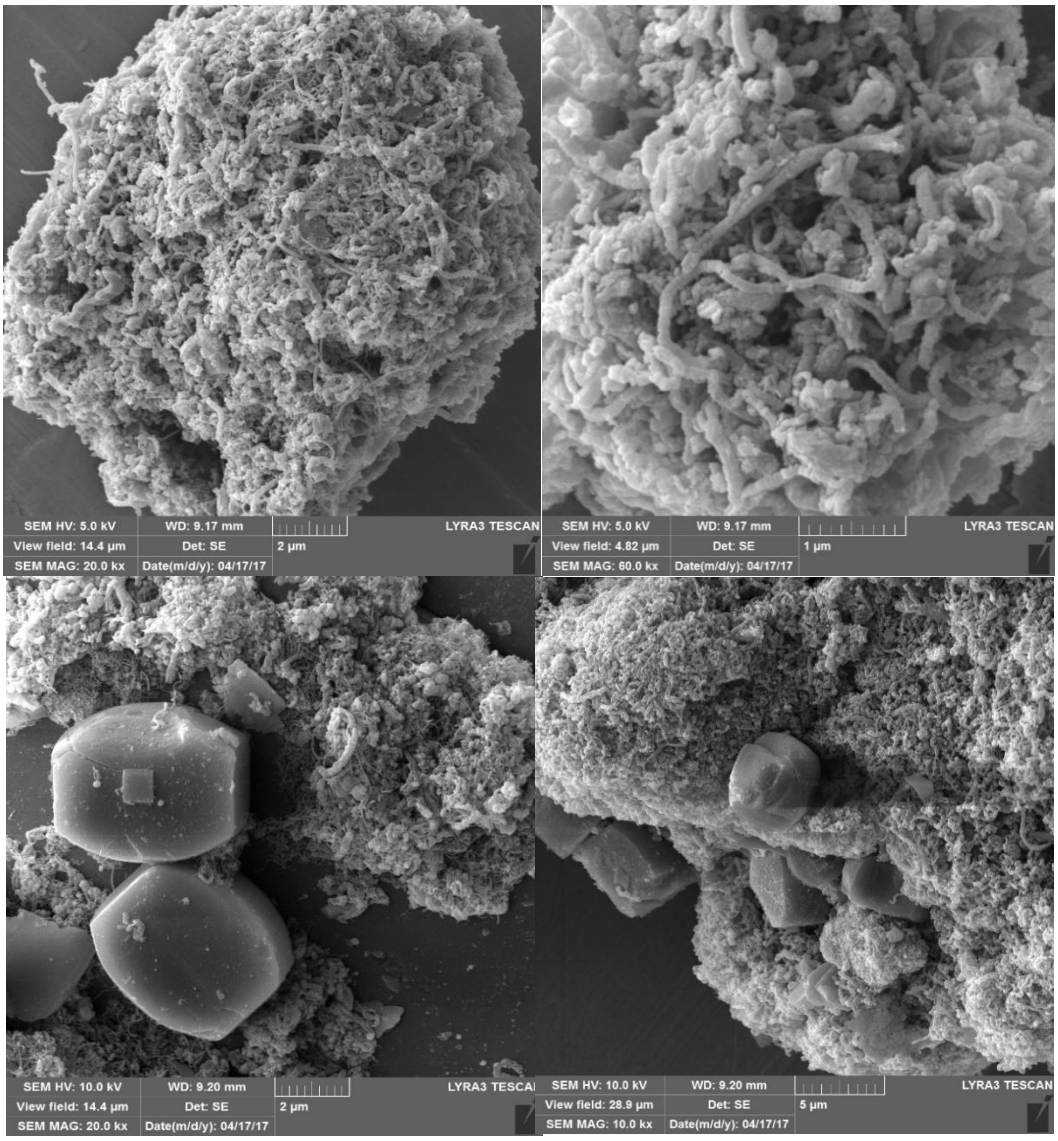

Figure 4-33. FE-SEM micro graphs of spent: top, 20Ni/Ce-S-1 and bottom, 20Ni/Y-S-1 catalysts.

As can observed from the TEM images in Figure 4-34 for the spent 20Ni/CeS-1 catalyst, carbon nanotubes can be seen to almost completely engulf the silicalite-1 particles. The presence of nickel clusters as wide as 100 nm can also be observed in the TEM images of fresh 20Ni/S-1 and spent 20Ni/CeS-1 catalysts—an indication that agglomeration and potential sintering of metal particles were controlled to a minimum. The presence of carbon nanotubes as observed in the TEM images corroborates with the observation from the SEM images of the spent catalysts as shown in Figure 4-33. This observation is also in agreement with the results obtained from TGA-DSC and Raman spectroscopy.

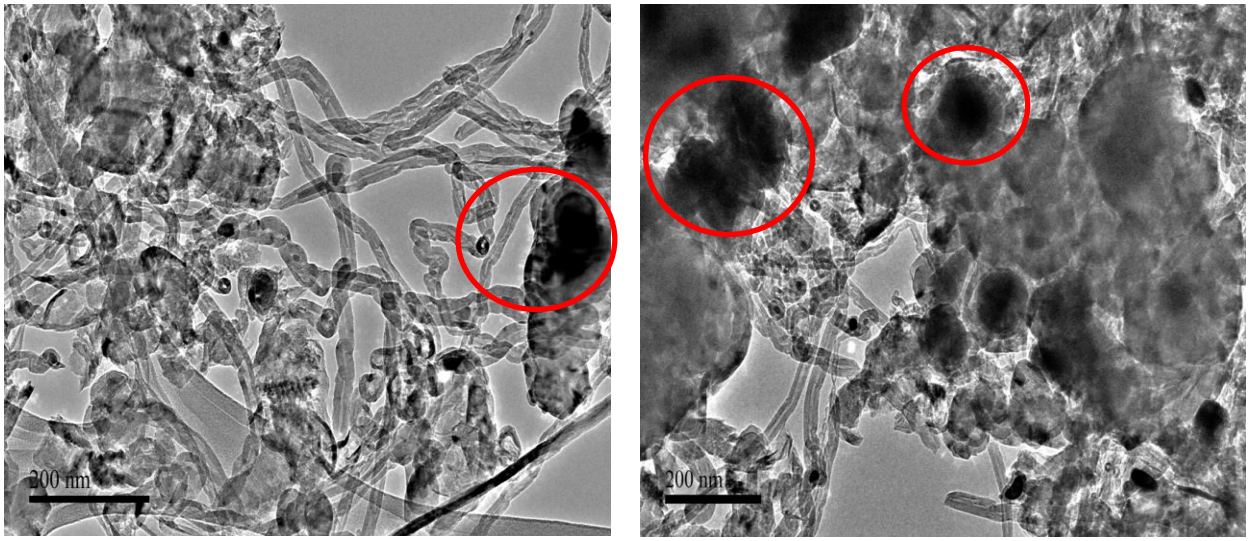

Figure 4-34. TEM image of spent 20Ni/CeS-1 catalyst after 12 h of reaction at 750 ^{o}C, 1 atm and 51,400 mL/h.g.

Chapter 5

CONCLUSIONS AND RECOMMENDATIONS

5.1 Conclusions

Ni particles were successfully dispersed on the surface of microwave synthesized silicalite-1. Nickel loading of 10 – 20 wt.% was found to be appreciably active in the conversion of CO_2 and CH_4 to syngas at a reaction temperature of 750 ^oC under a GHSV of 51400 mL/g.h. Increase in nickel loading caused a corresponding increase in H_2/CO ratio, resulting in the production of hydrogen-rich syngas. It was found that the activity and stability of the 20Ni/S-1 catalyst were improved after ion exchanging Na with the metals; Ce, Y and Zn. The Ce and Y ion-exchanged S-1 catalysts, despite high carbon deposition remained active after 11 h TOS – implying that these catalysts can be further modified to prevent or reduce carbon formation during the dry reforming reaction whilst maintaining the performance. In this study , we found that the MFI silicalite-1 zeolite is a suitable support material for dry reforming catalysts. Its good performance is ascribed to the high metal support interaction which minimized or prevented sintering of the nickel particles.

Overall, the 20Ni/CeS-1 catalysts had the best performance in terms of activity and stability. 4Ca-20Ni/S-1 catalyst produced syngas with H_2/CO ratio very close to unity. The superior performance of 20Ni/CeS-1 was attributed the oxygen storage capacity of Ce. This catalyst had higher mesoporosity owing to the post-synthesis treatment of the zeolite. The mesopores served to reduce mass transfer restrictions in the support

material. From the specific surface area measurements, the 20Ni/CeS-1 catalysts had the highest surface area. This high total surface area enables good dispersion of Ni particles thereby exposing more active sites for reaction to occur.

5.2 Recommendations

Based on these findings, we will recommend an investigation into the incorporation of both Ca and Ce into Ni-based silicalite-1 catalysts to further study their impacts in DRM reactions. We will also recommend studies of longer periods of stability tests of these catalysts in dry reforming of methane reactions. Mesoporosity was found to have a positive impact on the activity of the catalysts. We recommend further investigation into the effects of types of mesopores in the silicalite-1 (inter – or intracrystalline mesopores) on the methane reforming reaction. Relatively larger sizes of silicalite-1 particles are obtained when synthesis is done using the cheap template TPABr in alkaline medium. These crystals can be reduced by the sequential ball-milling-recrystallization procedure. We recommend a study on effect of sizes of silicalite-1 particles by this approach. There is room for incorporation of Al into the silicalite-1 framework. We therefore, further, recommend an investigation of the effect of Si/Al ratio on the performance of the 20Ni/CeS-1 catalysts.

References

1. Alkhathlan, K. and M. Javid, *Carbon emissions and oil consumption in Saudi Arabia.* Renewable and Sustainable Energy Reviews, 2015. **48**: p. 105-111 DOI: http://dx.doi.org/10.1016/j.rser.2015.03.072.
2. Haghighi, M., et al., *On the reaction mechanism of CO2 reforming of methane over a bed of coal char.* Proceedings of the Combustion Institute, 2007. **31**(2): p. 1983-1990 DOI: http://dx.doi.org/10.1016/j.proci.2006.07.029.
3. Aghamohammadi, S., M. Haghighi, and S. Karimipour, *A Comparative Synthesis and Physicochemical Characterizations of Ni/Al2O3–MgO Nanocatalyst via Sequential Impregnation and Sol–Gel Methods Used for CO2 Reforming of Methane.* Journal of Nanoscience and Nanotechnology, 2013. **13**(7): p. 4872-4882 DOI: 10.1166/jnn.2013.7588.
4. Lahijani, P., et al., *Conversion of the greenhouse gas CO2 to the fuel gas CO via the Boudouard reaction: A review.* Renewable and Sustainable Energy Reviews, 2015. **41**: p. 615-632 DOI: http://dx.doi.org/10.1016/j.rser.2014.08.034.
5. Khajeh Talkhoncheh, S. and M. Haghighi, *Syngas production via dry reforming of methane over Ni-based nanocatalyst over various supports of clinoptilolite, ceria and alumina.* Journal of Natural Gas Science and Engineering, 2015. **23**: p. 16-25 DOI: http://dx.doi.org/10.1016/j.jngse.2015.01.020.

6. Kumar, N., et al., *Bi-reforming of methane on Ni-based pyrochlore catalyst.* Applied Catalysis A: General, 2016. **517**: p. 211-216 DOI: http://dx.doi.org/10.1016/j.apcata.2016.03.016.

7. Lee, H.Y., et al., *Combined steam and CO2 reforming of CH4 using coke oven gas on nickel-based catalyst: Effects of organic acids to nickel dispersion and activity.* Chemical Engineering Journal, 2015. **280**: p. 771-781 DOI: http://dx.doi.org/10.1016/j.cej.2015.06.047.

8. de Sousa, H.S.A., et al., *Mesoporous catalysts for dry reforming of methane: Correlation between structure and deactivation behaviour of Ni-containing catalysts.* International Journal of Hydrogen Energy, 2012. **37**(17): p. 12281-12291 DOI: http://dx.doi.org/10.1016/j.ijhydene.2012.05.151.

9. Pan, L. and S. Wang, *Methanol steam reforming in a compact plate-fin reformer for fuel-cell systems.* International Journal of Hydrogen Energy, 2005. **30**(9): p. 973-979 DOI: http://dx.doi.org/10.1016/j.ijhydene.2004.10.012.

10. Laosiripojana, N. and S. Assabumrungrat, *Methane steam reforming over Ni/Ce–ZrO2 catalyst: Influences of Ce–ZrO2 support on reactivity, resistance toward carbon formation, and intrinsic reaction kinetics.* Applied Catalysis A: General, 2005. **290**(1–2): p. 200-211 DOI: http://dx.doi.org/10.1016/j.apcata.2005.05.026.

11. Pinheiro, A.N., et al., *Highly stable dealuminated zeolite support for the production of hydrogen by dry reforming of methane.* Applied Catalysis A: General, 2009. **355**(1–2): p. 156-168 DOI: http://dx.doi.org/10.1016/j.apcata.2008.12.007.

12. Rezaei, M., et al., *Autothermal reforming of methane over Ni catalysts supported on nanocrystalline MgO with high surface area and plated-like shape.* International

Journal of Hydrogen Energy, 2011. **36**(18): p. 11712-11717 DOI: http://dx.doi.org/10.1016/j.ijhydene.2011.06.056.

13. Cai, X., X. Dong, and W. Lin, *Autothermal Reforming of Methane over Ni Catalysts Supported on CuO-ZrO2-CeO2-Al2O3.* Journal of Natural Gas Chemistry, 2006. **15**(2): p. 122-126 DOI: http://dx.doi.org/10.1016/S1003-9953(06)60018-2.
14. Bobrova, L.N., et al., *Kinetic assessment of dry reforming of methane on Pt + Ni containing composite of fluorite-like structure.* Applied Catalysis B: Environmental, 2016. **182**: p. 513-524 DOI: http://dx.doi.org/10.1016/j.apcatb.2015.09.049.
15. Farniaei, M., et al., *Syngas production in a novel methane dry reformer by utilizing of tri-reforming process for energy supplying: Modeling and simulation.* Journal of Natural Gas Science and Engineering, 2014. **20**: p. 132-146 DOI: http://dx.doi.org/10.1016/j.jngse.2014.06.010.
16. Nikoo, M.K. and N.A.S. Amin, *Thermodynamic analysis of carbon dioxide reforming of methane in view of solid carbon formation.* Fuel Processing Technology, 2011. **92**(3): p. 678-691 DOI: http://dx.doi.org/10.1016/j.fuproc.2010.11.027.
17. Vollmar, H.E., et al., *Innovative concepts for the coproduction of electricity and syngas with solid oxide fuel cells.* Journal of Power Sources, 2000. **86**(1–2): p. 90-97 DOI: http://dx.doi.org/10.1016/S0378-7753(99)00421-8.
18. Pereñiguez, R., et al., *LaNiO3 as a precursor of Ni/La2O3 for CO2 reforming of CH4: Effect of the presence of an amorphous NiO phase.* Applied Catalysis B: Environmental, 2012. **123–124**: p. 324-332 DOI: http://dx.doi.org/10.1016/j.apcatb.2012.04.044.

19. Zhang, S., et al., *Ceria-Doped Ni/SBA-16 Catalysts for Dry Reforming of Methane.* ACS Catalysis, 2013. **3**(8): p. 1855-1864 DOI: 10.1021/cs400159w.

20. Niu, J., et al., *Dry (CO2) reforming of methane over Pt catalysts studied by DFT and kinetic modeling.* Applied Surface Science, 2016. **376**: p. 79-90 DOI: http://dx.doi.org/10.1016/j.apsusc.2016.01.212.

21. García-Diéguez, M., et al., *Transient study of the dry reforming of methane over Pt supported on different γ-Al2O3.* Catalysis Today, 2010. **149**(3–4): p. 380-387 DOI: http://dx.doi.org/10.1016/j.cattod.2009.07.099.

22. Stevens, R.W. and S.S.C. Chuang, *In Situ IR Study of Transient CO2 Reforming of CH4 over Rh/Al2O3.* The Journal of Physical Chemistry B, 2004. **108**(2): p. 696-703 DOI: 10.1021/jp0367530.

23. Múnera, J.F., et al., *Kinetics and reaction pathway of the CO2 reforming of methane on Rh supported on lanthanum-based solid.* Journal of Catalysis, 2007. **245**(1): p. 25-34 DOI: http://dx.doi.org/10.1016/j.jcat.2006.09.008.

24. Reddy, G.K., et al., *Reforming of methane with carbon dioxide over Pt/ZrO2/SiO2 catalysts—Effect of zirconia to silica ratio.* Applied Catalysis A: General, 2010. **389**(1–2): p. 92-100 DOI: http://dx.doi.org/10.1016/j.apcata.2010.09.007.

25. Sokolov, S., et al., *Stable low-temperature dry reforming of methane over mesoporous La2O3-ZrO2 supported Ni catalyst.* Applied Catalysis B: Environmental, 2012. **113–114**: p. 19-30 DOI: http://dx.doi.org/10.1016/j.apcatb.2011.09.035.

26. Mette, K., et al., *Stable Performance of Ni Catalysts in the Dry Reforming of Methane at High Temperatures for the Efficient Conversion of CO2 into Syngas.* ChemCatChem, 2014. **6**(1): p. 100-104 DOI: 10.1002/cctc.201300699.

27. Misture, S.T., et al., *Sulfur-resistant and regenerable Ni/Co spinel-based catalysts for methane dry reforming.* Catalysis Science & Technology, 2015. **5**(9): p. 4565-4574 DOI: 10.1039/C5CY00800J.

28. Kim, S.S., et al., *Effect of Ce/Ti ratio on the catalytic activity and stability of Ni/CeO2–TiO2 catalyst for dry reforming of methane.* Chemical Engineering Journal, 2015. **280**: p. 433-440 DOI: http://dx.doi.org/10.1016/j.cej.2015.06.027.

29. Ao, M., et al., *Structure and activity of strontium substituted LaCoO3 perovskite catalysts for syngas conversion.* Journal of Molecular Catalysis A: Chemical, 2016. **416**: p. 96-104 DOI: http://dx.doi.org/10.1016/j.molcata.2016.02.020.

30. Liu, G., et al., *Bi-metal Cu–Co from LaCo1 − xCuxO3 perovskite supported on zirconia for the synthesis of higher alcohols.* Fuel Processing Technology, 2014. **128**: p. 289-296 DOI: http://dx.doi.org/10.1016/j.fuproc.2014.07.010.

31. Fang, Y., et al., *Cu-Co bi-metal catalyst prepared by perovskite CuO/LaCoO3 used for higher alcohol synthesis from syngas.* Journal of Energy Chemistry, 2014. **23**(4): p. 527-534 DOI: http://dx.doi.org/10.1016/S2095-4956(14)60181-9.

32. Pecchi, G., et al., *Catalytic Performance of La_{0.6}Ca_{0.4}Fe_{1-x}Ni_xO₃ Perovskites in DME Oxidation.* Modern Research in Catalysis, 2015. **04**(04): p. 97-106 DOI: 10.4236/mrc.2015.44012.

33. Yang, E.-h., et al., *The effect of promoters in La0.9M0.1Ni0.5Fe0.5O3 (M = Sr, Ca) perovskite catalysts on dry reforming of methane.* Fuel Processing Technology, 2015. **134**: p. 404-413 DOI: http://dx.doi.org/10.1016/j.fuproc.2015.02.023.

34. Sutthiumporn, K., et al., *CO2 dry-reforming of methane over La0.8Sr0.2Ni0.8M0.2O3 perovskite (M = Bi, Co, Cr, Cu, Fe): Roles of lattice oxygen on C–H activation and carbon suppression.* International Journal of Hydrogen Energy, 2012. **37**(15): p. 11195-11207 DOI: http://dx.doi.org/10.1016/j.ijhydene.2012.04.059.

35. Moradi, G.R., M. Rahmanzadeh, and F. Khosravian, *The effects of partial substitution of Ni by Zn in LaNiO3 perovskite catalyst for methane dry reforming.* Journal of Co2 Utilization, 2014. **6**: p. 7-11 DOI: 10.1016/j.jcou.2014.02.001.

36. Wang, N., et al., *A comparison study on methane dry reforming with carbon dioxide over LaNiO3 perovskite catalysts supported on mesoporous SBA-15, MCM-41 and silica carrier.* Catalysis Today, 2013. **212**: p. 98-107 DOI: http://dx.doi.org/10.1016/j.cattod.2012.07.022.

37. Moradi, G.R., F. Khosravian, and M. Rahmanzadeh, *Effects of Partial Substitution of Ni by Cu in LaNiO3 Perovskite Catalyst for Dry Methane Reforming.* Chinese Journal of Catalysis, 2012. **33**(4–6): p. 797-801 DOI: http://dx.doi.org/10.1016/S1872-2067(11)60378-1.

38. Valderrama, G., A. Kiennemann, and M.R. Goldwasser, *La-Sr-Ni-Co-O based perovskite-type solid solutions as catalyst precursors in the CO2 reforming of methane.* Journal of Power Sources, 2010. **195**(7): p. 1765-1771 DOI: http://dx.doi.org/10.1016/j.jpowsour.2009.10.004.

39. Perez-Camacho, M.N., et al., *Self-cleaning perovskite type catalysts for the dry reforming of methane.* Chinese Journal of Catalysis, 2014. **35**(8): p. 1337-1346 DOI: 10.1016/s1872-2067(14)60187-x.

40. Sagar, T.V., et al., *Influence of method of preparation on the activity of La-Ni-Ce mixed oxide catalysts for dry reforming of methane.* Rsc Advances, 2014. **4**(91): p. 50226-50232 DOI: 10.1039/c4ra07098d.

41. Moradi, G., F. Khezeli, and H. Hemmati, *Syngas production with dry reforming of methane over Ni/ZSM-5 catalysts.* Journal of Natural Gas Science and Engineering, 2016. **33**: p. 657-665 DOI: http://dx.doi.org/10.1016/j.jngse.2016.06.004.

42. Luengnaruemitchai, A. and A. Kaengsilalai, *Activity of different zeolite-supported Ni catalysts for methane reforming with carbon dioxide.* Chemical Engineering Journal, 2008. **144**(1): p. 96-102 DOI: http://dx.doi.org/10.1016/j.cej.2008.05.023.

43. Usman, M., W.M.A. Wan Daud, and H.F. Abbas, *Dry reforming of methane: Influence of process parameters—A review.* Renewable and Sustainable Energy Reviews, 2015. **45**: p. 710-744 DOI: http://dx.doi.org/10.1016/j.rser.2015.02.026.

44. Xie, T., et al., *Immobilizing Ni nanoparticles to mesoporous silica with size and location control via a polyol-assisted route for coking- and sintering-resistant dry reforming of methane.* Chemical Communications, 2014. **50**(55): p. 7250-7253 DOI: 10.1039/C4CC01441C.

45. Liu, Z., et al., *Highly dispersed nickel loaded on mesoporous silica: One-spot synthesis strategy and high performance as catalysts for methane reforming with carbon dioxide.* Applied Catalysis B: Environmental, 2012. **125**: p. 324-330 DOI: http://dx.doi.org/10.1016/j.apcatb.2012.06.003.

46. Xu, L., et al., *Ordered mesoporous alumina supported nickel based catalysts for carbon dioxide reforming of methane.* International Journal of Hydrogen Energy, 2012. **37**(9): p. 7497-7511 DOI: http://dx.doi.org/10.1016/j.ijhydene.2012.01.105.

47. Sarkar, B., et al., *Highly nanodispersed Gd-doped Ni/ZSM-5 catalyst for enhanced carbon-resistant dry reforming of methane.* Journal of Molecular Catalysis A: Chemical, 2016. **424**: p. 17-26 DOI: http://dx.doi.org/10.1016/j.molcata.2016.08.006.

48. Dai, C., et al., *Hollow zeolite encapsulated Ni–Pt bimetals for sintering and coking resistant dry reforming of methane.* Journal of Materials Chemistry A, 2015. **3**(32): p. 16461-16468.

49. Frontera, P., et al., *Catalytic dry-reforming on Ni–zeolite supported catalyst.* Catalysis Today, 2012. **179**(1): p. 52-60 DOI: http://dx.doi.org/10.1016/j.cattod.2011.07.039.

50. Fakeeha, A.H., et al., *Stabilities of zeolite-supported Ni catalysts for dry reforming of methane.* Chinese Journal of Catalysis, 2013. **34**(4): p. 764-768 DOI: http://dx.doi.org/10.1016/S1872-2067(12)60554-3.

51. Foley, H.C., *Carbogenic molecular sieves: synthesis, properties and applications.* Microporous Materials, 1995. **4**(6): p. 407-433 DOI: http://dx.doi.org/10.1016/0927-6513(95)00014-Z.

52. Chang, J.-S., S.-E. Park, and H. Chon, *Catalytic activity and coke resistance in the carbon dioxide reforming of methane to synthesis gas over zeolite-supported Ni catalysts.* Applied Catalysis A: General, 1996. **145**(1): p. 111-124 DOI: http://dx.doi.org/10.1016/0926-860X(96)00150-0.

53. Zhang, W.D., et al., *Preparation of La2NiO4/ZSM-5 catalyst and catalytic performance in CO2/CH4 reforming to syngas.* Applied Catalysis A: General, 2005. **292**: p. 138-143 DOI: http://dx.doi.org/10.1016/j.apcata.2005.05.018.

54. Estephane, J., et al., *CO2 reforming of methane over Ni–Co/ZSM5 catalysts. Aging and carbon deposition study*. International Journal of Hydrogen Energy, 2015. **40**(30): p. 9201-9208 DOI: http://dx.doi.org/10.1016/j.ijhydene.2015.05.147.

55. Estephane, J., et al., *CO2 reforming of CH4 over highly active and stable yRhNix/NaY catalysts.* Comptes Rendus Chimie, 2015. **18**(3): p. 277-282 DOI: http://dx.doi.org/10.1016/j.crci.2014.08.007.

56. Nimwattanakul, W., A. Luengnaruemitchai, and S. Jitkarnka, *Potential of Ni supported on clinoptilolite catalysts for carbon dioxide reforming of methane.* International Journal of Hydrogen Energy, 2006. **31**(1): p. 93-100 DOI: http://dx.doi.org/10.1016/j.ijhydene.2005.02.005.

57. Khodakov, Y.S., et al., *Investigation of the structure and thermal stability of zeolites of types A, X, and Y, containing trivalent chromium.* Bulletin of the Academy of Sciences of the USSR, Division of chemical science, 1969. **18**(3): p. 465-470 DOI: 10.1007/bf00906959.

58. Trigueiro, F.E., et al., *Thermal stability of Y zeolites containing different rare earth cations.* Journal of Alloys and Compounds, 2002. **344**(1–2): p. 337-341 DOI: http://dx.doi.org/10.1016/S0925-8388(02)00381-X.

59. Kaengsilalai, A., et al., *Potential of Ni supported on KH zeolite catalysts for carbon dioxide reforming of methane.* Journal of Power Sources, 2007. **165**(1): p. 347-352 DOI: http://dx.doi.org/10.1016/j.jpowsour.2006.12.005.

60. Sarkar, B., et al., *Reforming of methane with CO2 over Ni nanoparticle supported on mesoporous ZSM-5.* Catalysis Today, 2012. **198**(1): p. 209-214 DOI: http://dx.doi.org/10.1016/j.cattod.2012.04.029.

61. Davis, M.E., *Ordered porous materials for emerging applications.* Nature, 2002. **417**(6891): p. 813-821.

62. Frontera, P., et al., *Effect of support surface on methane dry-reforming catalyst preparation.* Catalysis Today, 2013. **218–219**: p. 18-29 DOI: http://dx.doi.org/10.1016/j.cattod.2013.04.029.

63. Halliche, D., O. Cherifi, and A. Auroux, *Microcalorimetric studies and methane reforming by CO2 on Ni-based zeolite catalysts.* Thermochimica Acta, 2005. **434**(1–2): p. 125-131 DOI: http://dx.doi.org/10.1016/j.tca.2005.01.005.

64. Frontera, P., et al., *Zeolite-supported Ni catalyst for methane reforming with carbon dioxide.* Research on Chemical Intermediates, 2011. **37**(2-5): p. 267-279 DOI: 10.1007/s11164-011-0249-3.

65. Alotaibi, R., et al., *Ni catalysts with different promoters supported on zeolite for dry reforming of methane.* Applied Petrochemical Research, 2015. **5**(4): p. 329-337 DOI: 10.1007/s13203-015-0117-y.

66. Izquierdo, U., et al., *Ni and RhNi catalysts supported on Zeolites L for hydrogen and syngas production by biogas reforming processes.* Chemical Engineering Journal, 2014. **238**: p. 178-188 DOI: http://dx.doi.org/10.1016/j.cej.2013.08.093.

67. Vafaeian, Y., M. Haghighi, and S. Aghamohammadi, *Ultrasound assisted dispersion of different amount of Ni over ZSM-5 used as nanostructured catalyst for hydrogen production via CO2 reforming of methane.* Energy Conversion and Management, 2013. **76**: p. 1093-1103 DOI: http://dx.doi.org/10.1016/j.enconman.2013.08.010.

68. Jeong, H., et al., *Effect of promoters in the methane reforming with carbon dioxide to synthesis gas over Ni/HY catalysts.* Journal of Molecular Catalysis A: Chemical, 2006. **246**(1–2): p. 43-48 DOI: http://dx.doi.org/10.1016/j.molcata.2005.10.013.

69. Primo, A. and H. Garcia, *Zeolites as catalysts in oil refining.* Chemical Society Reviews, 2014. **43**(22): p. 7548-7561 DOI: 10.1039/C3CS60394F.

70. Gunther, W.R., et al., *Sn-Beta zeolites with borate salts catalyse the epimerization of carbohydrates via an intramolecular carbon shift.* Nat Commun, 2012. **3**: p. 1109 DOI: http://www.nature.com/ncomms/journal/v3/n10/suppinfo/ncomms2122_S1.html.

71. Na, K., et al., *Directing Zeolite Structures into Hierarchically Nanoporous Architectures.* Science, 2011. **333**(6040): p. 328-332 DOI: 10.1126/science.1204452.

72. Cundy, C.S. and P.A. Cox, *The Hydrothermal Synthesis of Zeolites: History and Development from the Earliest Days to the Present Time.* Chemical Reviews, 2003. **103**(3): p. 663-702 DOI: 10.1021/cr020060i.

73. Corma, A., *Inorganic Solid Acids and Their Use in Acid-Catalyzed Hydrocarbon Reactions.* Chemical Reviews, 1995. **95**(3): p. 559-614 DOI: 10.1021/cr00035a006.

74. Davis, R.J., *New perspectives on basic zeolites as catalysts and catalyst supports.* Journal of Catalysis, 2003. **216**(1–2): p. 396-405 DOI: http://dx.doi.org/10.1016/S0021-9517(02)00034-9.

75. Maesen, T.L.M., et al., *Shape-selective n-alkane hydroconversion at exterior zeolite surfaces.* Journal of Catalysis, 2008. **256**(1): p. 95-107 DOI: http://dx.doi.org/10.1016/j.jcat.2008.03.004.

76. Busca, G., *Bases and Basic Materials in Chemical and Environmental Processes. Liquid versus Solid Basicity.* Chemical Reviews, 2010. **110**(4): p. 2217-2249 DOI: 10.1021/cr9000989.

77. Schoonheydt, R.A., et al., *The framework basicity of zeolites.* Journal of Materials Chemistry, 2012. **22**(36): p. 18705-18717 DOI: 10.1039/C2JM31366A.

78. Barthomeuf∗, D., *Basic Zeolites: Characterization and Uses in Adsorption and Catalysis.* Catalysis Reviews, 1996. **38**(4): p. 521-612 DOI: 10.1080/01614949608006465.

79. Keller, T.C., et al., *Hierarchical high-silica zeolites as superior base catalysts.* Chemical Science, 2014. **5**(2): p. 677-684 DOI: 10.1039/C3SC51937F.

80. Romero, M.D., et al., *O Methylation of Phenol in Liquid Phase over Basic Zeolites.* Industrial & Engineering Chemistry Research, 2004. **43**(26): p. 8194-8199 DOI: 10.1021/ie049461+.

81. Hathaway, P.E. and M.E. Davis, *Base catalysis by alkali-modified zeolites.* Journal of Catalysis, 1989. **116**(1): p. 263-278 DOI: http://dx.doi.org/10.1016/0021-9517(89)90091-2.

82. Martins, L., W. Hölderich, and D. Cardoso, *Methylammonium-FAU zeolite: Investigation of the basic sites in base catalyzed reactions and its performance.* Journal of Catalysis, 2008. **258**(1): p. 14-24 DOI: http://dx.doi.org/10.1016/j.jcat.2008.05.018.

83. Joshi, U.D., et al., *Effect of nonframework cations and crystallinity on the basicity of NaX zeolites.* Applied Catalysis A: General, 2003. **239**(1–2): p. 209-220 DOI: http://dx.doi.org/10.1016/S0926-860X(02)00391-5.

84. Ono, Y., *Solid base catalysts for the synthesis of fine chemicals.* Journal of Catalysis, 2003. **216**(1–2): p. 406-415 DOI: http://dx.doi.org/10.1016/S0021-9517(02)00120-3.

85. Hattori, H., *Heterogeneous Basic Catalysis.* Chemical Reviews, 1995. **95**(3): p. 537-558 DOI: 10.1021/cr00035a005.

86. Corma, A., et al., *Sn-zeolite beta as a heterogeneous chemoselective catalyst for Baeyer-Villiger oxidations.* Nature, 2001. **412**(6845): p. 423-425 DOI: http://www.nature.com/nature/journal/v412/n6845/suppinfo/412423a0_S1.html.

87. Hwang, Y.K., et al., *Microwave Fabrication of MFI Zeolite Crystals with a Fibrous Morphology and Their Applications.* Angewandte Chemie International Edition, 2005. **44**(4): p. 556-560 DOI: 10.1002/anie.200461403.

88. Fan, W., et al., *Synthesis, Crystallization Mechanism, and Catalytic Properties of Titanium-Rich TS-1 Free of Extraframework Titanium Species.* Journal of the American Chemical Society, 2008. **130**(31): p. 10150-10164 DOI: 10.1021/ja7100399.

89. Hartmann, M. and L. Kevan, *Transition-Metal Ions in Aluminophosphate and Silicoaluminophosphate Molecular Sieves: Location, Interaction with Adsorbates and Catalytic Properties.* Chemical Reviews, 1999. **99**(3): p. 635-664 DOI: 10.1021/cr9600971.

90. Zhou, Y., et al., *One-Pot Synthesis of Zeolitic Strong Solid Bases: A Family of Alkaline-Earth Metal-Containing Silicalite-1.* Chemistry – A European Journal, 2015. **21**(43): p. 15412-15420 DOI: 10.1002/chem.201501894.

91. Gu, J., et al., *Unseeded organotemplate-free hydrothermal synthesis of heteroatomic MFI zeolite poly-nanocrystallites.* Journal of Materials Chemistry A, 2013. **1**(7): p. 2453-2460 DOI: 10.1039/C2TA01009G.

92. Corma, A., R.M. Martín-Aranda, and F. Sánchez, *Zeolites as base catalysts: Condensation of benzaldehyde derivatives with activated methylenic compounds on Germanium-substituted faujasite.* Journal of Catalysis, 1990. **126**(1): p. 192-198 DOI: http://dx.doi.org/10.1016/0021-9517(90)90057-Q.

93. Xu, B.-Q., et al., *Nano-MgO: novel preparation and application as support of Ni catalyst for CO2 reforming of methane.* Catalysis Today, 2001. **68**(1–3): p. 217-225 DOI: http://dx.doi.org/10.1016/S0920-5861(01)00303-0.

94. Wang, L., et al., *Ionothermal Synthesis of Magnesium-Containing Aluminophosphate Molecular Sieves and their Catalytic Performance.* Chemistry – A European Journal, 2008. **14**(34): p. 10551-10555 DOI: 10.1002/chem.200801383.

95. Saha, S.K., et al., *Synthesis of aluminophosphate molecular sieves with AFI topology substituted by alkaline earth metal and their application to solid acid catalysis.* Microporous and Mesoporous Materials, 2005. **81**(1–3): p. 289-303 DOI: http://dx.doi.org/10.1016/j.micromeso.2005.02.009.

96. Sato, S., et al., *Cu-ZSM-5 zeolite as highly active catalyst for removal of nitrogen monoxide from emission of diesel engines.* Applied Catalysis, 1991. **70**(1): p. L1-L5 DOI: http://dx.doi.org/10.1016/S0166-9834(00)84146-9.

97. Corma, A., et al., *A large-cavity zeolite with wide pore windows and potential as an oil refining catalyst.* Nature, 2002. **418**(6897): p. 514-517 DOI: http://www.nature.com/nature/journal/v418/n6897/suppinfo/nature00924_S1.html.

98. Vermeiren, W. and J.-P. Gilson, *Impact of Zeolites on the Petroleum and Petrochemical Industry.* Topics in Catalysis, 2009. **52**(9): p. 1131-1161 DOI: 10.1007/s11244-009-9271-8.

99. Xu, X., J. Wang, and Y. Long, *Zeolite-based Materials for Gas Sensors.* Sensors, 2006. **6**(12): p. 1751.

100. Jhung, S.H., et al., *Crystal morphology control of AFI type molecular sieves with microwave irradiation.* Journal of Materials Chemistry, 2004. **14**(2): p. 280-285 DOI: 10.1039/B309142B.

101. Jhung, S.H., et al., *Selective formation of SAPO-5 and SAPO-34 molecular sieves with microwave irradiation and hydrothermal heating.* Microporous and Mesoporous Materials, 2003. **64**(1–3): p. 33-39 DOI: http://dx.doi.org/10.1016/S1387-1811(03)00501-8.

102. Komarneni, S., R. Roy, and Q.H. Li, *Microwave-hydrothermal synthesis of ceramic powders.* Materials Research Bulletin, 1992. **27**(12): p. 1393-1405 DOI: http://dx.doi.org/10.1016/0025-5408(92)90004-J.

103. Jhung, S.H., et al., *Template-Free Synthesis of the Nanoporous Nickel Phosphate VSB-5 under Microwave Irradiation.* Chemistry of Materials, 2004. **16**(8): p. 1394-1396 DOI: 10.1021/cm035173c.

104. Ramaswamy, V., et al., *Structure and Redox Behavior of Zirconium in Microporous Zr-Silicalites Studied by EXAFS and ESR Techniques.* Journal of Catalysis, 2001. **200**(2): p. 250-258 DOI: http://dx.doi.org/10.1006/jcat.2001.3213.

105. Notari, B., *Microporous Crystalline Titanium Silicates*, in *Advances in Catalysis*, W.O.H. D.D. Eley and G. Bruce, Editors. 1996, Academic Press. p. 253-334.

106. Hartmann, M., *Hierarchical Zeolites: A Proven Strategy to Combine Shape Selectivity with Efficient Mass Transport.* Angewandte Chemie International Edition, 2004. **43**(44): p. 5880-5882 DOI: 10.1002/anie.200460644.

107. Lopez-Orozco, S., et al., *Zeolitic Materials with Hierarchical Porous Structures.* Advanced Materials, 2011. **23**(22-23): p. 2602-2615 DOI: 10.1002/adma.201100462.

108. Cundy, C.S., J.O. Forrest, and R.J. Plaisted, *Some observations on the preparation and properties of colloidal silicalites. Part I: synthesis of colloidal silicalite-1 and titanosilicalite-1 (TS-1).* Microporous and Mesoporous Materials, 2003. **66**(2–3): p. 143-156 DOI: http://doi.org/10.1016/j.micromeso.2003.08.021.

109. Burkett, S.L. and M.E. Davis, *Mechanism of Structure Direction in the Synthesis of Si-ZSM-5: An Investigation by Intermolecular 1H-29Si CP MAS NMR.* The Journal of Physical Chemistry, 1994. **98**(17): p. 4647-4653 DOI: 10.1021/j100068a027.

110. de Moor, P.-P.E.A., et al., *In Situ Investigation of Si-TPA-MFI Crystallization Using (Ultra-) Small- and Wide-Angle X-ray Scattering.* The Journal of Physical Chemistry B, 1997. **101**(51): p. 11077-11086 DOI: 10.1021/jp9724784.

111. de Moor, P.P.E.A., T.P.M. Beelen, and R.A. van Santen, *Influence of Aging and Dilution on the Crystallization of Silicalite-1.* Journal of Applied Crystallography, 1997. **30**(5 Part 2): p. 675-679 DOI: doi:10.1107/S002188989700174X.

112. Kragten, D.D., et al., *Structure of the Silica Phase Extracted from Silica/(TPA)OH Solutions Containing Nanoparticles.* The Journal of Physical Chemistry B, 2003. **107**(37): p. 10006-10016 DOI: 10.1021/jp035110h.

113. Flanigen, E.M., et al., *Silicalite, a new hydrophobic crystalline silica molecular sieve.* Nature, 1978. **271**(5645): p. 512-516.

114. Fujiyama, S., et al., *Adsorption structures of non-aromatic hydrocarbons on silicalite-1 using the single-crystal X-ray diffraction method.* Physical Chemistry Chemical Physics, 2014. **16**(30): p. 15839-15845 DOI: 10.1039/C4CP01860E.

115. Persson, A.E., et al., *The synthesis of discrete colloidal particles of TPA-silicalite-1.* Zeolites, 1994. **14**(7): p. 557-567 DOI: http://dx.doi.org/10.1016/0144-2449(94)90191-0.

116. de Moor, P.-P.E.A., et al., *Si-MFI Crystallization Using a "Dimer" and "Trimer" of TPA Studied with Small-Angle X-ray Scattering.* The Journal of Physical Chemistry B, 2000. **104**(32): p. 7600-7611 DOI: 10.1021/jp0006476.

117. Watson, J.N., et al., *TPA−Silicalite Crystallization from Homogeneous Solution: Kinetics and Mechanism of Nucleation and Growth.* The Journal of Physical Chemistry B, 1997. **101**(48): p. 10094-10104 DOI: 10.1021/jp971531l.

118. Yang, S., et al., *Study on Synthesis of TPA-Silicalite-1 from Initially Clear Solutions of Various Base Concentrations by in Situ Calorimetry, Potentiometry, and SAXS.* Chemistry of Materials, 2004. **16**(2): p. 210-219 DOI: 10.1021/cm030587r.

119. Schoeman, B.J., *A spectroscopic study of the initial stage in the crystallization of TPA-silicalite-1 from clear solutions.* Studies in Surface Science and Catalysis, 1997. **105**: p. 647-654 DOI: http://dx.doi.org/10.1016/S0167-2991(97)80612-X.

120. Schoeman, B.J., *A high temperature in situ laser light-scattering study of the initial stage in the crystallization of TPA-silicalite-1.* Zeolites, 1997. **18**(2): p. 97-105 DOI: http://dx.doi.org/10.1016/S0144-2449(96)00134-0.

121. Schoeman, B.J., *The homogeneous nature of clear TPA-silicalite-1 precursor solutions.* Microporous Materials, 1997. **9**(5): p. 267-271 DOI: http://dx.doi.org/10.1016/S0927-6513(96)00116-2.

122. de Moor, P.-P.E.A., et al., *SAXS and USAXS Investigation on Nanometer-Scaled Precursors in Organic-Mediated Zeolite Crystallization from Gelating Systems.* Chemistry of Materials, 1999. **11**(1): p. 36-43 DOI: 10.1021/cm9807079.

123. Cundy, C.S., B.M. Lowe, and D.M. Sinclair, *Direct measurements of the crystal growth rate and nucleation behaviour of silicalite, a zeolitic silica polymorph.* Journal of Crystal Growth, 1990. **100**(1): p. 189-202 DOI: http://dx.doi.org/10.1016/0022-0248(90)90622-R.

124. Watson, J.N., et al., *Detection of TPA-silicalite precursors nucleated during the room temperature aging of a clear homogeneous synthesis solution.* Journal of the Chemical Society, Faraday Transactions, 1998. **94**(15): p. 2181-2186 DOI: 10.1039/A801924J.

125. Kirschhock, C.E.A., et al., *Aggregation Mechanism of Nanoslabs with Zeolite MFI-Type Structure.* The Journal of Physical Chemistry B, 1999. **103**(50): p. 11021-11027 DOI: 10.1021/jp992272y.

126. Mintova, S., et al., *Mechanism of the Transformation of Silica Precursor Solutions into Si-MFI Zeolite.* Angewandte Chemie International Edition, 2002. **41**(14): p. 2558-2561 DOI: 10.1002/1521-3773(20020715)41:14<2558::AID-ANIE2558>3.0.CO;2-0.

127. Cheng, C.-H. and D.F. Shantz, *Silicalite-1 Growth from Clear Solution: Effect of the Structure-Directing Agent on Growth Kinetics.* The Journal of Physical Chemistry B, 2005. **109**(29): p. 13912-13920 DOI: 10.1021/jp050733b.

128. Wang, X.-s., X.-w. Guo, and G. Li, *Synthesis of titanium silicalite (TS-1) from the TPABr system and its catalytic properties for epoxidation of propylene.* Catalysis

Today, 2002. **74**(1–2): p. 65-75 DOI: http://dx.doi.org/10.1016/S0920-5861(01)00531-4.

129. Vasile, A. and A.M. Busuioc-Tomoiaga, *A new route for the synthesis of titanium silicalite-1*. Materials Research Bulletin, 2012. **47**(1): p. 35-41 DOI: http://dx.doi.org/10.1016/j.materresbull.2011.10.008.

130. Xu, L., et al., *Alkaline-promoted Co-Ni bimetal ordered mesoporous catalysts with enhanced coke-resistant performance toward CO2 reforming of CH4.* Journal of CO2 Utilization, 2017. **18**: p. 1-14 DOI: http://doi.org/10.1016/j.jcou.2017.01.003.

131. Ramanjaneya Reddy, G., S. Balasubramanian, and K. Chennakesavulu, *Zeolite encapsulated Ni(ii) and Cu(ii) complexes with tetradentate N2O2 Schiff base ligand: catalytic activity towards oxidation of benzhydrol and degradation of rhodamine-B.* Journal of Materials Chemistry A, 2014. **2**(37): p. 15598-15610 DOI: 10.1039/C4TA01869A.

132. Wang, N., et al., *Preparation and characterization of a plasma treated NiMgSBA-15 catalyst for methane reforming with CO2 to produce syngas.* Catalysis Science & Technology, 2013. **3**(9): p. 2278-2287 DOI: 10.1039/C3CY00299C.

133. Le Normand, F., et al., *Photoemission on 3d core levels of Cerium: An experimental and theoretical investigation of the reduction of cerium dioxide.* Solid State Communications, 1989. **71**(11): p. 885-889 DOI: http://dx.doi.org/10.1016/0038-1098(89)90555-3.

134. Ponchel, A., et al., *CeNiO and CeAlNiO solids studied by electron microscopy, XRD, XPS and depth sputtering techniques.* Physical Chemistry Chemical Physics, 2000. **2**(2): p. 303-312 DOI: 10.1039/A908283B.

135. Zhang, Q., et al., *A stable Ni/SBA-15 catalyst prepared by the ammonia evaporation method for dry reforming of methane.* RSC Advances, 2015. **5**(114): p. 94016-94024 DOI: 10.1039/C5RA18845H.

136. Coenen, J.W.E., *Characterization of the standard nickel/silica catalyst EuroNi-1.* Applied Catalysis, 1991. **75**(1): p. 193-223 DOI: http://dx.doi.org/10.1016/S0166-9834(00)83132-2.

137. Sanhoob, M.A., et al., *Steam catalytic cracking of heavy naphtha (C12) to high octane naphtha over B-MFI zeolite.* Applied Catalysis B: Environmental, 2017. **210**: p. 432-443 DOI: http://doi.org/10.1016/j.apcatb.2017.04.001.

138. Li, H., et al., *Ni/SBA-15 catalysts for CO methanation: effects of V, Ce, and Zr promoters.* RSC Advances, 2015. **5**(117): p. 96504-96517 DOI: 10.1039/C5RA15990C.

139. Takahashi, R., et al., *Addition of zirconia in Ni/SiO2 catalyst for improvement of steam resistance.* Applied Catalysis A: General, 2004. **273**(1): p. 211-215 DOI: https://doi.org/10.1016/j.apcata.2004.06.033.

140. Ranjbar, A. and M. Rezaei, *Dry reforming reaction over nickel catalysts supported on nanocrystalline calcium aluminates with different CaO/Al2O3 ratios.* Journal of Natural Gas Chemistry, 2012. **21**(2): p. 178-183 DOI: https://doi.org/10.1016/S1003-9953(11)60351-4.

141. Wang, H.Y. and C.T. Au, *Carbon dioxide reforming of methane to syngas over SiO2-supported rhodium catalysts.* Applied Catalysis A: General, 1997. **155**(2): p. 239-252 DOI: https://doi.org/10.1016/S0926-860X(96)00398-5.

142. Dresselhaus, M.S., et al., *Raman spectroscopy of carbon nanotubes.* Physics Reports, 2005. **409**(2): p. 47-99 DOI: http://dx.doi.org/10.1016/j.physrep.2004.10.006.

143. McFarlane, A.R., et al., *The application of inelastic neutron scattering to investigate the steam reforming of methane over an alumina-supported nickel catalyst.* Chemical Physics, 2013. **427**: p. 54-60 DOI: http://dx.doi.org/10.1016/j.chemphys.2013.10.012.

144. Liu, D., et al., *Methane reforming with carbon dioxide over a Ni/ZiO2–SiO2 catalyst: Influence of pretreatment gas atmospheres.* International Journal of Hydrogen Energy, 2012. **37**(13): p. 10135-10144 DOI: http://dx.doi.org/10.1016/j.ijhydene.2012.03.158.

145. Goula, M.A., A.A. Lemonidou, and A.M. Efstathiou, *Characterization of Carbonaceous Species Formed during Reforming of CH4with CO2over Ni/CaO–Al2O3Catalysts Studied by Various Transient Techniques.* Journal of Catalysis, 1996. **161**(2): p. 626-640 DOI: http://dx.doi.org/10.1006/jcat.1996.0225.

146. de Sousa, F.F., et al., *Nanostructured Ni-containing spinel oxides for the dry reforming of methane: Effect of the presence of cobalt and nickel on the deactivation behaviour of catalysts.* International Journal of Hydrogen Energy, 2012. **37**(4): p. 3201-3212 DOI: http://doi.org/10.1016/j.ijhydene.2011.11.072.

Vitae

Name : Abdul-Rashid Bawah

Nationality : Ghanaian

Date of Birth : July 4, 1988

Email : rashbawah@gmail.com

Address : P. O. Box 40, Gambaga, N/R, Ghana

EDUCATION

Master of Science, Chemical Engineering (November 2017)

King Fahd University of Petroleum and Minerals (KFUPM), Dhahran, Saudi Arabia

Bachelor of Science, Chemical Engineering (June 2013)

Kwame Nkrumah University of Science and Technology (KNUST), Kumasi, Ghana

EMPLOYMENT HISTORY

King Fahd University of Petroleum and Minerals (KFUPM), Dhahran, Saudi Arabia

- ***Graduate Research Student***; Hydrocarbon conversion & Catalysis Group, Centre for Research Excellence in Nanotechnology, Research Institute.

January 2016—Present

- Research, design, synthesis and characterization of catalysts for dry reforming of natural gas to syngas, conversion rates of upwards of 90% of both CO_2 and methane were achieved.
- Undertaking research in zeolite and metal based catalysts and their composites.
- Run reactors for methane dry reforming reactions and conversion of methanol to olefins.
- Operate XRD, TPx, FTIR, micro GC and UV-vis equipment for sample analysis.
- Compiled and processed data acquired from experiments.
- Prepare and write peer reviewed scientific articles.
- Prepare reports and deliver presentations on assigned projects.

- Process quotations, invoices and receipts for reimbursement and payment for procured items.
- In charge of maintenance of fixed bed reactor system.
- Maintain compliance with all laboratory and safety policies, protocols and procedures.
- Maintain professional relationship with research scientists, technicians, administrators and scientific advisors.

➢ ***Teaching Laboratory Technician***, Department of Chemical Engineering

September 2017—Present

- Supervise and train undergraduate students during laboratory sessions, on the proper use and operation of equipment.
- Oversee the safety of students and technician assistants.

➢ ***Teaching Assistant***, Department of Chemical Engineering

September 2016—May 2017

- Assisted professors in the administering of teaching duties to undergraduate students.
- Supervised quiz and minor exam sessions for undergraduate students.
- Assessed and graded homework for undergraduate students.

Kwame Nkrumah University of Science and Technology (KNUST), Kumasi, Ghana

➢ ***Teaching Assistant***, Department of Chemical Engineering

August 2013—July 2014

- Provided support for lecturers in the teaching of undergraduate courses.
- Responsible for the teaching of courses to students when the substantive lecturer had other duties and could not be in class.
- Conducted and supervised process engineering and unit operations laboratory sessions for undergraduate students.

Tema Oil Refinery (TOR), Tema, Ghana

- ***Engineering Intern,*** Projects Department and Residue Fuel Catalytic Cracking Unit

June 2011—August 2011

- Assisted engineers in the compilation of project documents.
- Involved in routine project inspections in the plant and at the TOR oil jetty at Tema habour.
- Attended monthly project meetings, chaired by the project department manager.
- Maintained professional and work relationship with all engineers.
- Performed specific assigned tasks.

Other Skills

- Advanced knowledge of MS Office Applications
- Intermediate knowledge of:
  - MatLab programming
  - C-programming
  - Java programming
  - HYSIS